THE UNIVERSITY of EDINBURGH

Planar Array Design and Analysis on Direction of Arrival Estimation for Mobile Communication Systems

Rahmat Sanudin

Degree of Doctor of Philosophy

The University of Edinburgh

2014

Table of Contents

Declaration of Originality

I hereby declare that the research reported in this thesis and the thesis itself was composed and originated entirely by myself in the School of Engineering at the University of Edinburgh.

Rahmat Sanudin

School of Engineering, University of Edinburgh

18 April 2014

Acknowledgements

All praises due to Allah, the most gracious, the most merciful. I would like to take this opportunity to thank those who have been involved and supported me towards the successful completion of my PhD study.

I would like to thank my supervisor Prof. Tughrul Arslan for his valuable suggestions, criticism and guidance. His invaluable efforts, expertise and patience towards developing my professional and technical skills are highly appreciated.

This appreciation also goes to Dr. Ahmed T. Erdogan for his valuable time and advice. To all my friends in the System Level Integration Group, your help and encouragement is greatly appreciated.

Special thanks to my financial sponsor, Universiti Tun Hussein Onn Malaysia (UTHM) and the Ministry of Education Malaysia (MoE) for the scholarship and administrative support.

Last but not least, my appreciation goes to my wife and my parents for their patience, understanding and support throughout the research that led to this thesis.

Abstract

The demand of wireless communication has increased significantly in the past few decades due to huge demand to deliver multimedia content instantly. The expansion of mobile content paired with affordable mobile devices has opened a new trend for having access to the latest information on mobile devices. This trend is made possible by the technology of smart antenna systems as well as array signal processing algorithms. Array signal processing is not limited to wireless communication, but also found in other applications such as radar, sonar and automotive. One of the important components in array signal processing is its ability to estimate the direction of incoming signals known as directional-of-arrival (DOA). The performance of DOA algorithms depends on the steering vector since it contains information about the direction of incoming signals.

One of the main factors to affect the DOA estimation is the array geometries since the array factor of the array geometries determines the definition of the steering vector. Another issue in DOA estimation is that the DOA algorithms are designed based on the ideal assumption that the antenna arrays are free from imperfection conditions. In practice, ideal conditions are extremely difficult to obtain and thus the imperfect conditions will severely degraded the performance of DOA estimation. The imperfect conditions include the presence of mutual coupling between elements and are also characteristic of directional antenna.

There are three topics being discussed in this thesis. The first topic being investigated is new geometry of antenna array to improve the performance of DOA estimation. Two variants of the circular-based array are proposed in this thesis: semi-circular array and oval array. Another proposed array is Y-bend array, which is a variant of V-shape array. The proposed arrays are being put forward to offer a better performance of DOA estimation and have less acquired area compared with the circular array. It is found out that the semi-circular array has 5.7% better estimation resolution, 76% lower estimation error, and 20% higher estimation consistency than the circular array. The oval array improves the estimation resolution by 33%,

estimation error by 60%, and estimation consistency by 20% compared with the circular array. In addition, for the same number of elements, the oval array requires 12.5% to 15% less area than the circular array. The third proposed array, Y-bend array, has 23% smaller estimation resolution, 88% lower estimation error, and 7% higher estimation consistency than the V-shape array. Among the proposed arrays, the semi-circular possessed the best performance with 25% smaller estimation resolution, ten times smaller estimation error, and 5% higher estimation consistency over the other proposed arrays.

Secondly, this thesis investigates the DOA estimation algorithm when using the directional antenna array. In this case, a new algorithm is proposed in order to suit the characteristics of the directional antenna array. The proposed algorithm is a modified version of the Capon algorithm, one of the algorithms in beamforming category. In elevation angle estimation, the proposed algorithm achieves estimation resolution up to 1°. The proposed algorithm also manages to improve the estimation error by 80% and estimation consistency by 10% compared with the Capon algorithm. In azimuth angle estimation, the proposed algorithm achieves 20 times lower estimation error and 20% higher estimation consistency than the Capon algorithm. These simulation results show that the proposed algorithm works effectively with the directional antenna array.

Finally, the thesis proposes a new method in DOA estimation process for directional antenna array. The proposed method is achieved by means of modifying covariance matrix calculation. Simulation results suggest that the proposed method improves the estimation resolution by 5° and the estimation error by 10% compared with the conventional method. In summary, this thesis has contributed in three main topics related to DOA estimation; array geometry design, algorithm for the directional antenna array, and method in DOA estimation process for the directional antenna array.

Lay Summary

For the last 40 years, the technology of mobile communication systems develops significantly due to increasing demand in accessing real-time information. Besides, apart from voice, the means of communication also expands into other forms such as message, picture, and video. It is important to understand that there is an operating system that works effectively to support the mobile communication systems.

One of important components in the operating system of mobile communication technology is the 'brain' to process the transmitted signals. Transmitted signals refer to the bulk of information, such as voice or picture, which must be sent through the communication system. The 'brain' in this case is called the algorithm of signal processing. In other words, the algorithm of signal processing is responsible for ensuring the transmitted signals reach the receiver in the best quality. For example, in a telephone conversation that involves voice signal, the algorithm will code the voice signal in a format that is compatible with the service provider requirement. Then, the coded signal is sent through the communication line, either in wired or wireless connection, between the caller and receiver. Once the coded signal reaches the other end of communication line, the algorithm will decode the received signal to retrieve the original voice signal.

In mobile communication system, there are several factors that affect the quality of received signal. These factors include the antenna design, the antenna configuration, and the choice of signal processing algorithm. All these factors will determine the quality of received signals, reliability of communication line, and electrical power required to support the communication line. Therefore, it is important to optimise those factors to produce a reliable and efficient mobile communication system.

This thesis investigates the issue of antenna configurations and algorithms of signal processing for mobile communication systems. This thesis identifies three main aims as the focus point of research. Firstly, analyse the effectiveness of existing antenna configurations in the mobile communication systems. Secondly, analyse the effectiveness of existing signal processing algorithms. Finally, propose optimised

antenna configurations and efficient signal processing algorithms to achieve a reliable communication system. This thesis also presents evaluation results to show the proposed antenna configuration and signal processing algorithms have achieved the desired performance for mobile communication system. In addition, this thesis suggests future work that is useful to have a better understanding in this research area.

List of Figures

List of Tables

List of Acronyms

1D	One-dimensional
2D	Two dimensional
DOA	Direction of arrival
ML	Maximum Likelihood
MUSIC	Multiple Signal Classification
RMSE	Root Mean Square Error
SIR	Signal to Interference Ratio
SNR	Signal to Noise Ratio

1 Introduction

1.1 Motivation

The development of smart antennas for wireless communication systems has triggered enormous interest in the past decades for its potential to provide better services and an increasing number of users. A smart antenna system, in general, consists of an array of antenna that has the intelligence to adjust its beam depending on the environment. In a smart antenna system, it is desirable to have the radiation pattern as narrow as possible and the directivity as high as possible. A smart antenna system is desirable; it has demonstrated a number of benefits in ongoing research. It is anticipated that the smart antenna system could contribute to [1]:

- Significant reduction of multi-path fading thus enhanced wireless communication system performance;
- Longer battery life for mobile devices since less power is needed to transmit signals to the base station;
- Major improvement to the signal-to-interference ratio (SIR) and thus increase the system capacity.

Smart antennas can be classified into two main categories; switched beam and adaptive antenna [2]. The switched beam antenna has a number of fixed antenna beams covering a specific sector. The system will turn on a beam towards a desired signal at a time in order to increase the received signal strength. If the received signal is changing direction or multiple desired signals exist, the system will turn on the appropriate beam so that all the desired signals can be covered. The adaptive antenna is capable of increasing the reception of intended signals and suppressing the interference signals. This capability is achieved through algorithms that are able to locate the direction of both desired and interference signals. This information is then used to steer the main beam towards the desired signals and place nulls on the interference signals.

One of the important signal processing blocks in smart antenna systems is the direction of arrival (DOA) algorithm. The main purpose of the DOA algorithm is to estimate the direction of incoming signals based on samples of received signals. The accuracy of estimation depends on the number of received signal samples (also known as a snapshot since the estimation is calculated from the expectation of the received signals). This is the crucial step for locating the direction of desired signals and later the smart antenna system will steer the beam in the estimated direction. DOA algorithms also provide the means in a smart antenna system to adapt its directivity in a changing environment of wireless communication. As the direction of desired signals keeps on changing due to the movement of the mobile station, the DOA algorithm will dynamically update the new direction of desired signals. For instance, an antenna array can be designed to detect a number of incoming signals and direct the main beam in certain directions only while rejecting signals that are declared as interference. This process explains the intelligence in smart antennas that are able to locate the specific direction of both desired and interference signals [3].

In general, DOA algorithms depend on two fundamental descriptions; steering vector and covariance matrix. Steering vector represents the response of the antenna array to a source in a certain direction. For multiple signals impinging an array, each signal direction will be associated with a unique steering vector. On top of that, the steering vector also describes the array geometry since different array configuration leads to unique expression. The covariance matrix involves the expectation of a received signal, but in practice this cannot be obtained; therefore, an average over a finite sample of received signals is normally used instead [2].

The quality of DOA estimation also depends on the shape of the antenna array, or the antenna array geometry. The antenna array geometry determines the array factor which is used to form the steering vector. Thus, the geometry of antenna array is an essential factor for achieving accurate estimation. The antenna array structure could be used either for one-dimensional or two-dimensional DOA estimation. One-dimensional estimation means the estimation is limited to elevation angle whereas two-dimensional estimation provides simultaneous estimation of both elevation and azimuth angles [4].

1.2 Objectives of the thesis

The objectives of this thesis are outlined as follows:

- To develop a new design of antenna array geometries that could improve the accuracy of DOA estimation. The design goal is to achieve an estimation with high resolution, minimum estimation error and high estimation consistency. A high estimation resolution means the estimator is able to distinguish two or more signal sources that are close to one another. Minimising estimation error means the estimator can achieve accurate results since the estimated DOA is very close to the true DOA. A high estimation consistency means the estimator has high percentage of the true DOA estimation.
- To formulate a new algorithm of DOA estimation when using directional antenna array. Directional antenna possess unique characteristic that must be taken into account when using them in antenna array processing such as DOA estimation. Since most of the existing DOA algorithms are designed to work with isotropic antenna, this thesis aims to address this problem by proposing a new DOA algorithm that could work with directional antenna.
- To propose a new method in the DOA estimation process when using the directional antenna array. The proposed method also takes into account directional antenna characteristics in order to produce accurate DOA estimation.

1.3 Contribution of the thesis

This thesis presents the following original contributions:

1. New design of circular-based planar antenna arrays for two-dimensional DOA estimation.

2. New design of planar antenna arrays based on combination of linear antenna arrays for two-dimensional DOA estimation.

3. A new DOA estimation algorithm for directional antenna array.

4. A new technique in DOA estimation to accommodate the characteristic of the directional antenna element.

1.4 Thesis structure

The remainder of the thesis is organised as follows:

- Chapter 2 presents the overview of wireless communication systems, antenna array characteristics, and the fundamentals of the DOA algorithm. The evolution of wireless communication systems is covered including the importance of smart antenna implementation to cater for the need to deliver information in mobile devices. A configuration of the smart antenna system is also presented along with how the system could improve reception of mobile devices. This chapter also introduces the DOA estimation process as an essential component in the signal processing block of smart antenna systems. In addition, the characteristic of the antenna element is discussed and how it could affect the quality of DOA estimation. On top of that, the effect of antenna array geometry on DOA estimation is also discussed. Several configurations of existing antenna array are also presented and compared in terms of their performance in DOA estimation. The final section of this chapter covers the fundamentals of DOA algorithms including how the incoming signals are modelled in order to formulate the direction estimation. Classification of the DOA estimation algorithms is presented and compared in terms of various criteria such as estimation resolution and consistency.

- Chapter 3 presents the design of planar antenna array geometries for azimuth DOA estimation. The focus of this chapter is to address the issues related to azimuth angle estimation such as estimation resolution and estimation error. There are three new planar antenna arrays being proposed, and the performance of each proposed array in DOA estimation is analysed. The first

two proposed antenna arrays are based on circular shape, and the third proposal is made of a combination of several linear arrays. The performance of the proposed antenna arrays on DOA estimation is compared with the existing antenna array configurations in terms of the estimation resolution, estimation error and estimation consistency. In addition, a comparison study between the three proposed arrays is also carried out.

- Chapter 4 presents the DOA estimation when directional antenna is being used to form the antenna array. Firstly, a comparison study of the DOA estimation process between isotropic antenna array and directional antenna array is presented. Secondly, a new algorithm is proposed in order to accommodate the characteristic of the directional antenna element in DOA estimation. The proposed algorithm is then applied on elevation angle estimation using a linear array. Finally, the proposed algorithm is applied on azimuth angle estimation using a semi-circular array.

- Chapter 5 presents a new technique in DOA estimation for directional antenna array. Firstly, the proposed technique is introduced and its application on elevation angle estimation using a linear array is discussed. Secondly, the proposed technique is further applied for azimuth estimation using a semi-circular array.

- Chapter 6 presents the thesis summary and general conclusions. Suggestions for future work are also laid out including short and long term goals.

1.5 List of publications

1. **R. Sanudin**, N.H. Noordin, A.O. El-Rayis, N. Haridas, A.T. Erdogan, T. Arslan, "Analysis of DOA estimation for directional and isotropic antenna arrays", *2011 Loughborough Antennas and Propagation Conference (LAPC)*, Loughborough, UK, pp.1-4, 14-15 Nov. 2011

2. **R. Sanudin**, N.H. Noordin, A.O. El-Rayis, N. Haridas, A.T. Erdogan, T. Arslan, "Capon-like DOA estimation algorithm for directional antenna arrays", *2011 Loughborough Antennas and Propagation Conference (LAPC),* Loughborough, UK, pp.1-4, 14-15 Nov. 2011

3. **R. Sanudin**, A.T. Erdogan, T. Arslan, "Modified linear prediction algorithm with low bias estimator", *IET International Conference on Radar Systems (Radar 2012)*, Glasgow, UK, pp. 1-5, 22-25 Oct. 2012

4. **R. Sanudin**, T. Arslan, "Semi-circular antenna array for azimuth DOA estimation", *2012 Loughborough Antennas and Propagation Conference (LAPC),* Loughborough, UK, pp.1-4, 12-13 Nov. 2012

5. **R. Sanudin**, N.H. Noordin, T. Arslan, "DOA estimation using modified covariance matrix", *2012 Loughborough Antennas and Propagation Conference (LAPC),* Loughborough, UK, pp.1-4, 12-13 Nov. 2012

2 Background

The demand for wireless communication systems has increased rapidly over the last few decades. This is fuelled by a vast supply of interactive content over the internet, affordable mobile devices and broadband packages, and most importantly the fact that it is the reliable wireless communication technology available today. Reliability of the wireless communication system depends heavily on the physical facilities to support the technology such as the base station and server to store the web. Furthermore, the wireless communication system also requires signal processing technology to enable the delivery of content over the wireless network.

This chapter will give an overview of the wireless communication systems and the signal processing technology that enables its functionality. There are three main points being discussed in this chapter. Firstly, the importance of the wireless communication system and its contribution to society is presented. Secondly, the background of antenna array geometry is discussed, which contributes to the performance of signal processing and in turn to the quality of the wireless communication system. Thirdly, the background of the DOA estimation algorithm is presented, one of the components in signal processing techniques for wireless communication.

2.1 Smart Antenna for Wireless Communication System

2.1.1 Mobile Wireless Communication System

Essentially, the main objective of any communication system is to pass on the intended message over its network in the most reliable way. This means the network should be able to minimise the error during transmission and reception. The network is also expected to deliver the information as fast as possible. The communication system has evolved over the past century from the analogue system to the digital communication system.

The wireless communication system can be described by the system block illustrated in Figure 2.1.

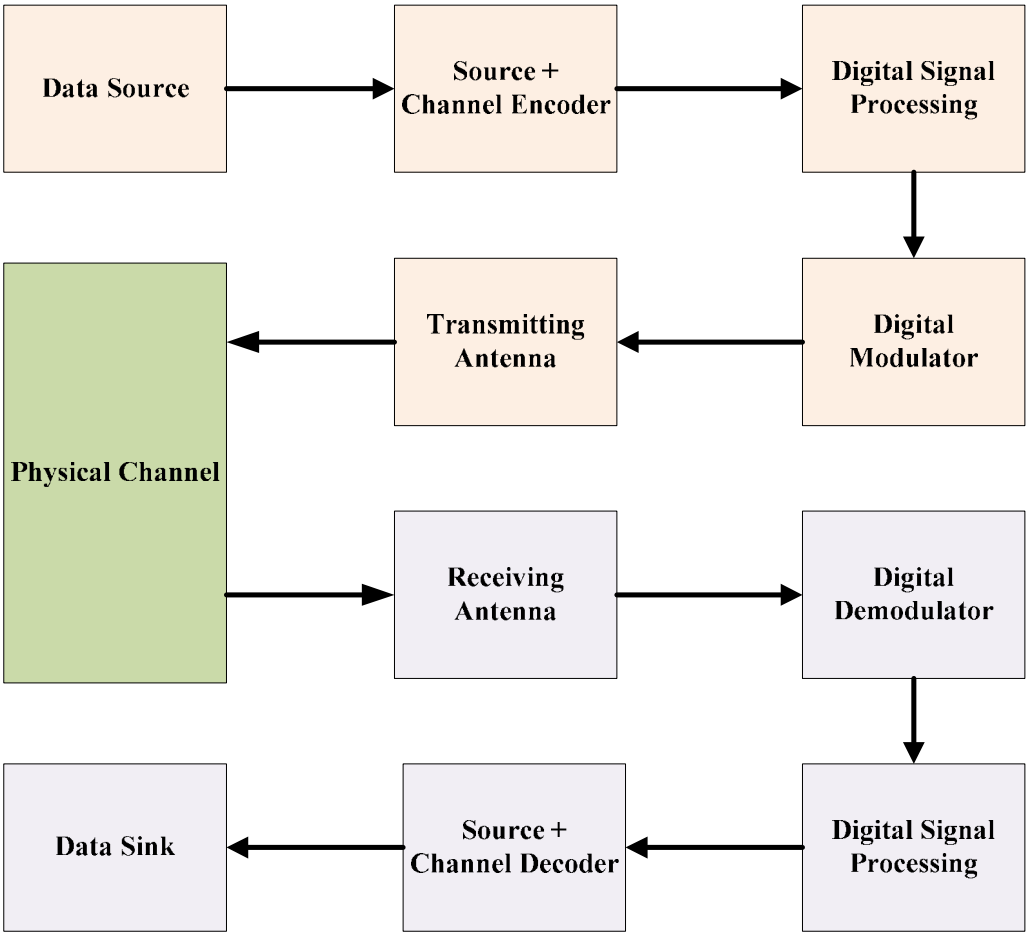

Figure 2.1: System block of wireless communication system [5]

A wireless communication system can be divided into three major blocks; transmission, channel and reception. In general, the transmission and reception blocks are performing the same process but in reverse order.

The transmission channel is susceptible to noise signal and other impairments that could corrupt the transmitted data. Reliability issues in the wireless communication system are closely related to the strength of radio waves that could be captured by the receiver [6]. This is inevitable since the radio waves could be reflected, diffracted, scattered or blocked during the transmission. Degradation of quality occurs because

the receiver experiences difference in attenuation, phase shift and delay of received signal. One phenomenon is that the radio waves can bounce on objects that exist along the transmission path, known as channel multipath fading, which greatly reduces the quality of the received signal [7, 8]. Another phenomenon is when the radio waves are blocked by a topological structure such as buildings or hills, known as shadow fading; this has a larger time-scale variation than multipath fading [9, 10].

In transmission block, a source encoder is used to ensure the channel will maximise the useful information to be sent over the transmission path. This is done by removing all the redundancy that exists in the information data, and hence the channel becomes more efficient [11]. Paired with the channel encoder, the efficiency of data transmission is improved by minimising the data error during transmission. This is made possible by employing error detection and error correction on the encoding process. The purpose of error detection is to find out if the transmitted data has been corrupted by noise in the transmission channel [12]. Error correction, on the other hand, performs a recovery of the original data when any error is detected on the specified received data [13, 14].

A digital signal processing block performs the processing of output from channel encoder for multiple channels of communication. This is done by means of digital beamforming, which maximises transmitted power onto a selected user and at the same time minimises the interference signals [15, 16].

In the modulation block, the process of putting the transmitted data into a carrier signal takes place. In other words, the digital form of transmitted data will be conveyed into another signal that can be physically transmitted in the wireless network. The modulation process will modify frequency, amplitude or phase of the carrier signal to ensure the data can be transmitted [17]. There are several techniques of digital modulation such as amplitude-shift keying, phase-shift keying, and frequency-shift keying.

The modulated signals are then supplied to the transmitter antenna to send the signals over the wireless channel. At the receiver end, the received modulated signal will be

stripped down to its baseband signal. Then the signal processing block will arrange the signal according to each sender. A channel decoder will perform error detection and error correction in order to recover the original data transmitted [11].

2.1.2 Smart Antenna System

The smart antenna system was originally introduced to solve limitations in wireless communication systems, such as a limited user capacity, received signal deterioration due to fading, and inefficient power management [18]. The system is designed in such a way that the user can point its power to a distinct area of intended signals and minimise power on interference signals [19]. The concentration of power on intended signals results in better reception of the audio signal during a voice call or data signal during internet browsing [20]. In addition, battery life can be extended since less power is wasted on interference signal [21]. The construction of the smart antenna system could also be seen as imitation of human audible system as shown in Figure 2.2. In this case, an antenna array acts as a pair of human ears and the signal processing block imitates a human brain to process the received signal.

Suppose the antenna array received one intended signal and an interference signal from different directions simultaneously. The signal processing block would determine the direction of each signal and the antenna array could therefore focus the received power entirely on the direction of the intended signal [22]. This case is similar to human hearing when someone can listen to two speeches simultaneously but still be able to concentrate on the content of the speech they are interested in [2]. This is made possible because the human brain can determine the direction of each speech and make a decision to concentrate only on the desired speech. The listener can also respond to the talker efficiently since the direction of the intended speech is clearly known. The same concept can be applied to mobile devices when listening to several base stations of different mobile service providers simultaneously. The mobile device can distinguish which signal is of the correct service provider and thus lock the received power into the desired direction [23].

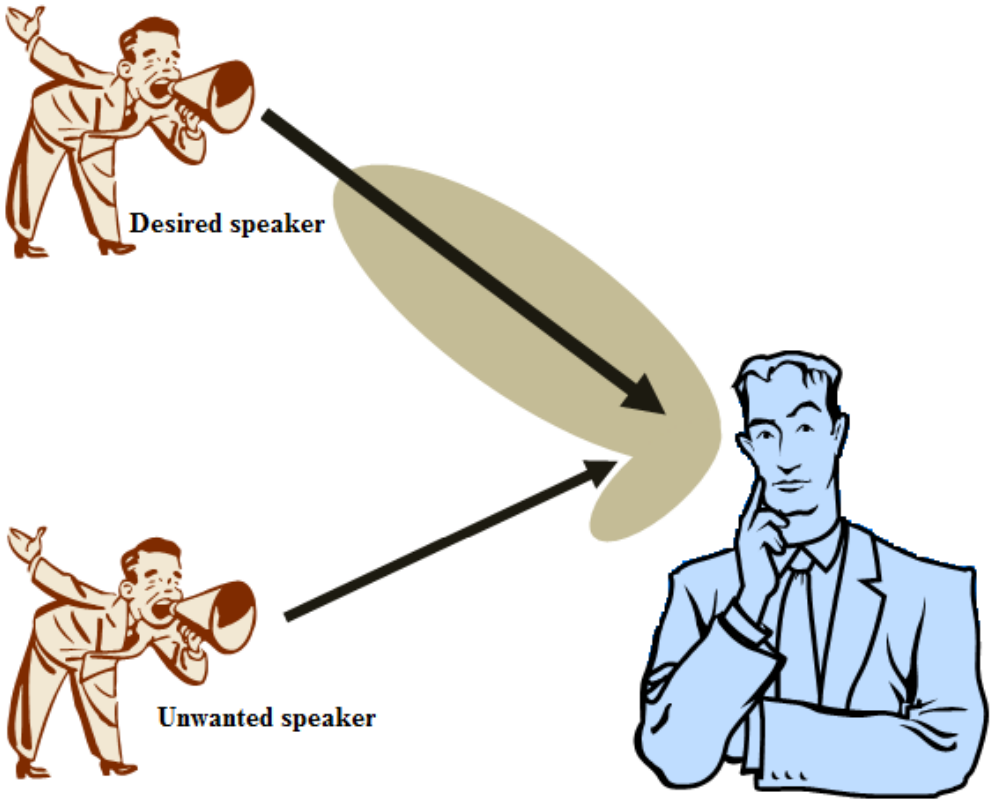

Figure 2.2: Human ear listening to two speeches simultaneously but only concentrating on one speech [2]

2.1.3 Configurations of smart antenna system

In general, the smart antenna can be configured either in switched-beam mode or adaptive mode [11]. In switched beam mode, the target area has been fixed and the direction is pre-determined. During the operation, the received power will be switched to a certain pre-determined area according to the direction of the received signal [24, 25]. The advantage of this approach is that it is easier to implement since the target area can be set offline. However, this approach may produce a low quality received signal since the received signal does not always come from the direction that has the maximum transmitted power [26, 27].

Adaptive mode, on the other hand, offers better flexibility as the antenna beam changes dynamically with respect to the direction of the desired signal [28]. This feature is made possible by assigning a weight to each element so that the antenna

array can focus its power in exact directions. In switched-beam mode, there is a possibility that the interference signal falls within the pre-determined beam that could deteriorate the quality of received signal. However, this problem is eliminated in adaptive mode since the location of both desired and interference signals are kept updated [29]. Figure 2.3 shows the beam pattern of smart antenna systems in both switched-beam and adaptive mode.

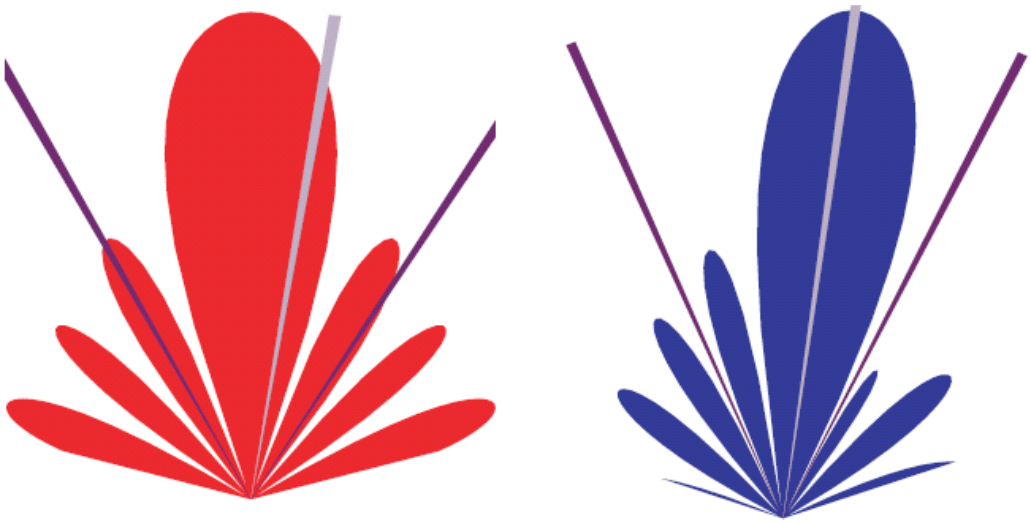

(a) (b)

Figure 2.3: Beam pattern of (a) switched-beam mode and (b) adaptive mode [2]

2.2 Antenna Array Geometry Characteristic

The smart antenna system requires a set of antenna to be arranged in an optimised configuration in order to achieve the functionalities of smart antenna. The arrangement of a group of antenna elements is known as the antenna array. Each configuration of antenna array will determine its property such as aperture, steering vector, gain and phase. This section will present key properties of antenna array and how these properties will affect the performance of DOA estimation.

2.2.1 Array aperture

The size of an antenna array is determined by the array aperture and in turn depends on the number of elements and the element spacing. In addition, the array aperture is also directly proportional to array gain, which means a bigger array will yield higher array gain [4]. The array aperture will increase if either the number of elements or the spacing element is increased [30]. However, increasing the number of elements will increase the computational complexity in array processing and the area occupied. Furthermore, increasing the element spacing increases the chance of having undesired grating lobes, which reduce array power efficiency [31]. Therefore, there needs to be a compromise in adjusting the array aperture in order to optimise the array performance.

In terms of DOA estimation, increasing the number of elements, which also increases the array aperture, will improve the accuracy of estimation [32]. However, for the same number of elements, reducing the element separation will reduce the accuracy of the DOA estimation. This is true especially for conventional DOA algorithms that heavily depend on the array aperture such as a conventional beamformer [33]. The common practice in array processing is to keep the element spacing equal to half of the signal wavelength [34]. This value is big enough to prevent significant grating lobes from existing, and small enough to effect good performance of the DOA estimation algorithm.

Sidelobe control is one of the areas that is being targeted to improve the array aperture. Several techniques have been proposed in sidelobe control such as

amplitude control, phase control [35] and weighting across array aperture [36]. Nevertheless, imposing sidelobe control causes the main beam to reduce and thus no significant improvement can be seen.

2.2.2 Array factor

By definition, array factor is a function of amplitude and phase weights, element placement, and frequency [4]. Array factor is also defined as the response of an array when an incoming signal impinges at a certain angle. When a signal comes at a certain angle, the wave will be received by all elements but at different time. In other words, the adjacent element will receive the signal after a certain amount of delay. The phase difference is important and must be considered when calculating the total array output [2]. Depending on the element positioning, the phase difference is a function of either elevation angle, θ, or azimuth angle, φ, or both. The elevation angle is measured with respect to the *z*-axis whereas the azimuth angle is measured from the *x*-axis as illustrated in Figure 2.4. In general, the array factor is given as follows:

$$AF = \sum_{n=1}^{N} w_n e^{j\psi_n} \tag{2.1}$$

where w_n is the complex weight of element n, ψ is the phase shift between signals from successive array elements, and N is the number of elements. It is obvious from (2.1) that the array factor heavily depends on the array configuration. Different array configurations will produce unique array factors. The next section will present further discussion of the array factor.

It is worth mentioning that array radiation pattern can be changed by manipulating the array factor. For example, the main beam of the array can be moved or steered by introducing phase shift to the element phase [37, 38]. The phase steering of the main beam, however, will cause the main beam to change its pointing direction as well. This feature enables the focus of the array main beam to change without moving the array [39, 40].

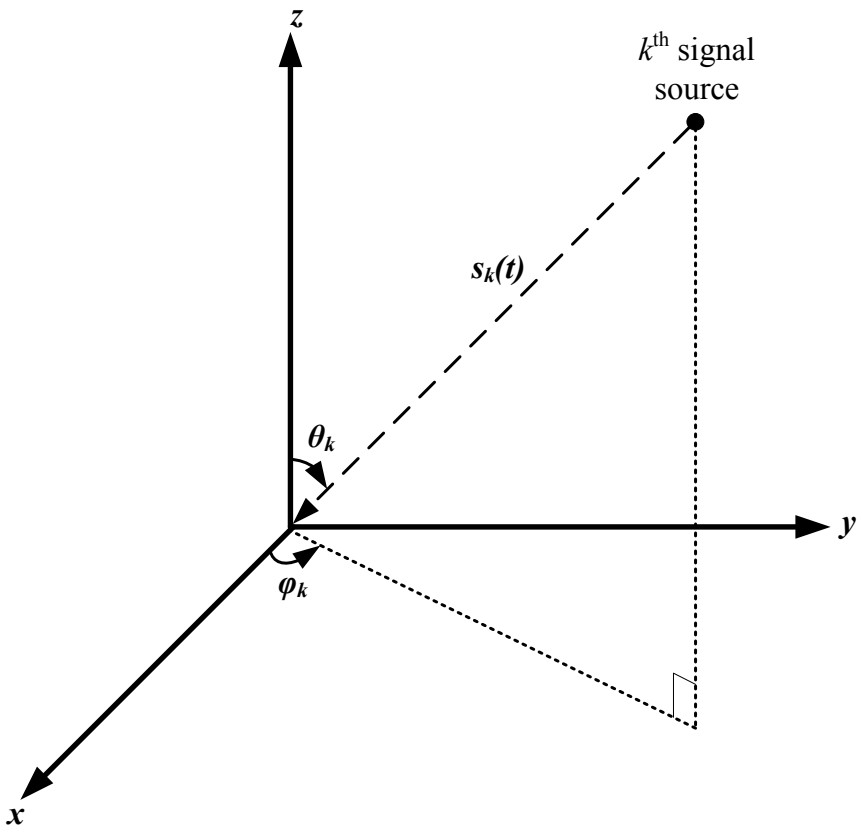

Figure 2.4: Definition of elevation angle, θ, and azimuth angle, φ [34]

2.2.3 Existing antenna array geometries

2.2.3.1 Linear antenna array

Linear antenna array is an array composed of several array elements aligned in a straight line on a plane, as shown in Figure 2.5. In general, the linear antenna array is easy to analyse compared with other array geometries due to its simple structure. This array configuration is also normally used as a starting point to demonstrate the functionality of a DOA algorithm [41]. However, there are two main issues in linear array that limits its usage for DOA estimation. Firstly, the capability of linear antenna array is limited to one-dimensional (1D) DOA estimation, which means it only could estimate the elevation angle, θ, of incoming signals [2, 34]. This limitation is unattractive for implementation in practical purposes since the direction

of incoming signals is defined by both azimuth, φ, and elevation angles, θ. Secondly, the total range of azimuth angle that can be estimated by the linear antenna array, which is limited to 180°, lies within (-90°<θ<90°), which represents half of the *x-y* plane. Nevertheless, it has been shown that the useful angle of coverage is not more than 120° due to deterioration of beam sharpness when |θ|>60° [42]. As a result, the accuracy of DOA estimation is greatly affected when the incoming signal is within the range of end-fire (70°<|θ|<90°).

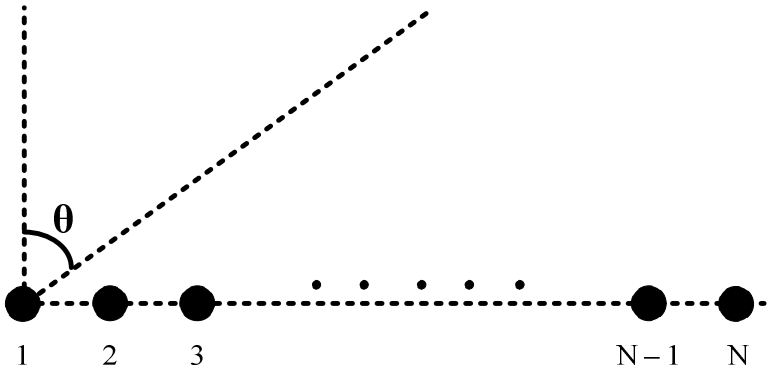

Figure 2.5: Linear antenna array

2.2.3.2 Rectangular and triangular antenna array

The need for two-dimensional (2D) DOA estimation has led to further development of array geometries. The 2D DOA estimation refers to estimation of both the elevation and azimuth angles simultaneously. There are three 'classic' array geometries being commonly used for 2D DOA estimation: namely triangular, rectangular, and circular arrays. Both triangular and rectangular antenna arrays are a combination of the linear arrays that resemble the shape of the triangle and rectangle respectively, as shown in Figure 2.6. The triangular and rectangular arrays offer a quick solution to 2D DOA estimation although they require a higher number of elements and computational load than the linear antenna arrays [43].

However, this additional cost is considered inevitable because the complexity is associated with simultaneous estimation of both azimuth and elevation angles. Furthermore, given the same number of elements, the linear antenna array would

never achieve the same estimation capability as either triangular or rectangular antenna arrays [34]. In phased antenna array design, the triangular antenna array is preferable to the rectangular antenna array since it can suppress the grating lobes effectively [44]. On the other hand, the rectangular array is able to maintain sharpness of its main beam in both broadside and endfire directions [45]. This advantage results in minimum discrepancy between estimated and true DOA of signal sources. However, both triangular and rectangular antenna arrays suffer from non uniform beam space due to their edge element that leads to poor DOA estimation [46].

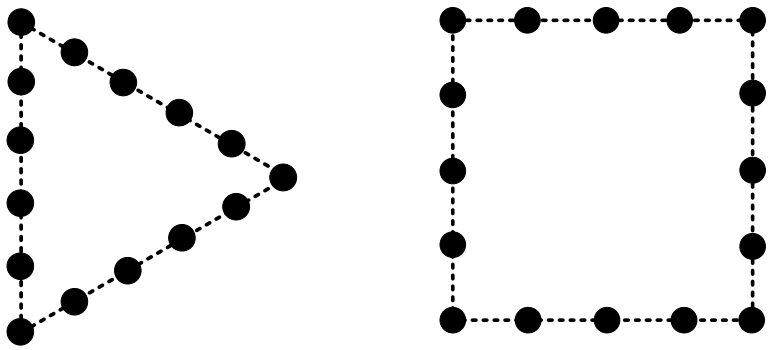

(a) (b)

Figure 2.6: Structure of (a) triangular and (b) rectangular antenna arrays

2.2.3.3 Circular antenna array

The circular antenna array offers unique features among antenna array configurations due to the symmetry of its design as shown in Figure 2.7. A notable advantage of the circular antenna array is that it can provide a uniform beam space since it does not have an edge element [46].

The symmetric property of the circular antenna array could also be exploited to improve DOA estimation by constructing the covariance matrix in the form of a Hermitian persymmetric matrix. The Hermitian persymmetric matrix form could improve DOA estimation result especially in low signal-to-noise ratio (SNR) and a

small number of snapshots [47]. Another study also found out that the circular antenna array produced better spatial resolution and narrower main beam compared with the rectangular antenna array [48]. An experimental work on mobile relay station using circular antenna array shows that a significant low estimation error, which is about 1°, can be achieved [49, 50]. Those advantages are very useful for smart antenna application. This observation is supported by the uniqueness in the circular antenna array, which could cover the whole azimuth angle in a uniform manner.

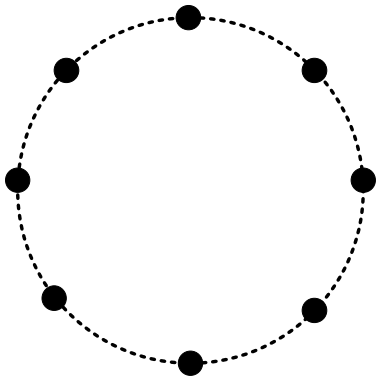

Figure 2.7: Structure of circular antenna array

2.2.3.4 V-shape and Y-shape antenna array

The most recent array geometries for 2D DOA estimation are V-shape antenna array, Y-shape antenna array, and L-shape antenna array. Recent development of antenna array design has been motivated to improve the estimation error and resolution of classic array geometries.

V-shape antenna array is considered as one of the most promising arrays for 2D DOA estimation based on its excellent performance [51, 52]. As shown in Figure 2.8, the V-shape antenna array is made of two linear antenna arrays separated by a pre-defined angle, known as V-angle, between them. Given a particular range of V-angle, the V-shape array could produce lower estimation error than the circular antenna array [51]. The same observation is also pointed out in [52], in which smaller estimation error is produced in the V-shape antenna array compared with the

circular antenna array for the same number of elements and element separation. However, the values of V-angle have a significant effect on the steering vector, and hence the quality of estimation results. Therefore, given a number of elements, the V-angle should be optimised in order to achieve an excellent estimation.

Another planar antenna array, known as Y-shape antenna array, has also been reported in several publications. As depicted in Figure 2.8, the structure of the Y-shape is a combination of three linear antenna arrays on the same plane separated by 60° between them. This structure makes the Y-shape have a balanced-symmetric property. The Y-shape antenna array is noted to have the best detection threshold, comparable with the circular antenna array [53]. A practical array design of quarter-wave monopole has also been proposed utilising the Y-shape antenna array, which produced an estimation error below 2° [54].

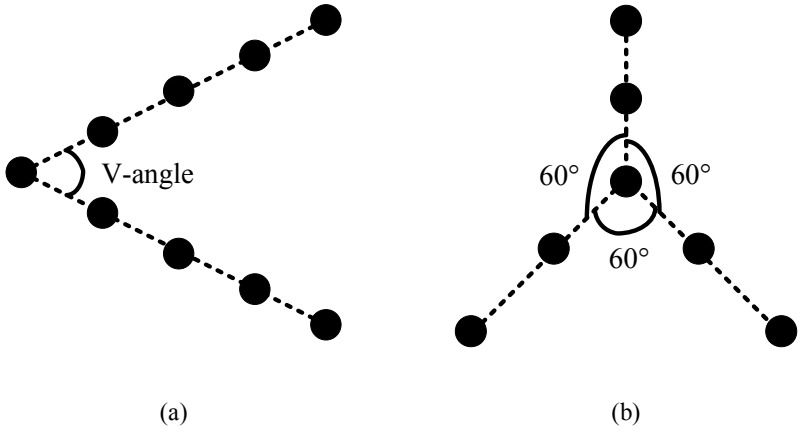

Figure 2.8: Structure of (a) V-shape and (b) Y-shape antenna array

2.2.3.5 L-shape antenna array

The performance of the L-shape antenna array in 2D DOA estimation has been discussed in several literatures. There are three variations of L-shape antenna array structure mentioned in the literature, as illustrated in Figure 2.9. The L-shape antenna array has been recognised as an excellent choice for 2D DOA estimation since its introduction in 1991 by Hua [55]. In this work, the L-shape antenna array was shown to have about 37% better accuracy than cross array. Joint estimation of both azimuth and elevation angle estimation with high resolution has been proposed in the L-shape

antenna array [56, 57]. These results suggest that the L-shape array could achieve estimation resolution as high as 2°.

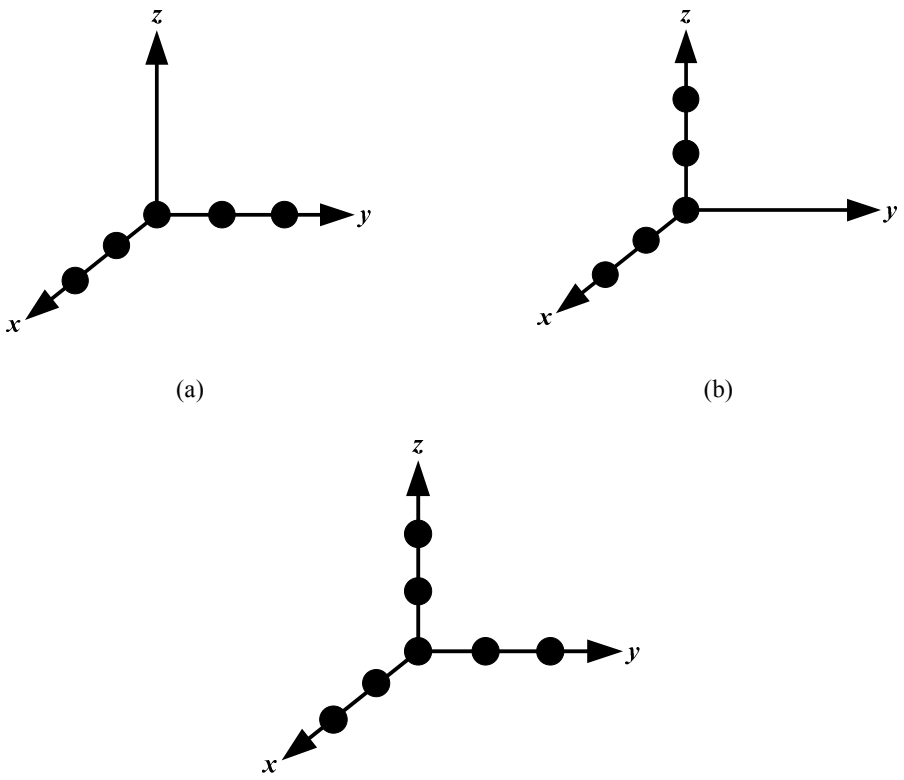

Figure 2.9: Variation of L-shape array structure (a) L-shape on x-y plane (b) L-shape on x-z plane (c) Double L-shape

Joint estimation using the L-shape antenna array with low computational complexity have also been reported [58-60]. The results in these works yield lower estimation error compared with the rectangular array for the same number of elements. The excellent performance is due to the fast convergence to achieve accurate angle estimation.

Another variation of the L-shape antenna array, known as double L-shape antenna array, has been introduced by Tayem et. al. [61]. The double L-shape antenna array helps to eliminate the problem of estimation failure in the L-shape antenna array for azimuth angle. The only notable drawback of the double L-shape antenna array is

that it needs 30% more elements than the L-shape antenna array. The additional elements in the double L-shape antenna array also leads to higher computational load compared to the L-shape array. The DOA estimation using the double L-shape array could also be improved by using the extended correlation matrix [62]. The proposed technique modifies the calculation of covariance matrix by adding a matrix of incoming signal DOA. The proposed method helps to reduce the estimation error in low SNR level on top of eliminating the estimation failure.

2.2.3.6 Comparison of antenna array geometry

There are seven antenna array geometries that have been discussed in this section. Table 2.1 shows the comparison of all the array geometries.

Table 2.1: Comparison of antenna array configuration

Antenna array geometry	Advantage	Drawback
Linear	1. Simple configuration 2. Easy to analyse.	Limited to elevation angle estimation.
Triangular	1. Simultaneous elevation and azimuth angles estimation. 2. Effective to suppress the grating lobes.	Poorer estimation than circular array due to non uniform main beam.
Rectangular	1. Simultaneous elevation and azimuth angle estimation. 2. Maintains sharpness of its main beam in both broadside and endfire directions.	Poorer estimation than circular array due to non uniform main beam.

Circular	1. Simultaneous elevation and azimuth angle estimation. 2. Better estimation resolution than rectangular and triangular arrays due to uniform beam space. 3. Narrower main beam than rectangular array.	Low resolution for elevation angle estimation.
V-shape	1. Simultaneous elevation and azimuth angle estimation. 2. Lower estimation error than the circular array. 3. Better estimation than rectangular array due to flexible V-angle.	An optimum value of V-angle is needed to achieve an accurate estimation.
Y-shape	1. Simultaneous elevation and azimuth angle estimation. 2. Has symmetric geometry structure.	Poor estimation at end-fire of elevation angle.
L-shape	1. Simultaneous elevation and azimuth angle estimation. 2. High resolution for azimuth estimation. 3. Produces lower estimation error than rectangular array.	Low estimation consistency than circular array.

2.2.4 Mutual coupling compensation methods

The ideal condition in DOA estimation assumes that the elements of an array are isotropic, which ignores the effect of the mutual coupling. However, in a practical application the array is affected by mismatch array manifold due to physical conditions such as mutual coupling [63, 64], phase uncertainties [65, 66], and sensor positioning perturbation [67].

Several methods have been proposed to improve the DOA estimation with the presence of mutual coupling. The main objective of compensation methods is to ensure that the effect of mutual coupling will be minimised in the performance of the DOA algorithm. This, in turn, will ensure that the estimation of direction of the incoming signal will be as accurate as possible. The mutual coupling compensation methods can be classified into two main categories; offline and online compensation methods. In general, offline methods estimate coupling coefficients before the array operates [68]. In contrast, online methods calculate the coupling coefficients during the operation of the array and update the values continuously [69].

2.2.4.1 Offline methods

Method of moment is one of offline methods being proposed to calculate and compensate for the mutual coupling effect in array processing [70, 71]. However, this method requires a priori knowledge of incoming signals such as the exact number of signals and the DOA. A maximum likelihood based method is also being proposed, one that exploits the source calibration [72]. It is very effective for determining the coupling coefficients, and could be extended to find gain/phase uncertainties and sensor positioning errors. Another method being proposed that also exploits source calibration is for known location in [73]. The drawback of both methods in [72, 73] is that the source calibration is difficult in practical applications.

2.2.4.2 Online Calibration

Unlike to offline methods, online methods are more adaptive to any changes since the calculation is performed during the array operation. The advantage of auto calibration is that it does not require source calibration and thus it could be done

offline. Auto-calibration is being proposed in [74, 75] which uses an iterative process to calculate both the DOA and coupling coefficients. Nevertheless, this method is not preferable in a real-time system since it involves many parameters and thus has high computational complexity [76, 77]. Furthermore, it has been reported that this method could take a considerable amount of time in order for the DOA calculation to converge [77]. Another method has been proposed to address the problem of computational complexity [78, 79]. This method is designed specifically for linear array [78] and circular array [79]. The simplicity in computation comes from the fact that the mutual coupling is inversely proportional to the element spacing in the array. In other words, the mutual coupling will reduce as the element is further apart. This fact leads to a simpler representation of the mutual coupling matrix since the mutual coupling is considered to be zero after several element spacing.

2.3 Fundamentals of DOA Estimation

One of the main functions in the signal processing block of the smart antenna system is to estimate the direction of the incoming signal. The DOA estimation will be used to feed the beamformer to steer the antenna beam in the desired signal direction. Thus, the intelligence of the smart antenna system lies in the accuracy of the DOA estimation, which determines if the system is able to maximise the received signal in the desired direction. The DOA estimation is made possible by DOA algorithms, the mathematical model that describes the received signal and antenna array output. In general, the DOA algorithms can be divided into three types; beamforming, subspace-based and maximum likelihood. These algorithms will be discussed in detail in section 2.3.4. There are several parameters used to gauge the performance of DOA algorithms such as estimation error, estimation resolution, and consistency of estimation.

2.3.1 Data model

In this section, the data model of DOA estimation used throughout this thesis will be presented. The covariance matrix of DOA estimation is discussed followed by an

overview of the existing DOA estimation algorithms. Finally, this section discusses the parameters that are used to measure the performance of DOA estimation algorithms.

There are several assumptions being made in the data model in order to obtain the DOA estimation result throughout this thesis. These assumptions are used throughout the thesis unless stated otherwise. The assumptions are as follow:

a) Far-field sources

There are *K* signal sources coming far-field points towards the antenna array. The source location is far enough in such a way that the wavefront of each source coming to each element is planar and equal direction of propagation. The assumption is valid if the distance between signal sources and antenna array is more than $\frac{2D^2}{\lambda}$, where D is the dimension of array and λ is the wavelength of incoming signal.

b) Narrowband signals

There are *K* signals coming from *K* sources with the same carrier frequency, f_c, and therefore the incoming signal of amplitude α and phase β can be described as:

$$s(t) = \alpha(t)\cos[2\pi f_c t + \beta(t)] \tag{2.2}$$

The narrowband signal has amplitude and phase which vary very slowly with respect to τ, time for incoming signal to propagate from one element to another. Thus, the complex envelope or phasor of incoming signals can be defined as:

$$s^{env}(t) = \alpha(t)e^{j\beta t} = \alpha(t)e^{j2\pi f_c t} \tag{2.3}$$

c) Noise signal

The noise signal is assumed to be a complex zero white Gaussian process, have zero mean and variance σ^2, and to be uncorrelated with the signal.

d) Isotropic elements

There are *N* isotropic elements in the antenna array, where each element has a gain of one and mutual coupling between the elements is zero.

2.3.2 Steering vector

Most DOA estimation algorithms require knowledge of the response of each antenna element when a signal is impinging the array. The response of the element is defined by a parameter known as steering vector. The steering vector depends heavily on the array structure and hence the array factor. This section will present a simple example of how a steering vector is determined.

Suppose that a signal arrives on a two-element linear array at an elevation angle θ. Assuming the signal source is in the far-field region, the signal would be considered a plane wave as shown in Figure 2.10. Since the signal wave arrives at an angle relative to the array plane, elements 1 and 2 will receive the signal at different time. Assuming element 1 as the reference, element 2 will receive the signal wave after delay of [2]:

$$\Delta\tau = \frac{d\sin\theta_s}{v_0} \tag{2.4}$$

Where *d* is the spacing between element 1 and 2, and v_0 is the signal velocity. The phase shift, ψ, can be expressed in term of the phase shift by using the carrier frequency, f_c, of the incoming signal [2]:

$$\Delta\psi = \frac{2\pi d\sin\theta_s}{\lambda_c} \tag{2.5}$$

where λ_c is the wavelength of carrier signal corresponding to carrier frequency. The equation (2.5) represents the output of element 2 with respect to element 1. In DOA estimation, (2.5) is also known as steering vector for this array.

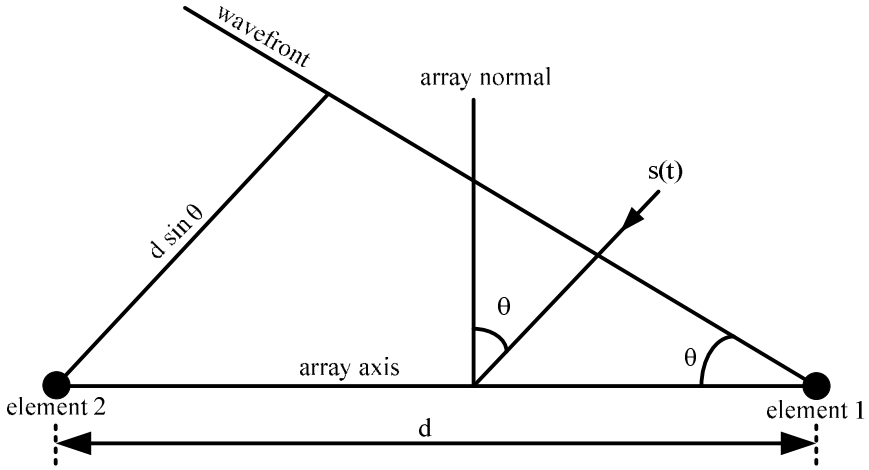

Figure 2.10: Signal arrives at angle θ on a linear array [2]

2.3.3 Covariance matrix

In general, covariance matrix represents the cross covariance of noise-corrupted signals that have impinged on the antenna array. The covariance matrix is an essential component in calculating the spatial power spectrum in order to estimate the DOA [2, 34]. In this section, the process of obtaining the covariance matrix from the antenna array output will be presented.

Suppose that there are *K* signals impinging on *N* element of a linear array as shown in Figure 2.11. Using the assumption of the data model described in 2.3.1, the received signal of all antenna elements can be given as [2]:

$$\mathbf{x}(t) = \sum_{k=1}^{K} \mathbf{a}(\theta_k) s_k(t) + \mathbf{n}(t) \tag{2.6}$$

where $\mathbf{x}(t)$ is the complex baseband received signal at the antenna array at time *t*, $s_k(t)$ is the signal coming from k^{th} sources at direction of θ_k, $\mathbf{a}(\theta_k)$ is the steering vector at direction of θ_k, and $\mathbf{n}(t)$ is the noise signal.

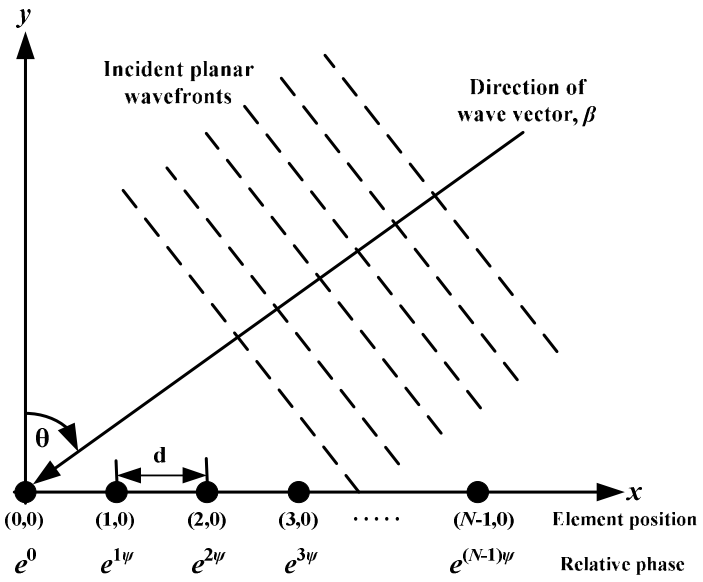

Figure 2.11: Steering vector of a linear array [2]

Equation (2.6) can be rewritten in vector form [2]:

$$x(t) = \begin{bmatrix} \mathbf{a}(\theta_1) & \mathbf{a}(\theta_2) & \cdots & \mathbf{a}(\theta_K) \end{bmatrix} \begin{bmatrix} s_1(t) \\ s_2(t) \\ \vdots \\ s_K(t) \end{bmatrix} + \mathbf{n}(t) \tag{2.7}$$

The first vector in (2.7) represents the array manifold of the linear array, which represents the response of each array element with respect to each incoming signal. It implies that the array manifold would have a total of $N \times K$ array response or steering vector. Each of the array manifold elements can be represented by the following:

$$\mathbf{a}(\theta_k) = \begin{bmatrix} 1 \\ e^{j\frac{2\pi d \sin\theta}{\lambda}} \\ e^{j\frac{2\pi(2d)\sin\theta}{\lambda}} \\ \vdots \\ e^{j\frac{2\pi(nd)\sin\theta}{\lambda}} \end{bmatrix} \tag{2.8}$$

It is also worth noting that the linear array covers π radian of elevation angle in the range of $-\frac{\pi}{2} < \theta < \frac{\pi}{2}$. In general, (2.6) – (2.8) complete the definition of the received signal, which includes the signal direction that needs to be estimated.

The received signal covariance matrix is calculated by finding expectation of multiplication of the received signal and its Hermitian as shown in the following:

$$R = E\left[\mathbf{x}(t)\mathbf{x}(t)^H\right] \tag{2.9}$$

where $(\cdot)^H$ and $E[\cdot]$ denote the Hermitian, and mean operation respectively. However, for a known limited number of signal samples or snapshots, (2.9) can be approximated as

$$R = \frac{1}{L}\sum_{l=1}^{L}\mathbf{x}(t)\mathbf{x}^H(t) \tag{2.10}$$

where L is the number of signal samples or snapshots. The expression of the covariance matrix in (2.10) is used in the DOA algorithm to find the estimation of DOA.

2.3.4 DOA estimation algorithm

In smart antenna systems, DOA estimation is an essential process for determining the direction of incoming signals and thus directing the beam of the antenna array towards the estimated direction. There are a large of number of DOA algorithms that have been proposed for this and they can be classified into three categories; beamforming, subspace-based and maximum likelihood. Each category differs in terms of computational complexity, spectral resolution and accuracy. Algorithms in

the beamforming category are straightforward and require low computation complexity. Nevertheless, algorithms in this category have low resolution and that leads to the introduction of algorithms in subspace-based category. Algorithms in the subspace-based category offer superior accuracy and high resolution estimation compared with algorithms in the beamforming category. However, the performance of algorithms this category heavily depends on the uncorrelated signal environment as well as high computational complexity. Furthermore, when the correlated signals exist due to multipath fading, the performance of algorithms in the subspace-based category will deteriorate significantly. In order to reduce the computational complexity, algorithms in the beamforming category can be applied but with the cost of lower resolution.

2.3.4.1 Beamforming category

In the beamforming category, the DOA is estimated whenever a maximum power is observed in the spatial power spectrum. The algorithm models the array to be steered across the entire angle range and power is measured at each steered angle [80]. Tabulation of power readings for the angle range will show the pattern of power distribution and the maximum power angle will be taken as the DOA for the incoming signal. The steering process would require knowledge of the array manifold for that particular array. In addition, during the steering process, the array beam will be likely to change its pattern. Therefore, in order to have a linear combination of array output for the whole steering process, a weight **w** is needed. The output of the array is given as [34]:

$$\mathbf{y} = \mathbf{w}^H \mathbf{x}(t) \tag{2.11}$$

Using the total output in (2.11), the average power for a limited number of snapshots is given as [34]:

$$P = \frac{1}{L}\sum_{l=1}^{L} |y(t_l)|^2 = \frac{1}{L}\sum_{l=1}^{L} \mathbf{w}(t_l)^H R\mathbf{w}(t_l)$$

$$P = \mathbf{w}^H R\mathbf{w} \tag{2.12}$$

The first algorithm for DOA estimation is known as a conventional beamformer or Bartlett algorithm [81]. In this algorithm, the weight **w** is set to be equal to the steering vector, or $\mathbf{w} = \mathbf{a}(\theta)$. In a linear array, for example, the weight **w** is given as [34]:

$$a(\theta_k) = \begin{bmatrix} 1 \\ e^{j\frac{2\pi d \sin\theta_k}{\lambda}} \\ \vdots \\ e^{j\frac{2\pi(N-1)d \sin\theta_k}{\lambda}} \end{bmatrix} \tag{2.13}$$

Therefore, the spatial power spectrum of the Bartlett algorithm in (2.12) can be expressed using the value of **w** given in (2.13) to obtain the following [34]:

$$P_B(\theta) = \mathbf{a}(\theta)^H \mathbf{R}\ \mathbf{a}(\theta) \tag{2.14}$$

For each direction of elevation angle θ, the power will be measured and then the power readings tabulated against θ. The maximum power will be observed at the direction of k^{th} signal source, or when $\theta = \theta_k$. This happens because the weight **w** aligns the phases of all signal outputs from each element and adds constructively. This algorithm is rather simple to implement, however, it lacks estimation resolution when compared to other algorithms. The only way to increase the resolution of the Bartlett algorithm is to have more antenna elements in the array [81]. However, having more elements means a larger area is required, which is not desirable in mobile devices due to their small size.

Another method in the beamforming category, known as the Capon algorithm, is proposed to overcome the drawbacks of a conventional beamformer [82]. The estimation method being proposed is forming the beam in the looking direction and putting a null on all other directions simultaneously. This is done by minimising the output power and maintaining unity gain in the looking direction. This condition can be described by the following constraint:

$$\min P(\mathbf{w}) \quad subject \quad to \quad \mathbf{w}^H \mathbf{a}(\theta) = 1 \tag{2.15}$$

The constraint shows that the signal in the looking direction will remain undistorted when the output power is being minimised. Therefore, the weight **w** and power spectrum can be calculated using the given constraint in (2.15) as given in (2.16) and (2.17) respectively [81]:

$$\mathbf{w}_{Capon} = \frac{\mathbf{R}^{-1}\mathbf{a}(\theta)}{\mathbf{a}(\theta)^H \mathbf{R}^{-1}\mathbf{a}(\theta)} \tag{2.16}$$

$$P_{Capon} = \frac{1}{\mathbf{a}(\theta)^H \mathbf{R}^{-1}\mathbf{a}(\theta)} \tag{2.17}$$

The improvement obtained from the Capon algorithm is a better estimation resolution compared with the Bartlett algorithm. However, the drawback of the Capon algorithm lies in its higher computational complexity than the Bartlett algorithm, and it cannot work for correlated signals. Since the Capon algorithm requires an inverse covariance matrix calculation in DOA estimation, the computational complexity will increase as the number of elements increases. The Capon algorithm also fails to work with correlated signals since the covariance matrix will become singular, and therefore the inverse covariance matrix cannot be determined [34]. The implementation of Bartlett and Capon algorithm is shown in Appendix A and B respectively.

2.3.4.2 Subspace-based category

In the subspace-based category, all the algorithms are utilising the eigen decomposition process of the covariance matrix [83]. In general, the covariance matrix can be partitioned into two subspaces, known as the signal subspace and the noise subspace. These subspaces can be found by performing eigen decomposition operations, where a set of eigenvalues and their eigenvectors are formed. The signal subspace is defined by eigenvector and associated with smaller eigenvalue whereas the noise subspace is defined by eigenvector associated with larger eigenvalue. The

most popular algorithm in the subspace-based category is Multiple Signal Classification (MUSIC) [84].

The essence of the MUSIC algorithm is to find the eigenvalues λ_n and their associated eigenvector $\mathbf{e}_n$ through eigen decomposition operation on the covariance matrix. The covariance matrix can be rewritten as [2]:

$$\mathbf{R} = \sum_{n=1}^{N} \lambda_n \mathbf{e}_n \mathbf{e}_n^H = \mathbf{E}_s \mathbf{\Lambda}_s \mathbf{E}_s^H + \mathbf{E}_n \mathbf{\Lambda}_n \mathbf{E}_n^H \tag{2.18}$$

where $\mathbf{E}_s = (\mathbf{e}_1, \mathbf{e}_2, \ldots, \mathbf{e}_K)$, $\mathbf{E}_n = (\mathbf{e}_{K+1}, \mathbf{e}_{K+2}, \ldots, \mathbf{e}_N)$, $\mathbf{\Lambda}_s = (\lambda_1, \lambda_2, \ldots, \lambda_K)$ and $\mathbf{\Lambda}_n = (\lambda_{K+1}, \lambda_{K+2}, \ldots, \lambda_N)$ represents the eigenvector of signal subspace, eigenvector of noise subspace, eigenvalue of signal subspace and eigenvalue of noise subspace respectively. Both vectors $\mathbf{E}_s$ and $\mathbf{E}_n$ also define the signal subspace and noise subspace respectively. DOA estimation processes in the MUSIC algorithm are based on the premise that all the steering vectors of signal DOA lie in the signal subspace. Since the signal subspace is orthogonal to noise subspace, all the steering vectors of signal DOA are orthogonal to noise subspace as well. Therefore, when the elevation angle equals the k^{th} signal DOA ($\theta = \theta_k$), it will minimise the cost function $\mathbf{a}(\theta)^H \mathbf{E}_n \mathbf{E}_n^H \mathbf{a}(\theta)$. At this point, a maximum power will be observed in the spatial power spectrum. Thus, the spatial power spectrum of MUSIC is given as:

$$P_{MUSIC} = \frac{1}{\mathbf{a}(\theta)^H \mathbf{E}_n \mathbf{E}_n^H \mathbf{a}(\theta)} \tag{2.19}$$

The signal DOA can be estimated by finding the peak in the spatial power spectrum. It is also expected that the same number of peaks would match the corresponding number of signal DOA. A clear advantage of the MUSIC algorithm is the high resolution estimation; this means it could distinguish DOA for closely spaced signals [83]. However, MUSIC has high computational complexity since it requires simultaneous search of DOA. Furthermore, MUSIC also requires knowledge of the exact number of incoming signals, which is not always the case in practical

applications [85]. The implementation of the MUSIC algorithm is shown in Appendix C.

2.3.4.3 Maximum likelihood

The third category of DOA estimation is maximum likelihood (ML) techniques, which exploit the statistical properties of received signals [80, 86]. This is not popular in system implementation though, due to its very high computational complexity. Nevertheless, the results using this technique produce the most accurate estimation and outperform other DOA estimators. The approach taken in ML is to reconstruct original data from the received signal $\mathbf{x}(t)$ using only the desired signals.

The reconstruction takes place by subtracting the estimate of the desired signal component $\hat{\mathbf{A}}(\theta)\hat{\mathbf{s}}(t)$ from the received signal $\mathbf{x}(t)$. The residual of $\left|\mathbf{x}(t)-\hat{\mathbf{A}}(\theta)\hat{\mathbf{s}}(t)\right|$ represents noise and interference signals. An extremely small value of the residual will reflect that the estimate of $\hat{\theta}$ and $\hat{\mathbf{s}}(t)$ are close enough to the exact values of θ and $\mathbf{s}(t)$. Therefore, it is desirable to minimise the cost function $\left|\mathbf{x}(t)-\hat{\mathbf{A}}(\theta)\hat{\mathbf{s}}(t)\right|$ in order to have an accurate estimation of both $\hat{\theta}$ and $\hat{\mathbf{s}}(t)$. The approach can be represented as the following [34]:

$$\min\left\langle\left\|\mathbf{x}(t)-\hat{\mathbf{A}}(\theta)\hat{\mathbf{s}}(t)\right\|^2\right\rangle \tag{2.20}$$

The desired signal can be expressed using the least square approach:

$$\hat{\mathbf{s}}(t)=\left(\mathbf{A}^H(\theta)\mathbf{A}(\theta)\right)^{-1}\mathbf{A}^H(\theta)\mathbf{x}(t_n)=\mathbf{w}^H\mathbf{x}(t_n) \tag{2.21}$$

Using the expression of $\hat{\mathbf{s}}(t)$ in (2.21) to substitute in the residual and minimise (2.20) will yield estimates of $\hat{\theta}$:

$$\mathbf{P}(\theta)=\mathbf{A}(\theta)\left(\mathbf{A}^H(\theta)\mathbf{A}(\theta)\right)^{-1}\mathbf{A}^H(\theta) \tag{2.22}$$

If the estimated value of $\hat{\theta}$ from (2.22) is the exact solution, then the reconstructed data will be given as:

$$\begin{aligned}\mathbf{X}(n)-\mathbf{A}(\theta)\mathbf{S}(n) &= \mathbf{X}(n)-\mathbf{P}(\theta)\mathbf{X}(n)\\ &= \left(\mathbf{A}(\theta)\mathbf{S}(n)+\mathbf{N}\right)-\left(\mathbf{A}(\theta)\mathbf{S}(n)+\mathbf{P}(\theta)\mathbf{N}\right)\\ &= \left(\mathbf{I}-\mathbf{P}(\theta)\right)\mathbf{N}\end{aligned} \tag{2.23}$$

The solution given in (2.23) is at the minimum value of the residual provided that the choice of $\hat{\theta} \cong \theta$ and the average power represents the power of the noise signal.

2.3.4.4 Comparison of DOA algorithms

There are three categories of DOA algorithm that have been discussed in this section. Table 2.2 shows the comparison of DOA algorithms in terms of their complexity, estimation resolution, estimation error, and estimation consistency [80, 87].

Table 2.2: Comparison of DOA algorithms

DOA performance parameter	DOA algorithm category		
	Beamforming	Subspace-based	Maximum likelihood
Computational complexity	The least complexity	More intensive than beamforming	The most intensive, required large samples
Estimation resolution	The worst resolution	The best resolution	Comparable with subspace-based
Estimation error	Comparable with subspace-based	The lowest error	Significantly large for finite sample
Estimation consistency	The best consistency	Inconsistent	Lower consistency than beamforming

2.4 Summary

This chapter has presented three sections covering the background information for this thesis. In the first section, the technology of wireless communication system was discussed, including the operation of the system. There are several shortcomings in wireless communication systems, such as a limited user capacity and received signal deterioration. This is where a smart antenna can mitigate these shortcomings. The ability of a smart antenna to concentrate its power on a narrow targeted area helps to improve received signals as well as increase battery life. Depending on the system complexity and performance, the smart antenna could be configured in either switched-beam or adaptive mode. The switched-beam mode offers simpler system implementation but the adaptive mode provides superior performance in a dynamic environment.

The next section discussed the array geometry configuration and its importance in DOA estimation. There are two factors in array geometry that determine the estimation results; the array aperture and array factor. The array aperture affects the array size and is also directly proportional to the number of elements and element spacing. It has also been pointed out that as the array aperture increases, the accuracy of DOA estimation will improve. The array factor describes the array response when there is a signal impinging at a certain angle. The response includes the amplitude, phase, element placement and frequency of the incoming signal. Since the array factor depends on the element positioning in an array, the configuration of an array will define a unique array factor. The importance of array factor is considered very high, to the extent that it could be used to change the array radiation pattern. In this section, classification of existing antenna arrays in the literature was also discussed. In general, antenna arrays can be classified as linear and planar arrays. Linear arrays are the basic structure of an antenna array and easier to analyse than other array structures. However, the linear arrays' capability is limited to one-dimensional DOA estimation, which means it can only estimate the elevation angle. This limitation is solved by using the planar arrays where both azimuth and elevation angles can be estimated simultaneously.

The final section in this chapter presented the fundamentals of DOA estimation. Assumptions that are being used in this thesis for DOA estimation were discussed, including signal source, noise signal and antenna elements. The essential components in DOA estimation, the steering vector, were introduced. The covariance matrix, another important component in DOA estimation, was also discussed. Most of the DOA algorithms heavily depend on the covariance matrix, especially the spectral-based or beamforming algorithms. In this section, classification of DOA algorithms and an overview of each category were given. The advantages and drawbacks of each category of algorithm were also highlighted.

In short, this chapter covered three topics related to the fundamental information in the DOA estimation process. Firstly, the importance of communication systems and how smart antennas fit into these systems. Secondly, the characteristics of array geometry and how those factors could affect the performance of DOA estimation. Several existing planar antenna array geometries for azimuth DOA estimation were also discussed. Finally, the classification of DOA algorithms was discussed, including the comparison between them.

3 Planar Antenna Array for Azimuth DOA Estimation

This chapter presents three new planar antenna array geometries and analyses the performance of each antenna array on azimuth DOA estimation. The three antenna arrays are named as semi-circular array, oval array and Y-bend array. The first two antenna arrays, semi-circular and oval, are configured based on the circular array. The third proposed antenna array, Y-bend, is configured based on the V-shape array. The main objective of the proposed antenna arrays is to improve the performance of DOA estimation. DOA estimation is measured based on three main criteria, estimation resolution, estimation error, and consistency of estimation.

For each proposed antenna array, two main points will be presented. Firstly, structure of the proposed antenna array is discussed with an associated data model to formulate the spatial power spectrum. Secondly, a comparison against the circular array and V-shape array is made to evaluate the improvement on DOA estimation performance. The comparison is made based on the three criteria mentioned above. The final section in this chapter compares the performance of DOA estimation among all proposed antenna arrays. In this chapter, results of DOA estimation simulation are obtained using MATLAB®.

3.1 Semi-circular array

3.1.1 Structure and data model

The structure of the semi-circular array is shown in Figure 3.1. There are N elements along the circumference of the semi-circular array with inter element spacing of 0.5λ, where λ is the wavelength of the incoming signals. The radius of r in the semi-circular array is measured from the centre of the circle to the elements of the array. Direction of the incoming signal is identified by elevation angle, denoted as θ, and azimuth angle, denoted as φ. The elevation angle is measured on the y-z plane from the z-axis to the path of the incoming signal. The azimuth angle, on the other hand, is

measured on the *x*-*y* plane from *x*-axis to the path of incoming signal. The same convention used in the circular array is also applied in the semi-circular array, where the element the *x*-axis is considered as the first element.

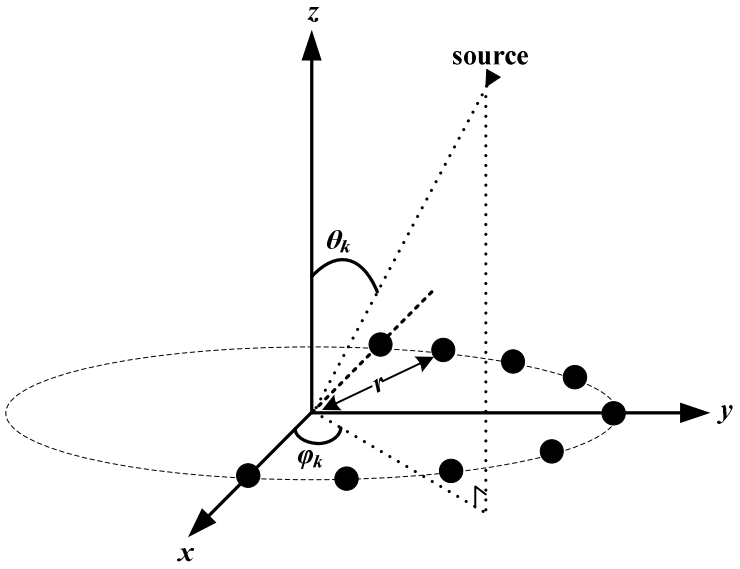

Figure 3.1: Structure of semi-circular array

The position of any element in the semi-circular array can be given as:

$$\varphi_n = \pi\left(\frac{n}{N}\right), \qquad n = 1,2,\ldots,N \tag{3.1}$$

The unit vector $\hat{\mathbf{a}}_r$ can be represented in Cartesian coordinates:

$$\hat{\mathbf{a}}_r = \mathbf{a}_x \sin\theta\cos\varphi + \mathbf{a}_y \sin\theta\sin\varphi + \mathbf{a}_z \cos\theta \tag{3.2}$$

Another unit vector $\hat{\mathbf{a}}_n$ from centre to the n^{th} element in semi-circular array can be written as:

$$\hat{\mathbf{a}}_n = \mathbf{a}_x \cos\varphi_n + \mathbf{a}_y \sin\varphi_n, \qquad n = 1,2,\ldots,N \tag{3.3}$$

Suppose the relative distance of signal wavefront reaches the n^{th} element relative to the origin is given as:

$$r_n = \mathbf{a}_r a \cos\alpha_n \tag{3.4}$$

For an incoming wavefront signal, α_n can be expressed as:

$$\begin{aligned}\cos\alpha_n &= -\mathbf{a}_r \bullet \mathbf{a}_n \\ &= -\left(\mathbf{a}_x \sin\theta\cos\varphi + \mathbf{a}_y \sin\theta\sin\varphi + \mathbf{a}_z \cos\theta\right)\bullet\left(\mathbf{a}_x \cos\varphi_n + \mathbf{a}_y \sin\varphi_n\right) \\ &= -\left(\sin\theta\cos\varphi\cos\varphi_n + \sin\theta\sin\varphi\sin\varphi_n\right) \\ &= -\sin\theta\cos\left(\varphi-\varphi_n\right) \qquad n = 1,2,\ldots,N\end{aligned} \tag{3.5}$$

Using (3.5), relative distance in (3.4) can be reduced to:

$$r_n = -\mathbf{a}_r a \sin\theta\cos\left(\varphi-\varphi_n\right), \qquad n = 1,2,\ldots,N \tag{3.6}$$

Therefore, the steering vector $\mathbf{a}_y\left(\theta_k,\varphi_k\right)$ of the semi-circular array on the *x*-*y* plane can be defined as follows:

$$\mathbf{a}_y\left(\theta_k,\varphi_k\right) = \left[\left(1,\ e^{-j\alpha_{y,1}},\ \ldots,\ e^{-j\alpha_{y,N}}\right)\right]^T \tag{3.7}$$

where

$$\alpha_{y,n} = \frac{2\pi(n-1)r\cos\left(\varphi-\varphi_k\right)\sin\theta_k}{\lambda} \tag{3.8}$$

The main difference of the semi-circular array from the circular array is the total circumference covered to place the array elements. As pointed out in (3.1), all the elements are spread in a length of π compared to 2π in the circular array. In a circular array, the spacing between elements can be expressed as the following:

$$d_{circ} = \frac{2\pi r_{circ}}{N} \tag{3.9}$$

For spacing between elements $d = \frac{\lambda}{2}$, this implies that the radius of the circular array is:

$$r_{circ} = \frac{N\lambda}{4\pi} \tag{3.10}$$

In the semi-circular array, the circumference is half of circumference is in the circular array. Therefore, the spacing between the elements can be expressed as:

$$d_{s-circ} = \frac{\pi r_{s-circ}}{N-1} \tag{3.11}$$

Maintaining the same spacing between elements $d = \frac{\lambda}{2}$ will yield the radius of the semi-circular array:

$$r_{s-circ} = \frac{(N-1)\lambda}{2\pi} \tag{3.12}$$

It is apparent that, for the same number of elements, the semi-circular array would have a larger radius than the circular array as shown in (3.10) and (3.12). As a result, as the number of elements increases, the area of the semi-circular increases significantly compared with the circular array.

3.1.2 Resolution of estimation

Resolution of estimation is a measurement of minimum separation required to distinguish two incoming signals. Higher estimation resolution means that two incoming signals separated by a smaller angle can still be distinguished. Assuming the same number of elements, there are two cases for comparing the estimation resolution between the circular array and the semi-circular array. Both cases use the following parameters: SNR is 0dB, the number of snapshots is 100, and the number of elements is eight.

In the first case, there are two signals impinging both arrays at (θ=90°, φ=100°) and (θ=90°, φ=115°). The result of DOA estimation of azimuth angle for both arrays is shown in Figure 3.2. The results show that the semi-circular array produced two distinct peaks, which corresponds to DOA of two source signals. However, the

circular array only managed to have a single peak, which means it is unable to distinguish the two source signals.

In the second case, there are two signals impinging both arrays at (θ=90°, φ=100°) and (θ=90°, φ=123°). The DOA estimation of azimuth angle for the two arrays is shown in Figure 3.3. Both the semi-circular array and circular array managed to have two distinct peaks that represent estimated DOA of two signal sources. The results in both cases clearly show that, given the same number of elements, the semi-circular array offers better resolution of estimation than the circular array by 8°.

Observations made in the simulation results suggest that the semi-circular array offers better estimation resolution compared to the circular array. This advantage, however, is compromised by larger area acquired by the semi-circular array. Therefore, in the case of the same number of elements, there is a compromise between acquired area of the array and the improvement in estimation resolution.

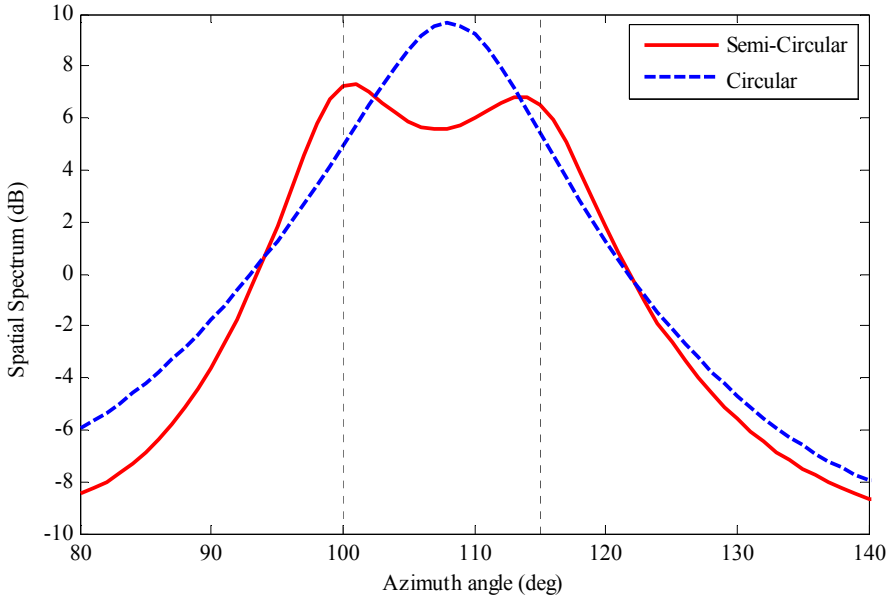

Figure 3.2: DOA estimation for two signals impinging at (θ=90°, φ=100°) and (θ=90°, φ=115°) using semi-circular and circular arrays. Dotted lines represent the true DOA.

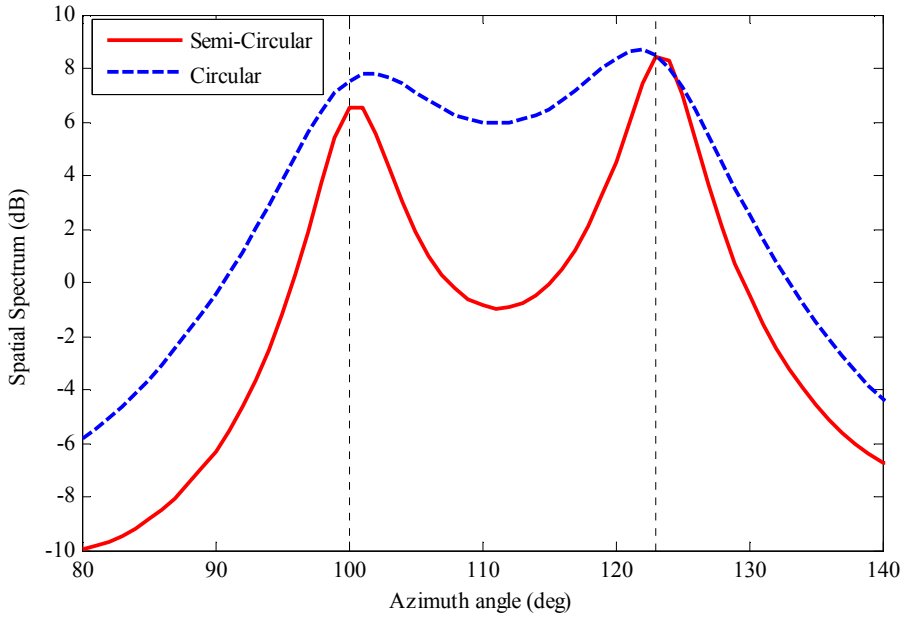

Figure 3.3: DOA estimation for two signals impinging at (θ=90°, φ=100°) and (θ=90°, φ=123°) using semi-circular and circular arrays. Dotted lines represent the true DOA.

3.1.3 Error of estimation

Estimation error is another statistical property used to measure the accuracy of DOA estimation. It represents how much the estimated DOA deviates from the true DOA. All the simulation results in this subchapter use the root-mean-square error (RMSE) to measure the estimation error, which is given as:

$$RMSE = \sqrt{\frac{1}{T}\sum_{i=1}^{T}\left(\theta - \hat{\theta}\right)^2} \tag{3.13}$$

where T is the number of trials, θ is the true DOA and $\hat{\theta}$ is the estimated DOA of the i^{th} trial.

The following parameters are used throughout in the simulations:

number of elements in both arrays is eight,

two signals impinging the array at (θ=90°, φ=100°) and (θ=90°, φ=120°),

the radii are 0.64λ and 1.27λ for circular and semi-circular array respectively,

RMSE produced by both arrays are compared against three parameters; the number of snapshots, SNR and separation of DOA. In the first case, the RMSE of azimuth angles is investigated against the number of snapshots. Figure 3.4 shows the RMSE for both circular and semi-circular arrays when the SNR is fixed at 0dB. In general observation, as the number of snapshots is increased, the performance of both arrays is improved. It is also apparent that the semi-circular array generated better estimation error than the circular array. The result shows that the semi-circular array achieved about 86% lower estimation error compared with the circular array.

Next, estimation error is compared against the SNR with the number of snapshots as 100. Both arrays show improvement in RMSE as the SNR is increased, as illustrated in Figure 3.5. The circular array exhibited a better rate of improvement, which is about 93% compared with 90% in the semi-circular array. However, on average, the semi-circular array has about 85% lower estimation errors than the circular array.

Finally, the estimation error is compared against DOA separation between two signals as depicted in Figure 3.6. In this case, azimuth angle of the first signal is fixed at 100°, and the second signal is varied between 115° and 125°. Both arrays show improvement as the second signal is moving away from the first signal. The circular array enjoys a better rate of error changes compared with the semi-circular array, a similar observation to that in the second scenario. Nevertheless, it is noted that the semi-circular array has a lower average estimation error than the circular array, roughly about 76%.

In all three comparisons of estimation error, the simulation results suggest that, for the same number of elements, the semi-circular array outperforms the circular array by producing lower estimation error. In general, the semi-circular array managed to achieve estimation within less than 1° from the true DOA. The circular array, on the other hand, estimates the true DOA off by 1° to 3°.

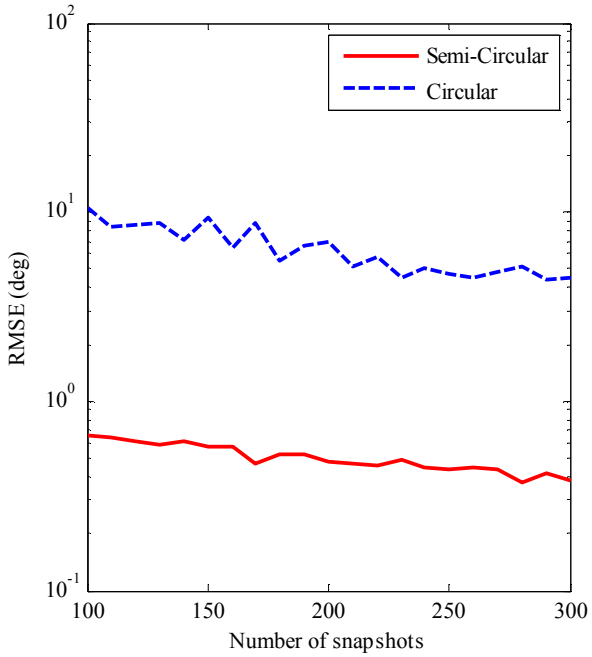

Figure 3.4: RMSE versus number of snapshots for both arrays with SNR as 0dB. The DOAs are at ($\theta = 90°$, $\varphi = 100°$) and ($\theta = 90°$, $\varphi = 120°$).

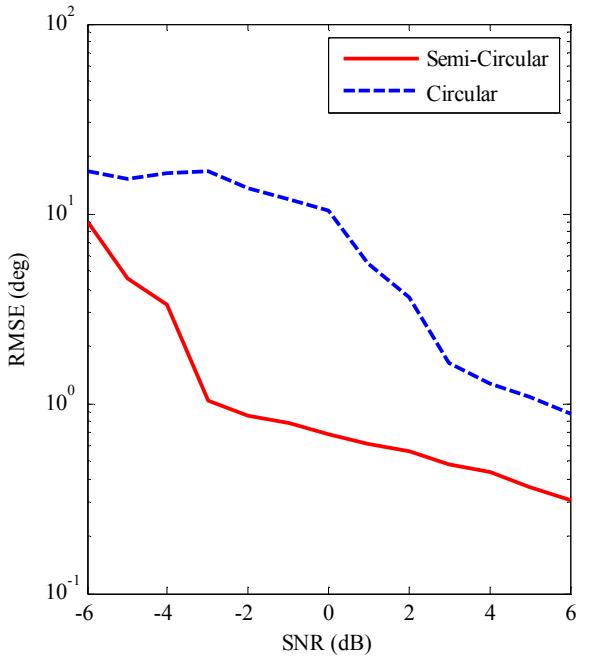

Figure 3.5: RMSE versus SNR for both arrays with number of snapshots as 100. The DOAs are at ($\theta = 90°$, $\varphi = 100°$) and ($\theta = 90°$, $\varphi = 120°$).

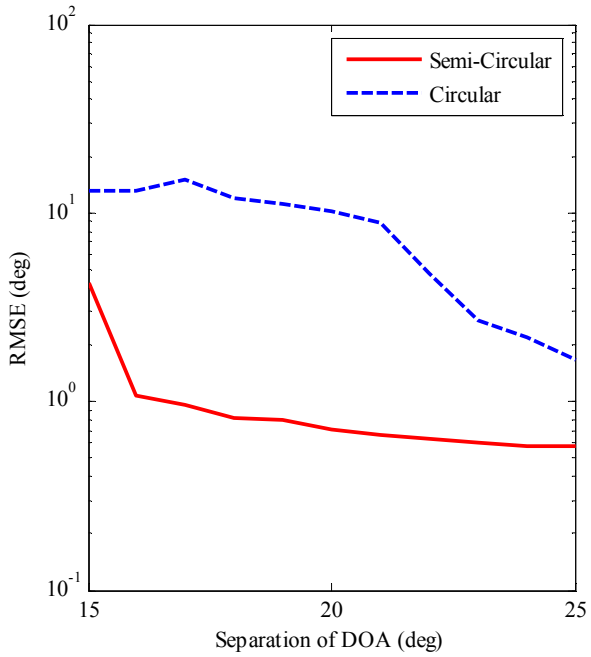

Figure 3.6: RMSE of DOA estimation for various signal separation when number of snapshots as 100 and SNR as 0dB. The DOAs are at ($\theta = 90°$, $\varphi = 100°$) and ($\theta = 90°$, $115°<\varphi<125°$).

3.1.4 Consistency of estimation

This section presents the third criterion to measure the DOA performance. This criterion represents the consistency of estimating the true DOA over a number of trials. Consistency of estimation is a measured based on the following:

$$Consistency = \frac{number \quad of \quad trials \quad for \quad true \quad DOA \quad estimation}{number \quad of \quad trials} \times 100\% \qquad (3.14)$$

In this section, a comparison of estimation consistency is presented between the semi-circular and the circular array. It is assumed that the number of snapshots is 100, SNR level is 0dB, and the number of elements in each array is eight. As shown in Figure 3.7 and Figure 3.8, the semi-circular array and the circular array have 80% and 58% estimation consistency respectively. The results suggest that the semi-circular possessed better consistency than the circular array by more than 20%.

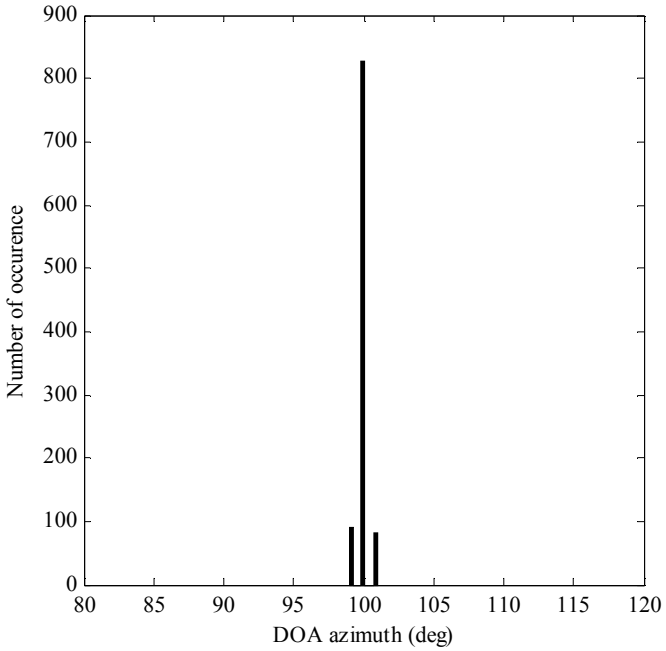

Figure 3.7: Histogram of azimuth estimation using the semi-circular array. The DOA is at (θ=90°, φ=100°).

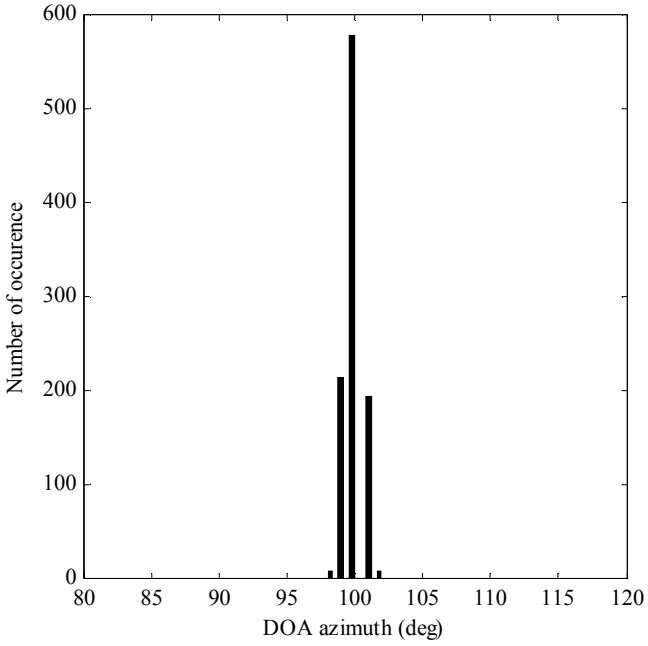

Figure 3.8: Histogram of azimuth estimation using the circular array. The DOA is at (θ=90°, φ=100°).

3.2 Oval array

Another variation of the circular-based array is proposed in this chapter, it is termed oval array. The oval array offers more flexibility compared with the circular array since the shape of the oval array is defined by two radii, major and minor radius.

3.2.1 Structure and data model

The structure of the oval array is shown in Figure 3.9. There are N elements with inter element spacing of 0.5λ, where λ is the wavelength of incoming signals. The oval array is defined by two radii; major radius labelled as a, and minor radius labelled as b. Unlike in the circular array, circumference and area of the oval array depends on both radii a and b, which is defined in (3.15) and (3.16).

$$\begin{aligned} C &\approx \pi\left(3(a+b)-\sqrt{(3a+b)(a+3b)}\right) \\ &= \pi\left(3(a+b)-\sqrt{10ab+3\left(a^2+b^2\right)}\right) \end{aligned} \tag{3.15}$$

$$A = \pi ab \tag{3.16}$$

The ratio of major radius to minor radius is defined as flattening factor as given in (3.17), which reflects how to flatten the oval shape.

$$g = 1-\frac{b}{a} \tag{3.17}$$

In this case, a flattening factor of 0.5 is being used, or $b = 0.5a$, to derive the steering vector. The elements are placed along the circumference as the following:

$$\varphi_n = 2\pi\left(\frac{n}{N}\right), \qquad n = 1,2,\ldots,N \tag{3.18}$$

The unit vector $\hat{\mathbf{a}}_r$ can be represented in Cartesian coordinate:

$$\hat{\mathbf{a}}_r = \mathbf{a}_x \sin\theta\cos\varphi + \mathbf{a}_y \sin\theta\sin\varphi + \mathbf{a}_z \cos\theta \tag{3.19}$$

Another unit vector $\hat{\mathbf{a}}_{rn}$ from centre to the n^{th} element in semi-circular array can be written as:

$$\hat{\mathbf{a}}_r = \mathbf{a}_x \cos\varphi_n + \mathbf{a}_y \sin\varphi_n, \qquad n = 1,2,\ldots,N \tag{3.20}$$

Suppose relative distance of signal wavefront reaches the n^{th} element relative to the origin is given as:

$$r_n = \mathbf{a}_r a \cos\alpha_n \tag{3.21}$$

For an incoming wavefront signal, α_n can be expressed as:

$$\begin{aligned}\cos\alpha_n &= -\mathbf{a}_r \bullet \mathbf{a}_n \\ &= -\left(\mathbf{a}_x \sin\theta\cos\varphi + \mathbf{a}_y \sin\theta\sin\varphi + \mathbf{a}_z \cos\theta\right) \\ &\quad \bullet \left(\mathbf{a}_x \cos\varphi_n + \mathbf{a}_y \sin\varphi_n\right) \\ &= -\left(\sin\theta\cos\varphi\cos\varphi_n + \sin\theta\sin\varphi\sin\varphi_n\right) \\ &= -\sin\theta\cos\left(\varphi - \varphi_n\right) \qquad n = 1,2,\ldots,N\end{aligned} \tag{3.22}$$

Using (3.22), relative distance in (3.21) can be reduced to:

$$r_n = -\mathbf{a}_r a \sin\theta\cos\left(\varphi - \varphi_n\right), \qquad n = 1,2,\ldots,N \tag{3.23}$$

Therefore, the steering vector $\mathbf{a}_y(\theta_k, \varphi_k)$ of oval array can be defined as follows:

$$\mathbf{a}_y(\theta_k, \varphi_k) = \left[\left(1,\ e^{-j\alpha_{y,1}},\ \ldots,\ e^{-j\alpha_{y,N}}\right)\right]^T \tag{3.24}$$

where

$$\alpha_{y,n} = \frac{\pi\left(3(a+b) - \sqrt{10ab + 3\left(a^2 + b^2\right)}\right)(n-1)\cos\left(\varphi - \varphi_k\right)\sin\theta_k}{\lambda} \tag{3.25}$$

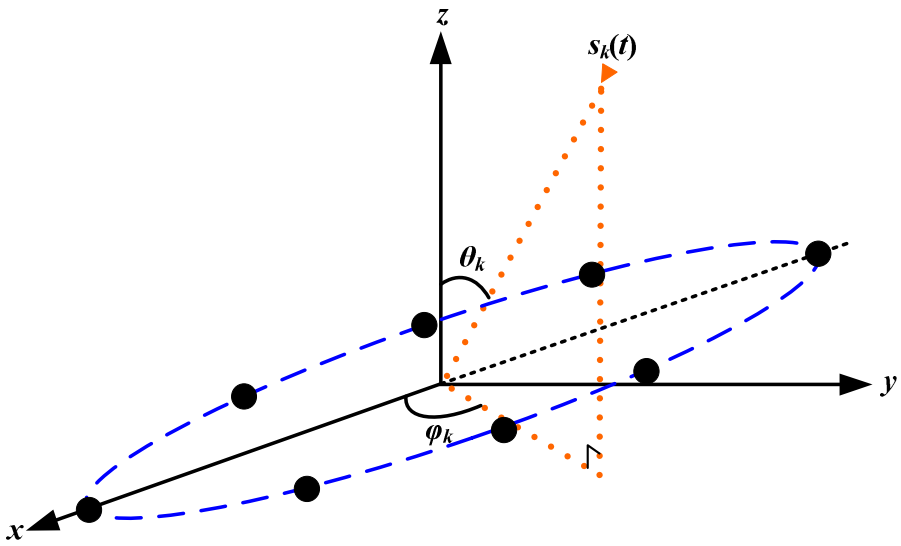

Figure 3.9: Structure of oval antenna array

An advantage of the oval array is that, given the same length of circumference, it acquired less area than the circular array. The comparison of the area, circumference length, and radius length is illustrated in Table 3.1. Since the array elements in both oval and circular arrays are placed along their circumference, this implies that the oval array would have less area than the circular array for the same number of elements.

Another factor that affects the array area is the flattening factor, which relates the major and minor radii. Given the same number of elements, the area of the circular array is compared with the oval array with different flattening factor as shown in Figure 3.10. It is apparent from the comparison result that the flattening factor and the array area are inversely proportional, which means that as the flattening factor is increased the array area would decrease significantly.

Table 3.1: Comparison of array area and circumference between the circular array and the oval array

Circumference (cm)	Circular array		Oval array		
	Radius, r (cm)	Area (cm^2)	Major radius, a (cm)	Minor radius, b (cm)	Area (cm^2)
1.00	0.16	0.08	0.20	0.10	0.07
1.50	0.24	0.18	0.30	0.15	0.15
2.00	0.32	0.32	0.40	0.21	0.27
2.50	0.40	0.50	0.52	0.26	0.42
3.00	0.48	0.72	0.62	0.31	0.60
3.50	0.56	0.97	0.72	0.36	0.82
4.00	0.64	1.27	0.84	0.42	1.07

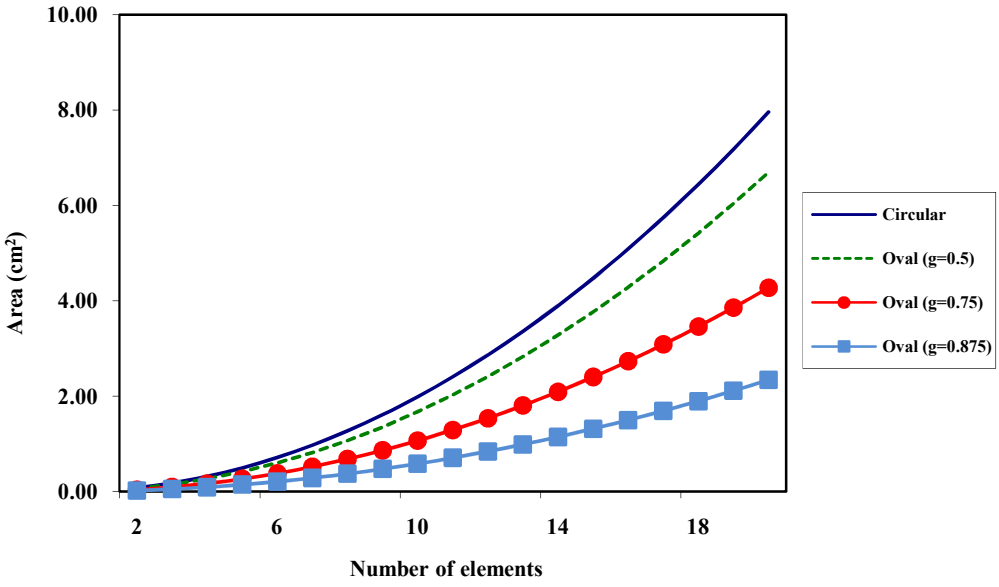

Figure 3.10: The area of both oval and circular arrays are compared in terms of number of elements

3.2.2 Resolution of estimation

Estimation resolution of both oval and circular arrays is investigated in order to find the minimum signal separation that can be distinguished in each array. In all cases, the number of snapshots is 100, SNR level is 0dB, and the number of elements in each array is eight. In the first case, it is assumed that there are two signal sources impinging the array at (θ=90°, φ=100°) and (θ=90°, φ=120°). Figure 3.11 shows that the oval array produces two distinct peaks on the spatial spectrum, which means the two signal sources can be distinguished.

The circular array, on the other hand, only managed to produce a single peak, which means it cannot distinguish the signal sources. The result suggests that the resolution of the oval array is about 20°. The circular array has lower estimation resolution, which is about 30° as illustrated in Figure 3.12. Therefore, given the same number of elements, the oval array could improve the estimation resolution of the circular array.

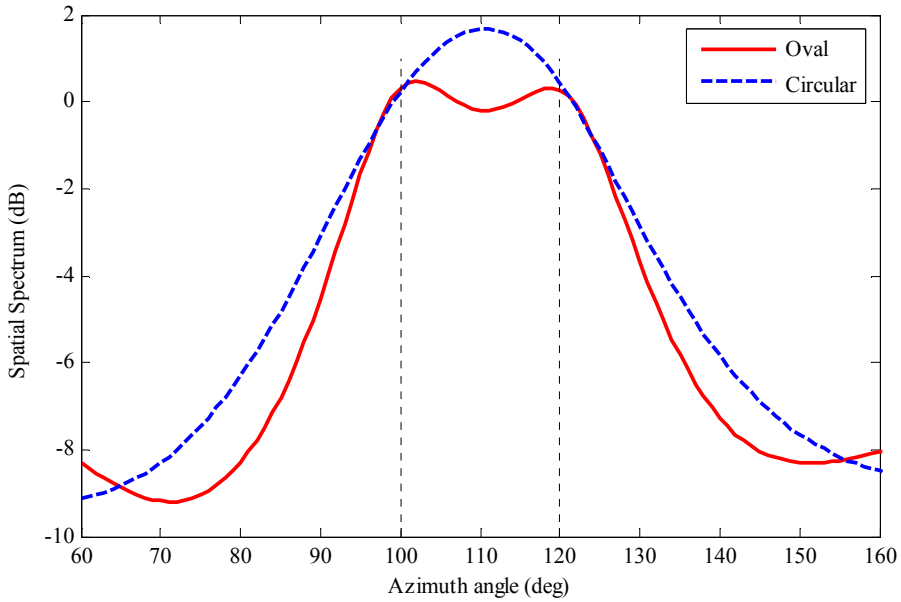

Figure 3.11: DOA estimation for two signals impinging at (θ=90°, φ=100°) and (θ=90°, φ=120°) using oval and circular arrays. Dotted lines represent the true DOA.

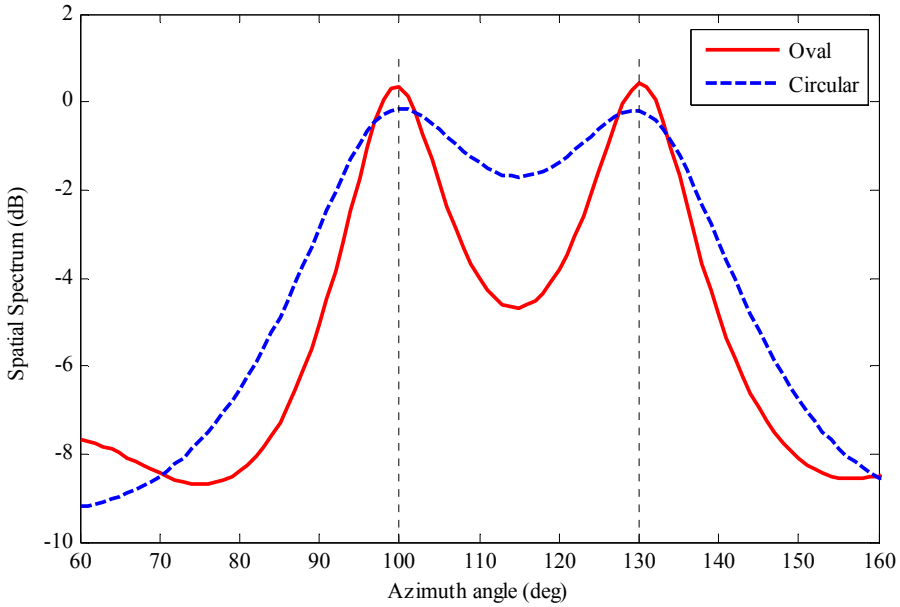

Figure 3.12: DOA estimation for two signals impinging at (θ=90°, φ=100°) and (θ=90°, φ=130°) using oval and circular arrays. Dotted lines represent the true DOA.

3.2.3 Error of estimation

The RMSE of the oval array is presented and compared with the circular array in four scenarios. First scenario compares the RMSE of both oval and circular arrays versus the SNR. Figure 3.13 shows that the oval array has lower RMSE than the circular array with minimum estimation error at 0.6°. The minimum RMSE achieved by the oval array is 76% lower than the minimum RMSE achieved by the circular array. However, the circular array shows better improvement of RMSE from 14° to 2.8°, which represents an 80% reduction. Compared with the oval array, the reduction is only about 50% from its maximum estimation error. On average, the oval array has reduced the estimation error of the circular array by no less than 85%, which is a notable improvement.

Next, the RMSE versus the number of snapshots is investigated. In general, both arrays show an improvement in estimation error as the number of snapshots is increased, as shown in Figure 3.14. The oval array reduced the estimation error of the

circular array by 64% and achieves its minimum RMSE at 0.5°. The oval array possessed a larger percentage of improvement compared with the circular array when the number of snapshots is increased from 50 to 65.

In the third scenario, the effect of DOA separation between two signal sources on RMSE is investigated. In this case, the first signal remains at 110°, and the second signal is varied between 130° and 140°. As illustrated in Figure 3.15, both arrays have almost the same estimation error when the signal sources are separated by 20°. However, as the separation is increased from 21° to 25°, the oval array has a significant reduction in RMSE from 15° to 0.8°. From that point on, the estimation error in the oval array settles down to its minimum value at 0.7°. Estimation error in the circular array is almost unchanged until the signal separation reaches 24°. As the signal separation increased to more than 24°, the RMSE gradually decreased and the circular array achieved its minimum estimation error at 1.8°. Comparing the minimum RMSE achieved by both arrays, the oval array managed to improve the estimation error in the circular array by 60%.

Simulation results show that the oval array shows notable improvement of estimation error in the circular array. On average, the improvement of estimation error by the oval array is between 60% and 80% compared with the circular array. Although both arrays show an identical trend in the improvement of estimation error in all cases, the oval array clearly outperforms the circular array by having lower estimation error.

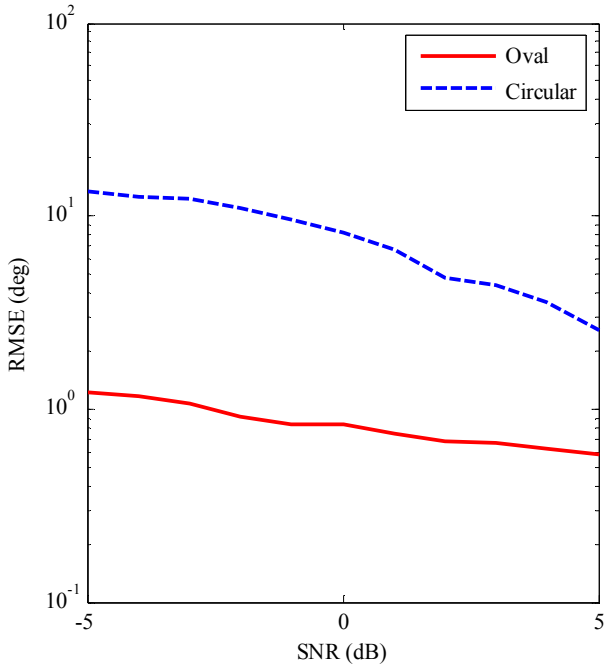

Figure 3.13: RMSE of DOA estimation for various SNR when number of snapshots is 100. The DOAs are at ($\theta = 90°$, $\varphi = 110°$) and ($\theta = 90°$, $\varphi = 135°$).

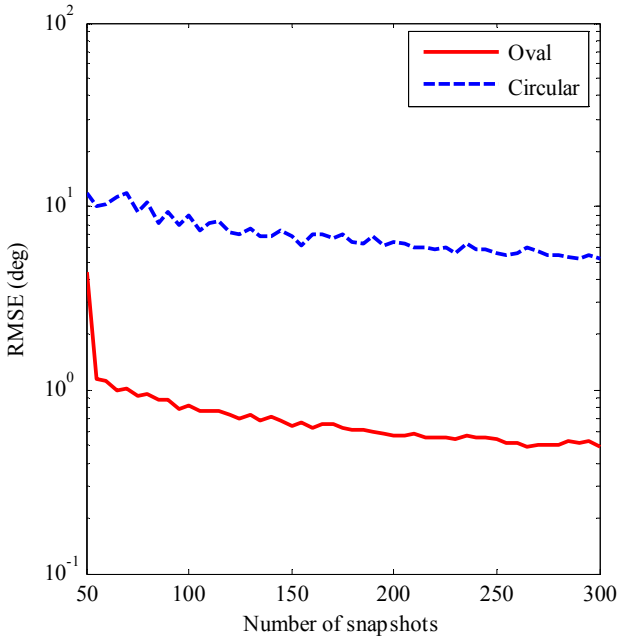

Figure 3.14: RMSE of DOA estimation versus number of snapshots when SNR is 0dB. The DOAs are at ($\theta = 90°$, $\varphi = 110°$) and ($\theta = 90°$, φ=135°).

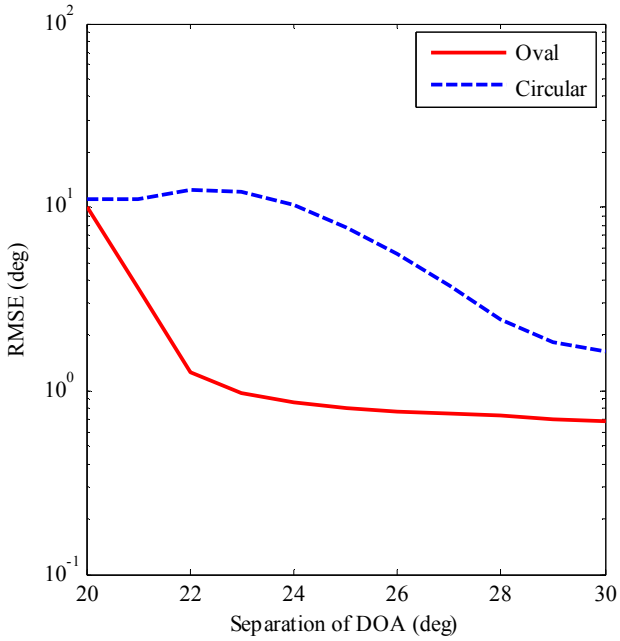

Figure 3.15: RMSE of DOA estimation for various signal separation when number of snapshots is 100 and SNR is 0dB. The DOAs are at ($\theta = 90°$, $\varphi = 110°$) and ($\theta = 90°$, $130° < \varphi < 140°$).

3.2.4 Consistency of estimation

This section presents the comparison of estimation consistency between the oval array and the circular array using the formula described in (3.14). In both cases, the number of snapshots is 100, SNR level is 0dB, and the number of elements in each array is eight.

Figure 3.16 and Figure 3.17 show that the oval array and the circular array exhibit 78% and 58% of estimation consistency respectively. Similar to the semi-circular array, the oval array also has about 20% higher consistency than the circular array.

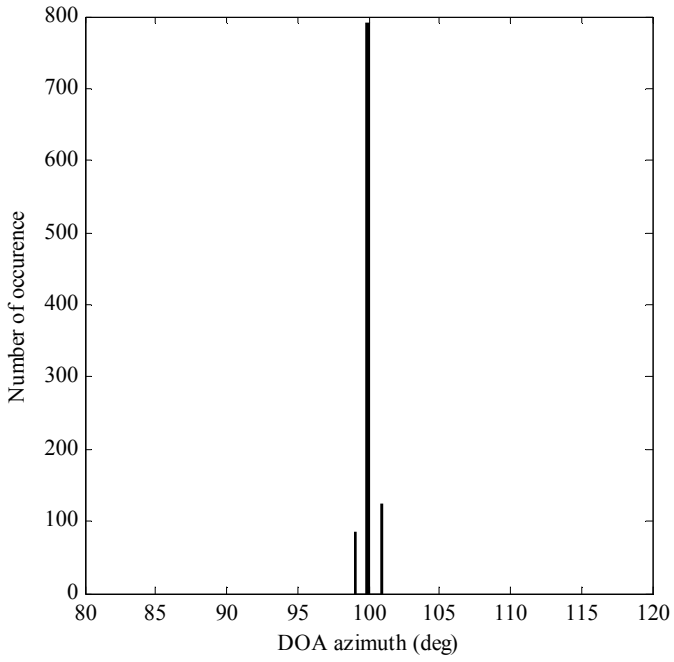

Figure 3.16: Histogram of azimuth estimation using the oval array. The DOA is at (θ=90°, φ=100°).

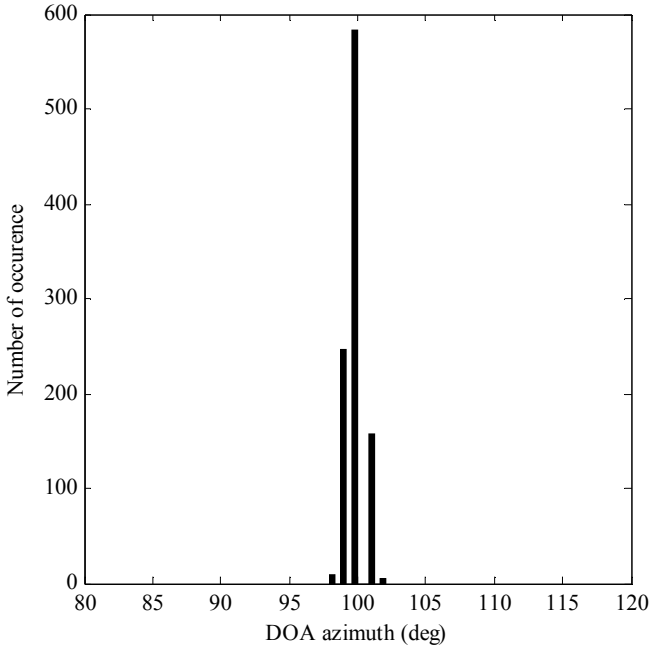

Figure 3.17: Histogram of azimuth estimation using the circular array. The DOA is at (θ=90°, φ=100°).

3.3 Y-bend array

The last section in this chapter investigates another shape antenna array for 2D DOA estimation. Unlike the previous sections which focus on the circular-based shape arrays, this section is looking at a planar array that is made from a combination of several linear arrays. Planar arrays of a similar concept have been proposed in the literature such as L-shape, V-shape and Y-shape arrays.

3.3.1 Structure and data model

The structure of the proposed array, which we term Y-bend, is shown in Figure 3.18. It is composed of three sub-arrays on the *x*-*y* plane. Two sub-arrays, *U* and *V*, are on both sides of the *y*-axis, with an element-dependent angle separating them, denoted α. Another sub-array, *W*, is placed exactly along the *y*-axis. Each sub-array consists of *N* elements; therefore the proposed array would have a total of 3*N*-2 elements. The position of both sub-arrays *U* and *V* are flexible within $0°<\varphi<180°$ and have the same distance from the *y*-axis, whereas the sub-array *W* is fixed along the *y*-axis.

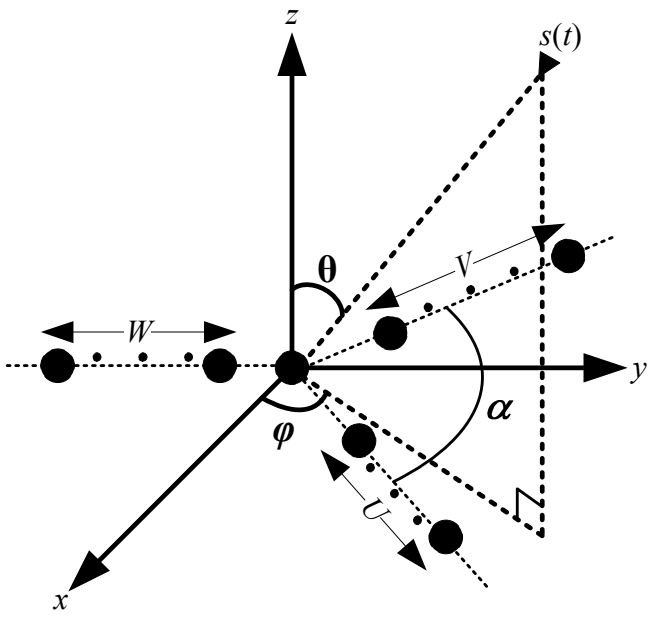

Figure 3.18: Structure of Y-bend antenna array

The received signal at sub-arrays *U*, *V* and *W* can be represented as follows:

$$x_U(t) = \mathbf{A_U} s(t) + n(t) \tag{3.26}$$

$$x_V(t) = \mathbf{A_V} s(t) + n(t) \tag{3.27}$$

$$x_W(t) = \mathbf{A_W} s(t) + n(t) \tag{3.28}$$

where $s(t)$ is the source signal, and $n(t)$ is the Gaussian white noise signal of zero mean and variance σ^2. $\mathbf{A_U}$, $\mathbf{A_V}$ and $\mathbf{A_W}$ are the steering matrices for sub-arrays *U*, *V* and *W* respectively and defined as:

$$\mathbf{A_U} = \begin{bmatrix} 1 & 1 & \cdots & 1 \\ e^{-j\gamma_1} & e^{-j\gamma_2} & \cdots & e^{-j\gamma_K} \\ \vdots & \vdots & \ddots & \vdots \\ e^{-jN\gamma_1} & e^{-jN\gamma_2} & \cdots & e^{-jN\gamma_K} \end{bmatrix} \tag{3.29}$$

$$\mathbf{A_V} = \begin{bmatrix} 1 & 1 & \cdots & 1 \\ e^{-j\beta_1} & e^{-j\beta_2} & \cdots & e^{-j\beta_K} \\ \vdots & \vdots & \ddots & \vdots \\ e^{-jN\beta_1} & e^{-jN\beta_2} & \cdots & e^{-jN\beta_K} \end{bmatrix} \tag{3.30}$$

$$\mathbf{A_W} = \begin{bmatrix} 1 & 1 & \cdots & 1 \\ e^{-j\mu_1} & e^{-j\mu_2} & \cdots & e^{-j\mu_K} \\ \vdots & \vdots & \ddots & \vdots \\ e^{-jN\mu_1} & e^{-jN\mu_2} & \cdots & e^{-jN\mu_K} \end{bmatrix} \tag{3.31}$$

$$\gamma_k = -\frac{2\pi d \sin\theta_k \sin\left(\varphi_k + \frac{\alpha}{2}\right)}{\lambda} \qquad k = 1,2,\ldots,K \tag{3.32}$$

$$\beta_k = \frac{2\pi d \sin\theta_k \sin\left(\varphi_k - \frac{\alpha}{2}\right)}{\lambda} \qquad k = 1,2,\ldots,K \tag{3.33}$$

$$\mu_k = -\frac{2\pi d \sin\theta_k \sin\varphi_k}{\lambda} \qquad k = 1,2,\ldots,K \tag{3.34}$$

where λ is the wavelength of incoming signal, *d* is the spacing between elements expressed in term of λ, and the angle α separating the *U* and *V* sub-arrays is defined as:

$$\alpha = 2 \times \left(\frac{\sqrt{N^2 + 2}}{2N} \right) \tag{3.35}$$

3.3.2 Resolution of estimation

The Y-bend array is evaluated using 13 elements, which means there are five elements in each sub-array. The spacing between the array elements is 0.5λ, and there are two signal sources present at (θ = 90°, φ = 65°) and (θ = 90°, φ = 75°).

Firstly, the estimation resolution is examined with the number of snapshots as 100, and SNR level as 0dB. As depicted in Figure 3.19, the Y-bend array manages to produce two distinct peaks on the spatial spectrum which represent two DOA of signal sources as estimated. The V-shape array, in contrast, only shows a single peak which corresponds to only one DOA of signal source being estimated although there are two signals impinging the array. This means that when there are two signals present and separated by 10° or less, the V-shape array fails to estimate both signals.

Figure 3.20 shows the estimation result when the azimuth angles of incoming signals are separated by 14°. Both arrays managed to produce two distinct peaks, which implies that they are able to estimate the direction of both signals. This result also means that the estimation resolution of the V-shape is roughly about 13°, less than the estimation resolution in the Y-bend array. Based on the observation in both cases, it appears that the Y-bend array has better estimation resolution than the V-shape array by 4°. However, the improvement in estimation resolution needs 30% more elements than the V-shape array.

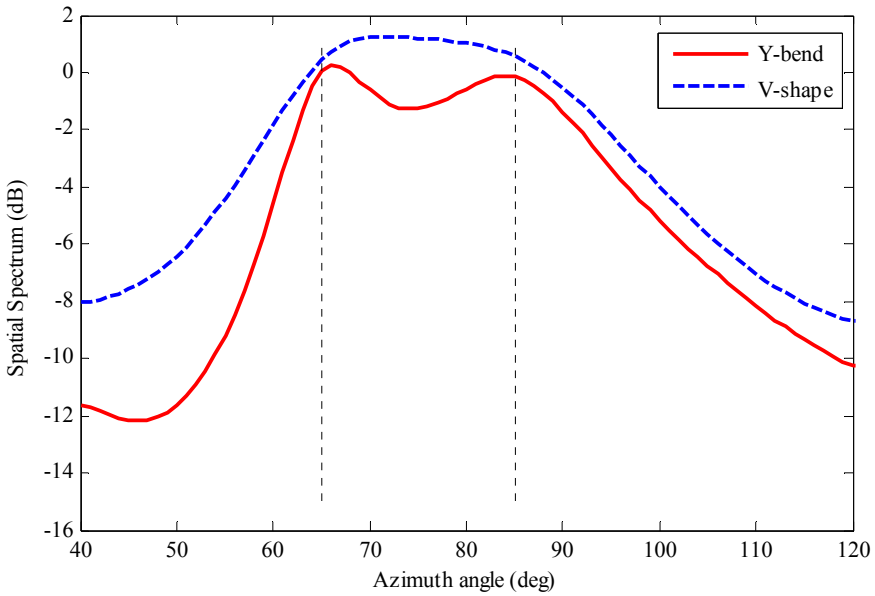

Figure 3.19: Azimuth estimation of two signal sources at (θ = 90°, φ = 65°) and (θ = 90°, φ = 85°) using Y-bend and V-shape arrays. Dotted lines represent the true DOA.

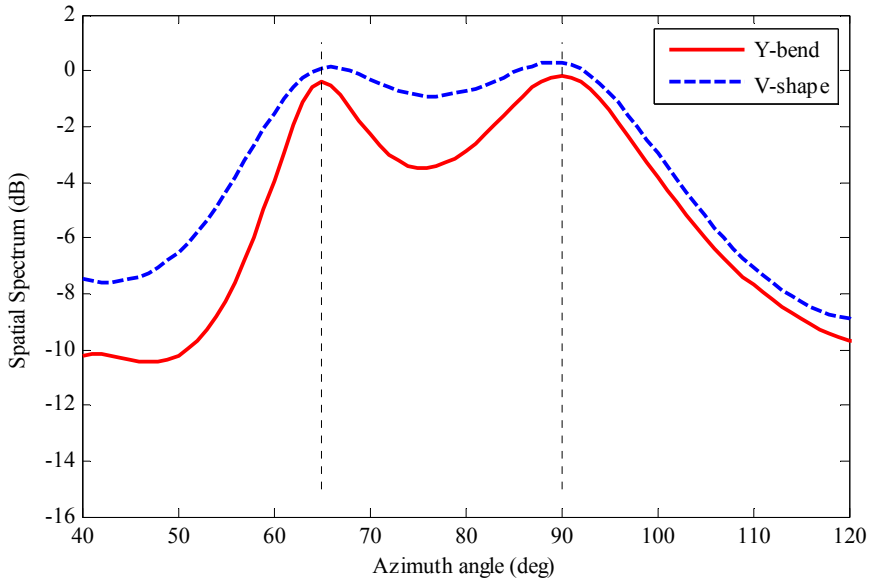

Figure 3.20: Azimuth estimation of two signal sources at (θ = 90°, φ = 65°) and (θ = 90°, φ = 90°) using Y-bend and V-shape arrays. Dotted lines represent the true DOA.

3.3.3 Error of estimation

The RMSE simulation of the Y-bend array is presented and compared with the V-shape array. The parameters of simulation are the same as in the previous section where there are eight elements in each sub-array, and there are two signal sources at ($\theta = 90°$, $\varphi = 65°$) and ($\theta = 90°$, $\varphi = 85°$).

Firstly, the RMSE versus the SNR of both arrays are investigated. As shown in Figure 3.21, the Y-bend array has 22% lower estimation error than the V-shape array at low SNR. However, as the SNR level improves, the estimation error of the Y-bend array drops drastically and clearly outperforms the V-shape array. At one point, 5dB to be exact, the Y-bend array has reduced the estimation error of the V-shape by 88%.

Secondly, the RMSE is investigated against the separation between two DOA of signal sources. In this case, the azimuth of the first signal remains at 65° and the second signal varies between 80° and 90°. As illustrated in Figure 3.22, RMSE in the Y-bend array reduced significantly as the second signal moved further away from the first signal. On the other hand, RMSE in the V-shape array remained almost constant until the signals were apart by more than 20°. It is noted that RMSE of the Y-bend array has roughly improved estimation error in the V-shape array by 78%.

Thirdly, the RMSE of both arrays are investigated versus the number of snapshots. In general, the number of snapshots does not have a significant impact on the RMSE as shown in Figure 3.23. The Y-bend managed to improve RMSE of the V-shape by 86%. This result also reveals a superior performance of the Y-bend over the V-shape array in term of estimation error.

Simulation results show that the Y-bend array manages to improve the estimation error of the V-shape array up to more than 80%. The simulation results suggest that the Y-bend array clearly outperforms the V-shape array in the estimation error criterion.

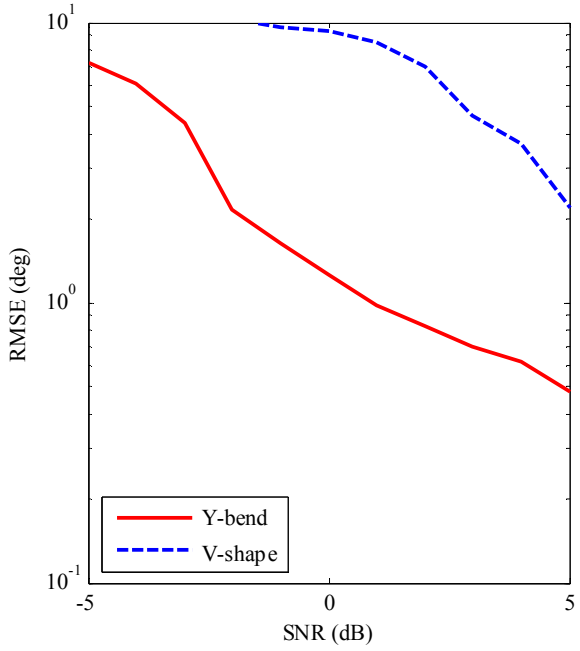

Figure 3.21: RMSE of DOA estimation for various SNR when number of snapshots is 100. The DOAs are at ($\theta = 90°$, $\varphi = 65°$) and ($\theta = 90°$, $\varphi = 85°$).

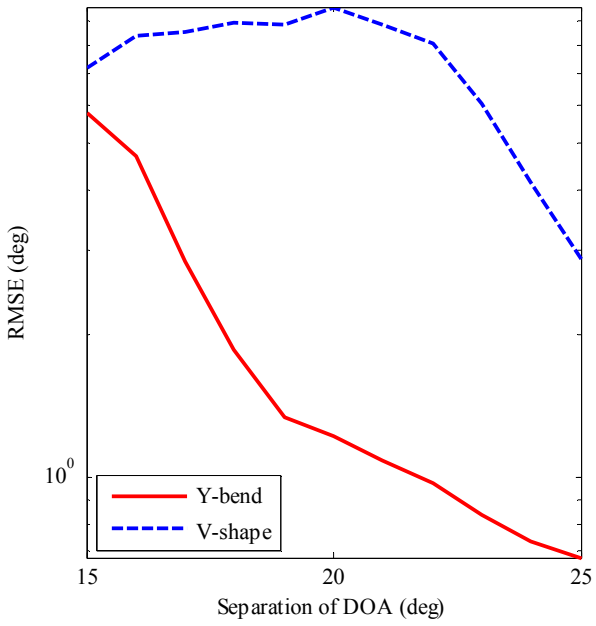

Figure 3.22: RMSE of DOA estimation for various signal separation when number of snapshots is 100 and SNR is 0dB. The DOAs are at ($\theta = 90°$, $\varphi = 65°$) and ($\theta = 90°$, $80° < \varphi < 90°$).

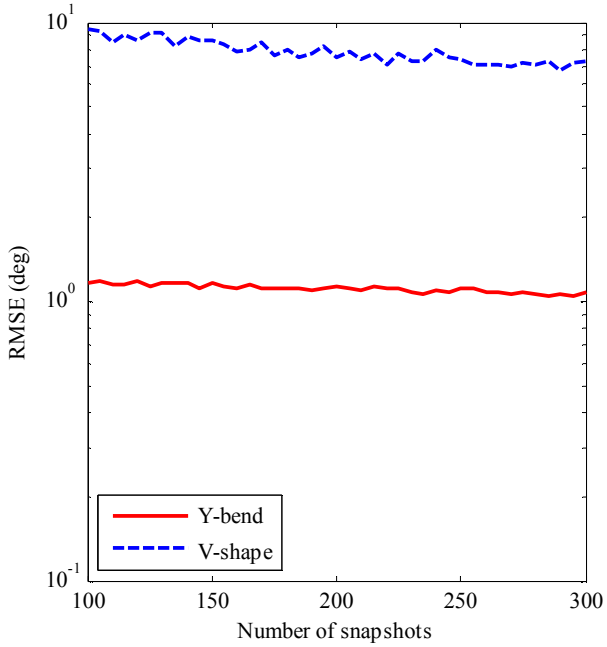

Figure 3.23: RMSE of DOA estimation versus number of snapshots when SNR is 0dB. The DOAs are at ($\theta = 90°$, $\varphi = 65°$) and ($\theta = 90°$, $\varphi=85°$).

3.3.4 Consistency of estimation

This section presents the comparison of estimation consistency between the Y-bend array and the V-shape array using formula described in (3.14). In both cases, the number of snapshots is 100, SNR level is 0dB, and the number of elements in each sub-array is five. Figure 3.24 and Figure 3.25 show that the Y-bend array and the V-shape array produce 42% and 35% of estimation consistency respectively. The results imply that the Y-bend possesses 7% higher estimation consistency than the V-shape array. Nevertheless, the results also illustrate that both arrays have almost the same dispersion of azimuth estimation: between 97° and 103°.

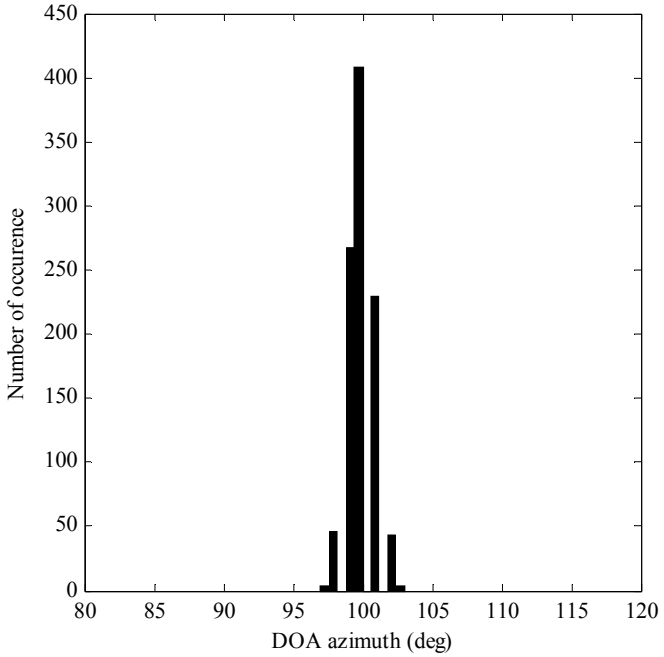

Figure 3.24: Histogram of azimuth estimation using the Y-bend array. The DOA is at (θ=90°, φ=100°).

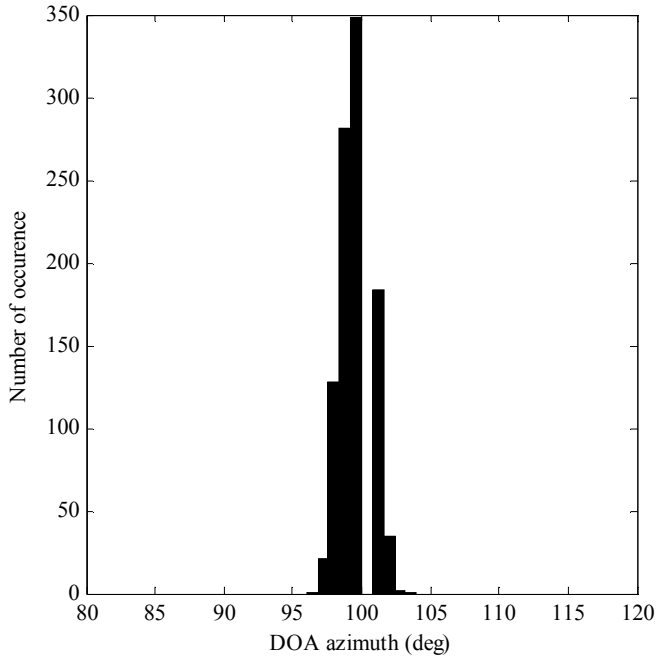

Figure 3.25: Histogram of azimuth estimation using the V-shape array. The DOA is at (θ=90°, φ=100°).

3.4 Comparison of the proposed arrays

This section presents a comparison study between all proposed arrays; the semi-circular array, the oval array, and the Y-bend array. All proposed arrays are compared based on three criteria; resolution of estimation, error of estimation and consistency of estimation. It is assumed that for each array geometry has ten elements in all comparison criteria.

3.4.1 Resolution of estimation

In this sub-section, the main objective is to find the minimum estimation resolution for each of the proposed arrays. All simulations have assumed that the number of snapshots is 100, and the SNR level is 0dB.

In the first case, it is assumed that there are two signal sources impinging the array at (90°, φ=60°) and (θ=90°, φ=85°). Figure 3.26 shows that all antenna arrays managed to produce two distinct peaks that represent DOA of two signals separated by 25°. In the second case, it is assumed that the signal separation is reduced to 20° with signal DOA at (θ=90°, φ=60°) and (θ=90°, φ=80°). The results in Figure 3.27 show that the Y-bend array fails to produce two distinct peaks, as opposed to the oval and semi-circular arrays. The third case considers a smaller resolution which is about 15°. Figure 3.28 shows that only the semi-circular array is able to distinguish both incoming signals. This result reflects that the semi-circular has the smallest estimation resolution among the three arrays. The final result in Figure 3.29 shows that all the arrays fail to estimate both incoming signals when the estimation resolution is 10°.

Therefore, in term of resolution of estimation, the semi-circular possesses the best performance among the proposed arrays. This is followed by the oval array and the Y-bend array.

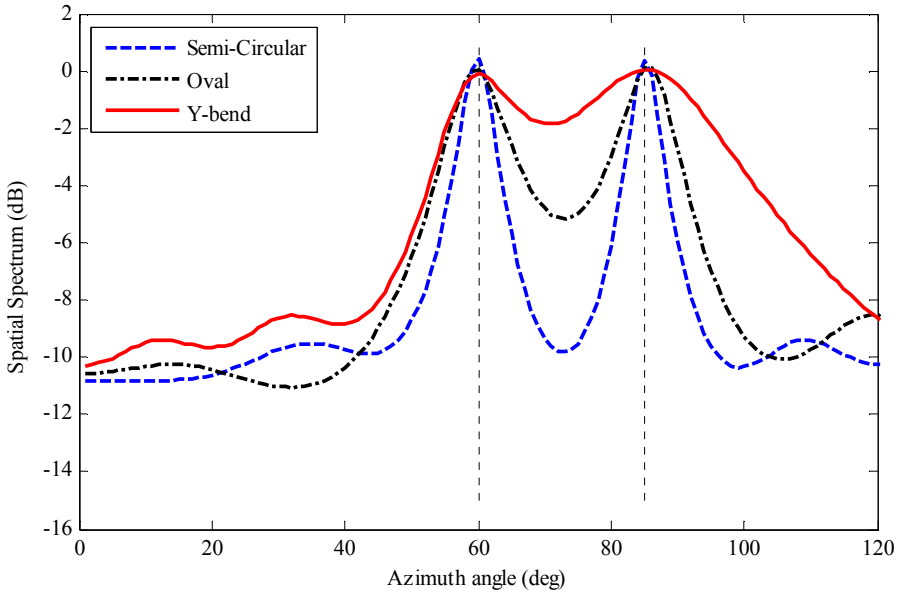

Figure 3.26: Azimuth estimation of two signal sources at (θ = 90°, φ = 60°) and (θ = 90°, φ = 85°) using semi-circular, oval and Y-bend array. Dotted lines represent the true DOA.

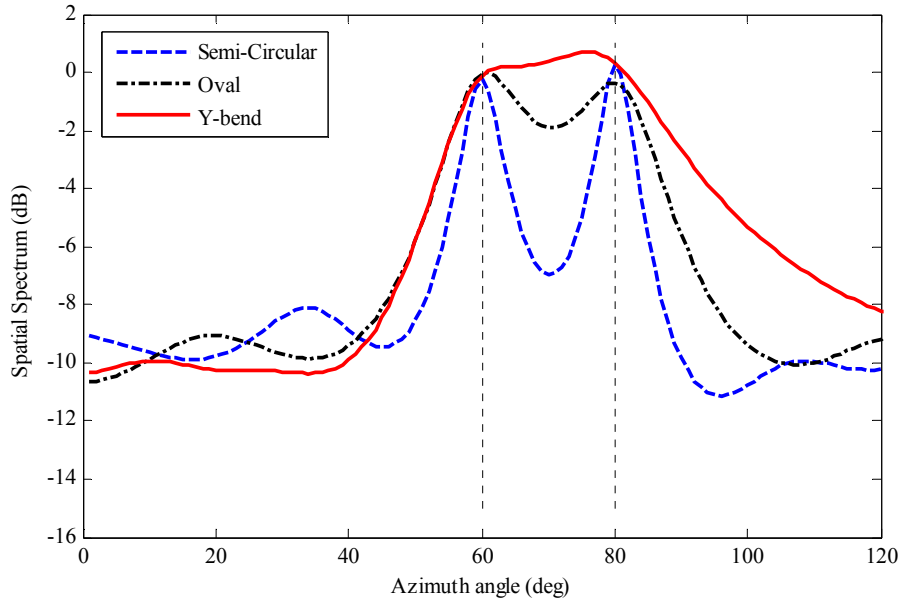

Figure 3.27: Azimuth estimation of two signal sources at (θ = 90°, φ = 60°) and (θ = 90°, φ = 80°) using semi-circular, oval and Y-bend array. Dotted lines represent the true DOA.

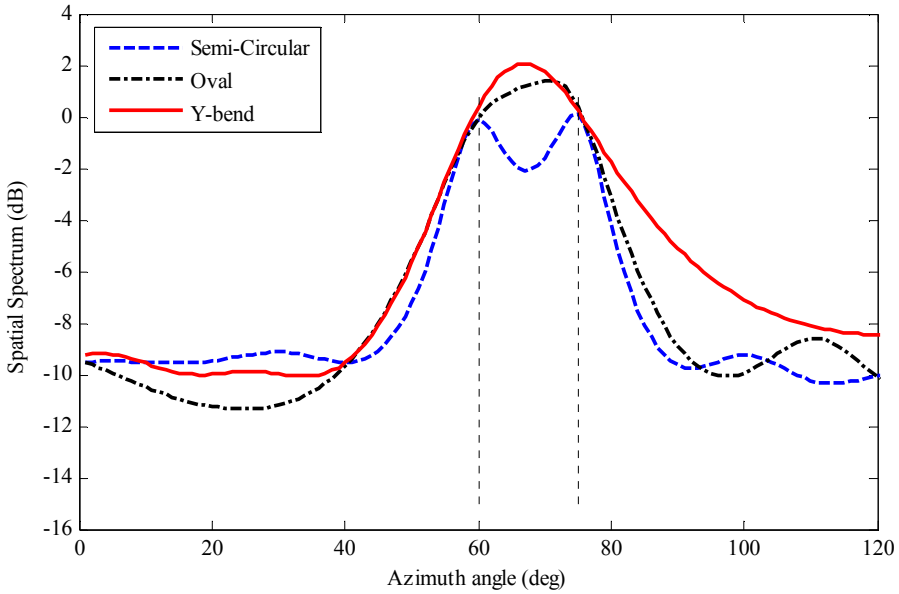

Figure 3.28: Azimuth estimation of two signal sources at (θ = 90°, φ = 60°) and (θ = 90°, φ = 75°) using semi-circular, oval and Y-bend array. Dotted lines represent the true DOA.

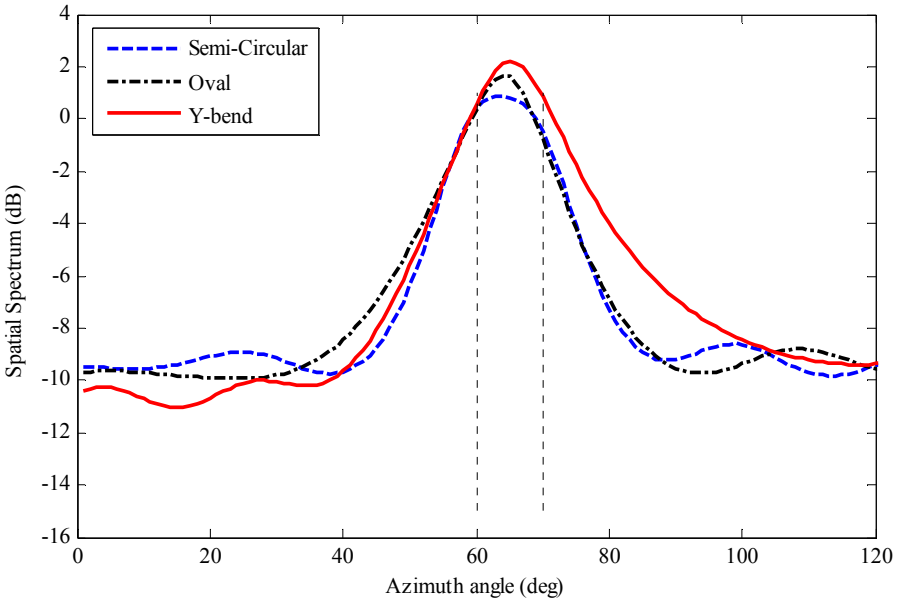

Figure 3.29: Azimuth estimation of two signal sources at (θ = 90°, φ = 60°) and (θ = 90°, φ = 70°) using semi-circular, oval and Y-bend array. Dotted lines represent the true DOA.

3.4.2 Error of estimation

Comparison of RMSE for all the proposed arrays is presented in this section. The RMSE of all arrays are first compared against the SNR. It is assumed that there are two signal sources: ($\theta = 90°$, $\varphi = 60°$) and ($\theta = 90°$, $\varphi = 80°$), and the number of snapshots is 100. Simulation results in Figure 3.30 illustrate that the semi-circular array has the smallest RMSE, which is about 0.05°. The RMSE of semi-circular array is 88% lower than that of the oval array and 20 times smaller than that of the Y-bend array. Figure 3.31 shows that, for a varying number of snapshots, the semi-circular array has the smallest RMSE among all the arrays. The RMSE of the semi-circular array has reduced from 0.2° to 0.05°. In contrast, the RMSE for both oval and Y-bend arrays are almost unchanged at 2° and 0.5° respectively. The third case compares RMSE when the signal separation is varied between 15° and 25°. Results in Figure 3.32 illustrate that the semi-circular array has 70% lower RMSE than the oval array. The semi-circular array also has ten times smaller RMSE than the Y-bend array.

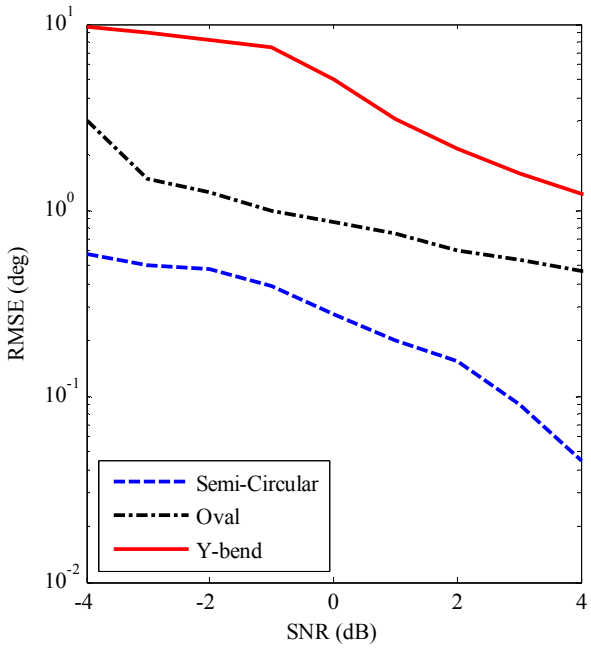

Figure 3.30: RMSE of DOA estimation for various SNR when number of snapshots is 100. The DOAs are at ($\theta = 90°$, $\varphi = 60°$) and ($\theta = 90°$, $\varphi=80°$).

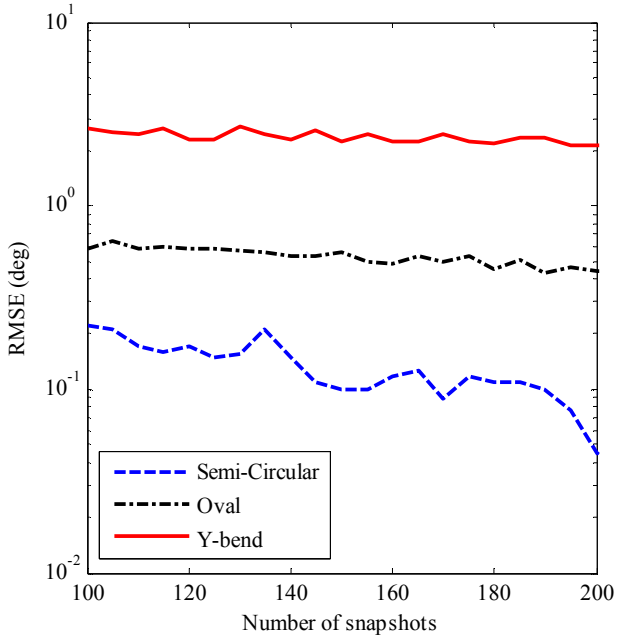

Figure 3.31: RMSE of DOA estimation versus number of snapshots when SNR is 0dB. The DOAs are at (θ = 90°, φ = 60°) and (θ = 90°, φ=80°).

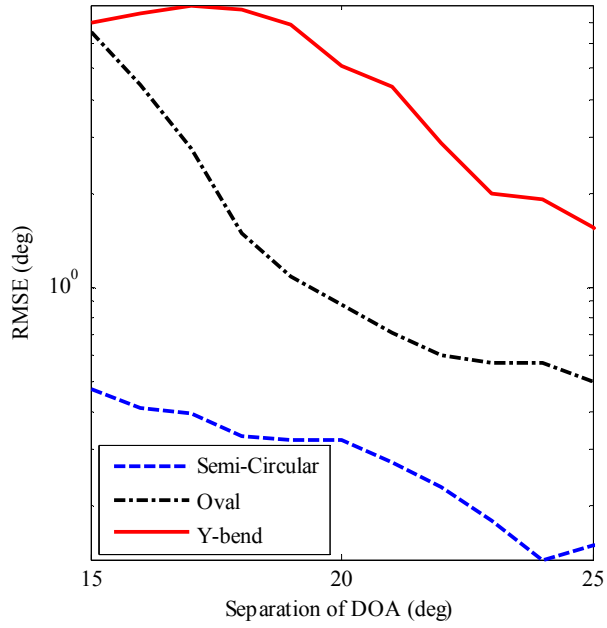

Figure 3.32: RMSE of DOA estimation for various signal separations when number of snapshots is 100 and SNR is 0dB. The DOAs are at (θ = 90°, φ = 60°) and (θ = 90°, 75°<φ<85°).

In general, the semi-circular array possesses the best performance among all the proposed arrays in terms of estimation error.

3.4.3 Consistency of estimation

This section presents the comparison of estimation consistency between all the proposed arrays. It is assumed that the number of snapshots is 100, SNR level is 0dB, and the number of elements in each array is ten. Simulation results shown in Figure 3.33, Figure 3.34 and Figure 3.35 represent estimation consistency of the semi-circular array, the oval array and the Y-bend arrays respectively. It exhibits that the semi-circular array and the oval array have a very high consistency, which is more than 90%. On the other hand, the Y-bend array posseses only 43% of consistency, which is less than half the consistency of both the semi-circular and oval arrays.

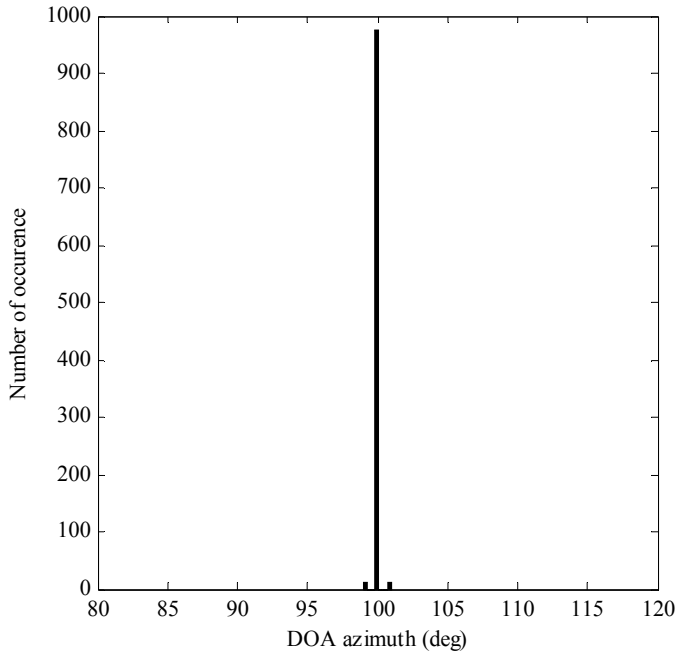

Figure 3.33: Histogram of azimuth estimation using the semi-circular array. The DOA is at (θ=90°, φ=100°).

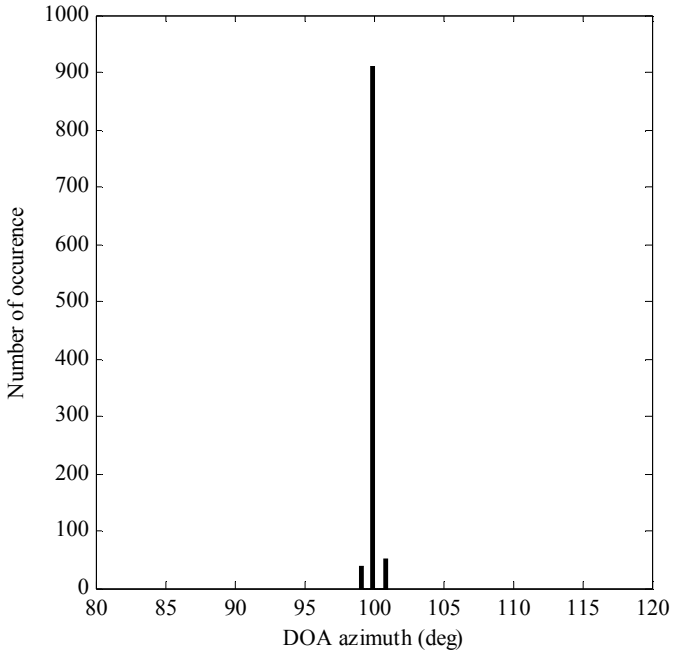

Figure 3.34: Histogram of azimuth estimation using the oval array. The DOA is at (θ=90°, φ=100°).

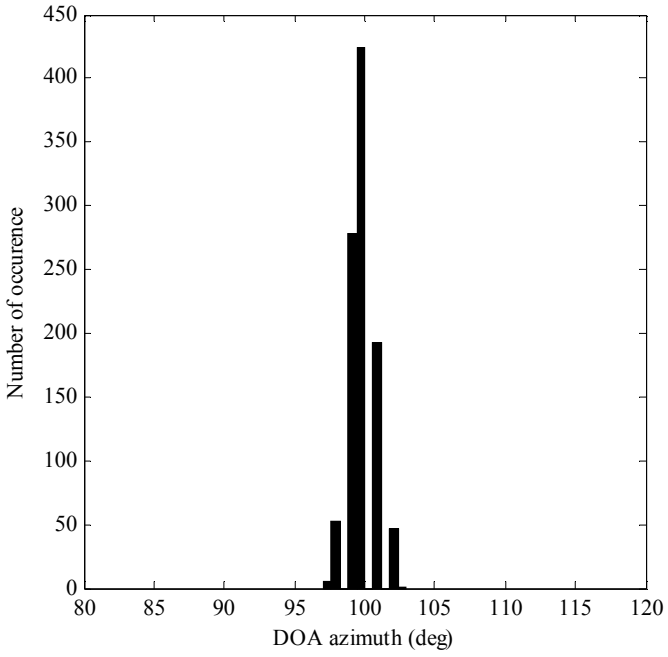

Figure 3.35: Histogram of azimuth estimation using the Y-bend array. The DOA is at (θ=90°, φ=100°).

3.4.4 Summary of comparison

Table 3.2 summarises the performance of estimation consistency for all the proposed arrays. In general, the semi-circular array holds the best performance of DOA estimation among all the proposed arrays. The oval array also has a comparable performance to the semi-circular array especially in the estimation consistency criterion. By contrast, the V-shape array possesses slightly larger estimation resolution and estimation error, but shows a very poor performance in estimation consistency.

Table 3.2: Comparison of array geometry based on DOA estimation performance

Antenna array geometry	Criteria of DOA estimation performance		
	Minimum resolution (deg)	Minimum RMSE (deg)	Consistency of estimation (%)
Semi-circular	15	0.05	95
Oval	20	0.50	90
Y-bend	25	1.50	40

3.5 Summary

This chapter has presented and discussed three new planar antenna arrays; the semi-circular array, the oval array, and the Y-bend array. The semi-circular array is proposed as a variation of the circular array. This chapter has shown that the semi-circular array outperforms the circular array in terms of estimation resolution, estimation error and estimation consistency. In particular, the semi-circular array improves the estimation resolution by 5.7%, the estimation error by at least 76%, and the estimation consistency by 20%. This implies that the estimation performance can be improved by concentrating the elements on one side of the circular configuration.

Furthermore, a comparison among the three proposed arrays also shows that the semi-circular array exhibits the best performance of DOA estimation. In this comparison, the semi-circular array achieves 25% smaller estimation resolution, ten times smaller estimation error, and 5% higher estimation consistency than the other two proposed arrays. These advantages suggest that the semi-circular array is an excellent choice of circular-based array for DOA estimation.

Another proposed array, the oval array, offers less area than the circular array. It has been shown that, with the same length of the circumference, the oval array has between 12.5% and 15% less area than the circular array. This, in turn, implies that the oval array would have less area than the circular array for the same number of elements. In addition, it has been shown that the oval array has improved the estimation resolution by 33%, the estimation error by at least 60%, and the estimation consistency by 20% of the circular array. These observations indicate that the DOA performance of the circular-based array could be improved by using the oval-shape configuration.

The third proposed array, Y-bend array, also shows significant improvement of DOA estimation over the V-shape array. Simulation results show that the Y-bend array improves the estimation resolution of the V-shape array by 23%. In addition, the Y-bend array achieves up to 88% lower estimation error and 7% higher estimation consistency than the V-shape array. However, the reduction in estimation error comes with larger array size, which is 33% more than the V-shape array.

This chapter has proposed three new antenna arrays that could improve DOA estimation performance over existing arrays. The improvement in estimation resolution, estimation error and estimation consistency has been shown numerically in simulation results. The next step is to investigate another factor that greatly influences the DOA estimation result, the DOA algorithm. The next chapter will propose a new DOA algorithm and apply it in elevation and azimuth angle estimation.

4 DOA Algorithm for Directional Antenna Arrays

This chapter presents DOA estimation using directional antenna arrays. The chapter starts by considering the difference of the estimation process using an isotropic antenna array and a directional antenna array. Next, a new DOA algorithm for directional antenna array is presented. The analysis of the proposed algorithm for elevation DOA estimation is also discussed. Finally, the proposed DOA estimation is applied in azimuth DOA estimation using the semi-circular array. In this chapter, DOA estimation is simulated using MATLAB®, and the directional antenna array is simulated using CST Microwave Studio®.

4.1 DOA estimation using isotropic and directional antenna arrays

4.1.1 Isotropic and directional element arrays

Isotropic elements radiate the energy equally in all directions as shown in Figure 4.1. The isotropic elements are often used as a reference to compare its radiation characteristics with directional elements. Directional elements, on the other hand, are defined as the elements that are able to concentrate the power primarily in certain directions or angular regions. Figure 4.2 shows a circular patch element that represents a directional element. The advantage of directional elements is that they can focus their power in a desired direction and suppress noise signal simultaneously. Power consumption is also reduced since power is only directed towards a certain narrow angle.

Figure 4.1: Radiation pattern of isotropic element

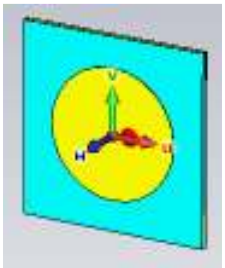

Figure 4.2: Circular patch antenna element

4.1.2 Comparison of estimation process

A comparison of the estimation process for an isotropic element array and a directional element array will be presented in this section by means of MATLAB simulation. The results of DOA estimations are then analysed to gauge how the algorithm performs in estimating the direction of incoming signals.

Simulation parameters for the isotropic array are as follows: element separation is 0.5λ, number of snapshots is 100, and it is assumed that there are sources of signal at (θ = -50°), (θ = 0°) and (θ = 60°). The result of the DOA estimation is shown in Figure 4.3. The position of peaks of spatial power spectrum indicates the estimation of direction of incoming signals. The results clearly indicate that all incoming signals could be estimated simultaneously using the isotropic antenna array.

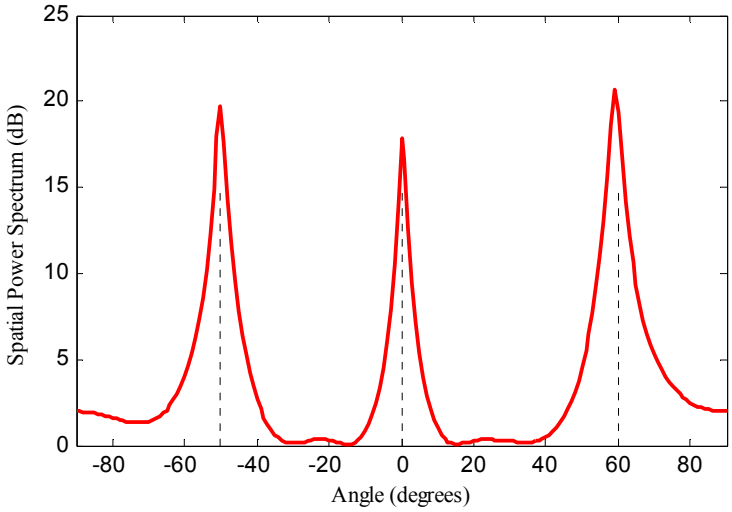

Figure 4.3: Spatial power spectrum of isotropic antenna array

The simulation is repeated with an array of directional elements, and the effect of mutual coupling is taken into account in order to obtain its radiation pattern. In the simulation, a linear array of eight circular patch elements with element separation of 0.5λ is used, as illustrated in Figure 4.4. The reflection loss of the array means the array approximately operates at 2.45GHz, as shown in Figure 4.5 and its radiation pattern, which has a narrow beam, is depicted in Figure 4.6.

Suppose the main beam of the array is pointed at 0° as shown in Figure 4.7. The DOA estimation process is performed by calculating the gain at different angular positions. The DOA estimation results clearly show only a single peak present in the spatial power spectrum, which is at an angle of 0°, as depicted by Figure 4.8.

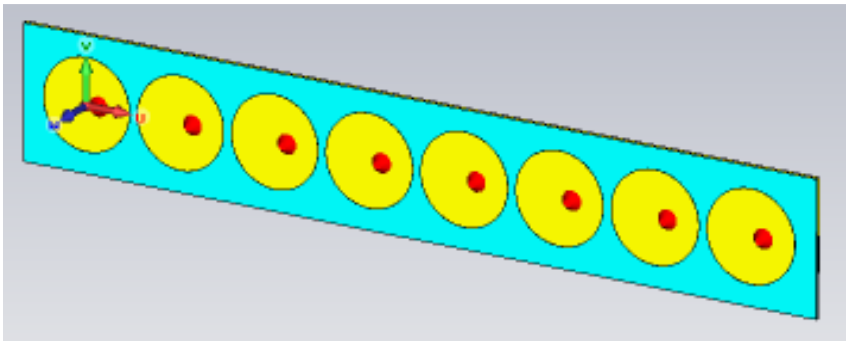

Figure 4.4: Circular patch antenna array

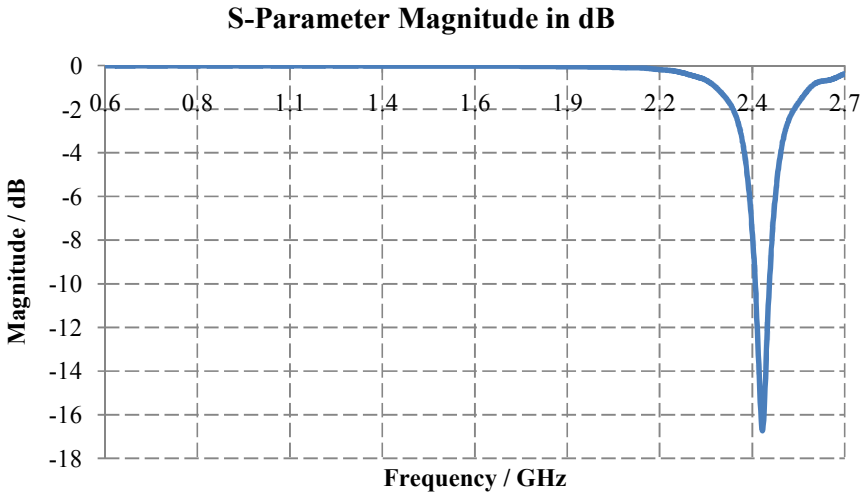

Figure 4.5: Reflection coefficient of the directional antenna array

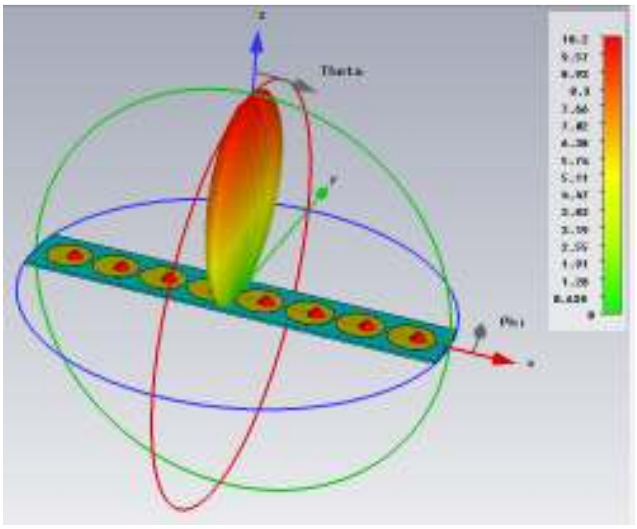

Figure 4.6: Radiation pattern of the linear antenna array

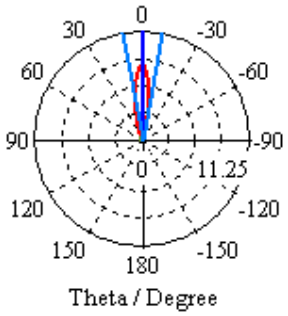

Figure 4.7: Radiation pattern of the directional antenna array with its main beam at 0°

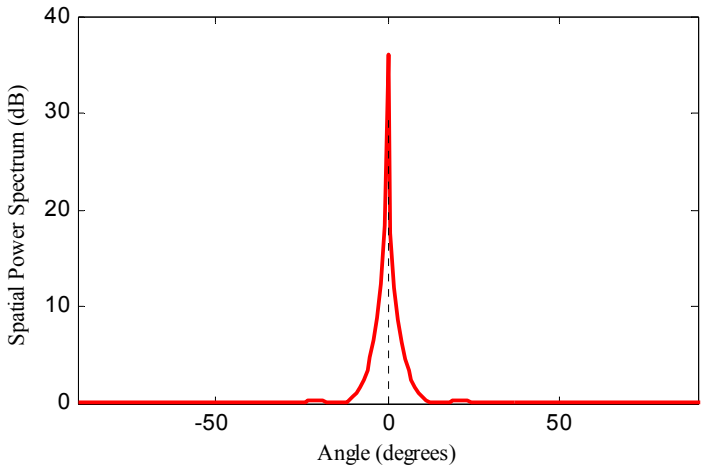

Figure 4.8: DOA estimation using the directional antenna array with its main beam at 0°

It appears that the position of the main beam determines the range of the angle of arrival that could be detected at any instant. This observation is verified as the main beam is moved to -50° and 60°, as shown in Figure 4.9 and Figure 4.11 respectively. The same process of DOA estimation is used in order to obtain the spatial power spectrum at both angular positions. The results shown in Figure 4.10 and Figure 4.12 confirm that the incoming signals can only be detected when they are within the range of the main beam position.

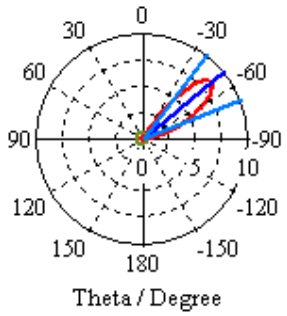

Figure 4.9: Radiation pattern of the directional antenna array with its main beam at -50°

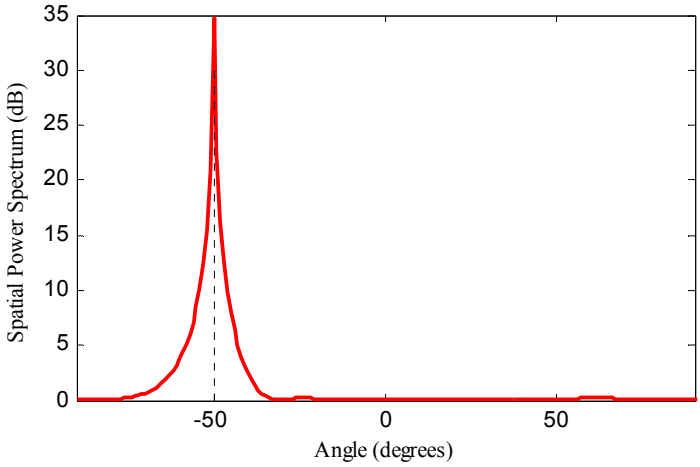

Figure 4.10: DOA estimation using the directional antenna array with its main beam at -50°

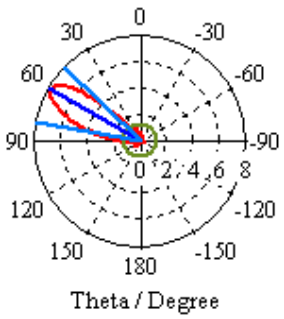

Figure 4.11: Radiation pattern of the directional antenna array with its main beam at 60°

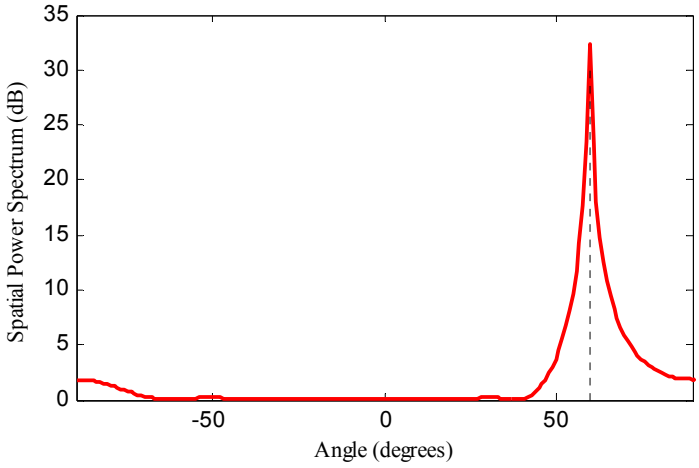

Figure 4.12: DOA estimation using the directional antenna array with its main beam at 60°

This observation also emphasises the importance of the position of the main beam during the DOA estimation process. In order to have an accurate estimation of the direction of the incoming signal, it is essential to ensure that the main beam can fully cover the angular position range required. Increasing the angular position range will increase the complexity of the estimation process.

4.1.3 Analysis of estimation in directional antenna array

There are several observations that can be made from the simulation results of DOA estimation. Firstly, simulation using isotropic antenna array generates multiple peaks in the spatial power spectrum, which indicates it is capable of detecting multiple signals simultaneously. It also implies that the DOA algorithm only needs to be performed once in order to acquire the estimation of angle of arrival for all incoming signals. On the other hand, the directional antenna array can only detect the incoming signals that fall within the range of the main beam position at one time. Therefore, in order to estimate all the angle of arrivals, the DOA algorithm should be applied repeatedly as the main beam moves to different angular positions.

Secondly, to ensure that the directional antenna array is able to estimate all angles of arrival, the main beam should be shifted to each possible elevation angles θ, in which ($-90° < \theta < +90°$). This is to ensure that the direction of incoming signals will coincide with the maximum gain of the array, and thus the DOA can be estimated correctly. However, performing this process will increase the processing time and computational complexity. Nevertheless, in order to reduce the complexity, the shifting process can be made in a pre-determined angle step, for example, at every 10°.

Thirdly, the gain of directional antenna array determines the height of the peak produced in the spatial power spectrum. This observation also explains the reason that the directional antenna array cannot detect signals beyond the range of the main beam at any instant. This is because the gain of the array is extremely low outside the main beam for an incoming signal to yield a significant output in spatial power spectrum. In short, the process of DOA estimation in a directional antenna array depends on the beam position, which affects the gain, as well as the DOA algorithm performance.

4.2 DOA algorithm for directional antenna arrays

In this section, a new DOA algorithm is proposed to suit the characteristic of directional antenna arrays. It has been shown that DOA estimation using the directional antenna array depends on the position of the main beam and its gain strength. The gain strength will fluctuate depending on the shape of the radiation pattern as the main beam moves from one angular position to another. Therefore, it is important to consider the gain values of the directional antenna array at any angular position of the main beam.

4.2.1 Motivation

The existing DOA algorithms work perfectly well with isotropic antenna arrays but cannot be used directly with directional antenna arrays for three reasons. Firstly, the radiation patterns of directional elements are narrow compared with isotropic elements. Secondly, the mutual couplings between the directional elements are quite significant and cannot be ignored. Thirdly, directional elements have different gains for distinct signal directions due to the narrow shape of the radiation pattern. All of these factors lead to the difficulty of using the existing DOA algorithms in directional antenna arrays. As a result, the directional antenna arrays require a DOA algorithm that would fit the characteristic of directional elements.

In this section, a new algorithm is proposed to suit the characteristic of directional antenna elements. The proposed algorithm is similar to the Capon algorithm in one aspect, which is to minimise power from all directions subject to distinct gain in the 'look direction'; hence it is named the Capon-like algorithm.

4.2.2 Data model

At time t, suppose there are K narrowband, uncorrelated signals impinging on an array of N elements and $K < N$. The signal output at the i^{th} element can be written as:

$$x_i(t) = \sum_{k=1}^{K} a_i(\theta_k) s_k(t) + n_i(t) \tag{4.1}$$

where $a(\theta)$, $s(t)$ and $n(t)$ are the steering vector, desired signal and noise signal respectively. In vector notation, (4.1) can be rewritten as:

$$\mathbf{x}(t) = \mathbf{A}(\theta)\mathbf{s}(t) + \mathbf{n}(t) \tag{4.2}$$

where

$$\mathbf{x}(t) = [x_1(t) \;\; x_2(t) \;\; \cdots \;\; x_N(t)]^T \tag{4.3}$$

$$\mathbf{s}(t) = [s_1(t) \;\; s_2(t) \;\; \cdots \;\; s_N(t)]^T \tag{4.4}$$

$$\mathbf{n}(t) = [n_1(t) \;\; n_2(t) \;\; \cdots \;\; n_N(t)]^T \tag{4.5}$$

$$\mathbf{A}(\theta) = [a_1(\theta) \;\; a_2(\theta) \;\; \cdots \;\; a_N(\theta)]^T \tag{4.6}$$

Moreover, when there are only L snapshots available for the estimation process, the signal data model becomes:

$$\mathbf{X} = \mathbf{AS} + \mathbf{N} \tag{4.7}$$

Next, assuming that the signals are second-order, stationary random process with the noise supposed to be white, the covariance matrix can be computed as follows:

$$\mathbf{R} = E[\mathbf{X}\mathbf{X}^H] \tag{4.8}$$

where $(\cdot)^H$ denotes complex conjugate transpose operation. However, since only limited L snapshots are available, the estimated covariance matrix computation becomes:

$$\hat{\mathbf{R}} = \frac{1}{L}\mathbf{X}\mathbf{X}^H \tag{4.9}$$

4.2.3 Capon-like algorithm

In the Capon algorithm, the DOA is estimated by minimising the received power of the incoming signal in all directions while maintaining a unity gain in 'look direction'. The constraint imposed on this algorithm is given as:

$$\min_{\mathbf{w}} \mathbf{w}^H \hat{\mathbf{R}} \mathbf{w} \quad subject\ to\ \mathbf{w}^H \mathbf{a}(\theta) = 1 \tag{4.10}$$

where **w** is the weight to be calculated. Applying the Lagrange optimisation method to the constraint yields the optimised weight:

$$\mathbf{w} = \frac{\hat{\mathbf{R}}^{-1}\mathbf{a}(\theta)}{\mathbf{a}^H(\theta)\hat{\mathbf{R}}^{-1}\mathbf{a}(\theta)} \tag{4.11}$$

The spatial power spectrum of the Capon algorithm can be determined using the optimised weight in (4.11) and given as:

$$P_{Capon} = \frac{1}{\mathbf{a}^H(\theta)\hat{\mathbf{R}}^{-1}\mathbf{a}(\theta)} \tag{4.12}$$

The proposed algorithm is a modified version of the Capon algorithm that is targeted to work with the directional antenna array. As shown in 4.1, it is essential to express the steering vector with its corresponding gain when using directional antenna. Therefore, the steering vector in the directional antenna array can be expressed as the following:

$$\mathbf{a}_d(\theta_i) = g(\theta_i)\mathbf{a}(\theta_i) \tag{4.13}$$

where $g(\theta_i)$ is the array gain in a distinct direction θ. For antenna arrays with isotropic elements, $g(\theta_i)$ is equal to 1 for i = 1,2,…,N. However, in the case of antenna arrays with directional elements, $g(\theta_i)$ is determined from the array gain pattern and thus significantly affects the values of $a(\theta_i)$. Consequently, for K incoming signals impinging a directional array, the array manifold is also changed as the following:

$$\begin{aligned}\mathbf{A} &= \left[g(\theta_1)\mathbf{a}(\theta_1) \;\; g(\theta_2)\mathbf{a}(\theta_2) \;\; \cdots \;\; g(\theta_K)\mathbf{a}(\theta_K)\right] \\ &= \left[\mathbf{a}_d(\theta_1) \;\; \mathbf{a}_d(\theta_2) \;\; \cdots \;\; \mathbf{a}_d(\theta_K)\right]\end{aligned} \tag{4.14}$$

Furthermore, since the array response is affected by the gain pattern in a 'look direction', the constraint in the Capon-like algorithm can be given by:

$$\min_{\mathbf{w}} \mathbf{w}^H \hat{\mathbf{R}} \mathbf{w} \quad \textit{subject to } \mathbf{w}^H \mathbf{a}(\theta) = \mathbf{g}(\theta) \tag{4.15}$$

Applying Lagrange optimisation technique to the constraint in (4.15) yields the Lagrange multiplier, λ, and weight $\mathbf{w}$ given by (4.16) and (4.17) respectively.

$$\lambda = -\frac{\mathbf{g}^H(\theta)}{\mathbf{a}^H(\theta)\hat{\mathbf{R}}^{-1}\mathbf{a}(\theta)} \tag{4.16}$$

$$\mathbf{w} = \frac{\hat{\mathbf{R}}^{-1}\mathbf{a}(\theta)\mathbf{g}^H(\theta)}{\mathbf{a}^H(\theta)\hat{\mathbf{R}}^{-1}\mathbf{a}(\theta)} \tag{4.17}$$

Finally, the power spectrum of the Capon-like algorithm is given as:

$$P = \frac{\mathbf{a}^H(\theta)\mathbf{a}(\theta)}{\mathbf{a}^H(\theta)\hat{\mathbf{R}}^{-1}\mathbf{a}(\theta)} \tag{4.18}$$

4.2.4 Angular estimation

Computer simulations are conducted to evaluate the performance of the Capon-like algorithm. This section compares the performance of the Capon-like and the Capon algorithms in elevation angle estimation. The simulation results presented in this section use a linear array of circular patch shown in Figure 4.4. Suppose there is a signal impinging the directional antenna array at 30°, SNR is fixed at 0dB, and the number of snapshots is 100.

Figure 4.13 shows a comparison of DOA estimation between the Capon and Capon-like algorithms. Estimation result using the Capon algorithm yields many spurious peaks in the spatial power spectrum that could lead to inaccurate estimation. Although there is a peak appearing at 30°, the DOA will be estimated based on the

highest peak strength, which appears at -50°. On the other hand, the Capon-like algorithm manages to estimate the DOA correctly and suppress the spurious peaks. The simulation is repeated for multiple signals with the same SNR and number of snapshots, and the signals are assumed at elevation angles of 5°, 20° and 35°.

Results in Figure 4.14 also show that the Capon-like algorithm managed to estimate the direction of all three signals correctly without any spurious peaks. In contrast, the Capon algorithm produced many spurious peaks and was unable to estimate the true DOA. Therefore, the observations in both results show that the Capon-like algorithm has better performance compared to the Capon algorithm.

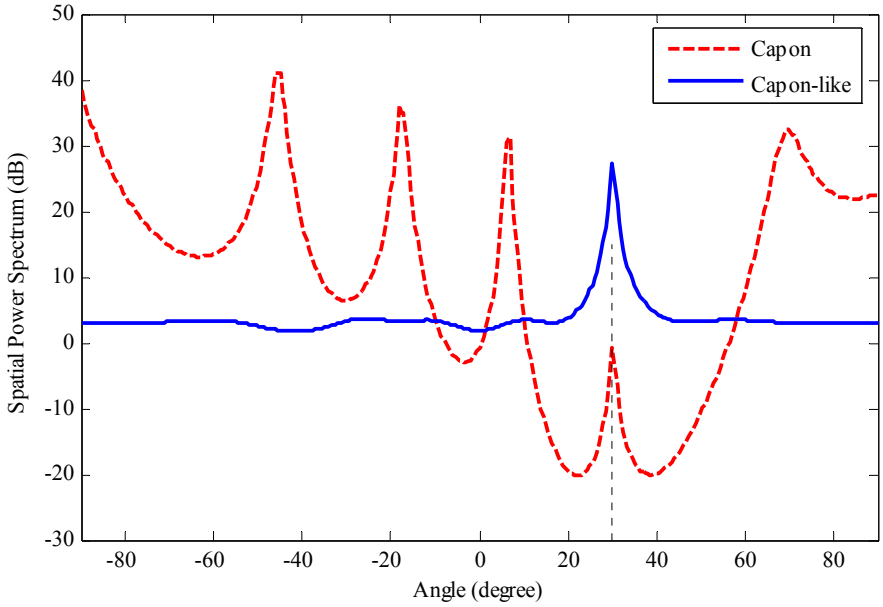

Figure 4.13: Comparison of DOA estimation between the Capon and Capon-like algorithms for single signal impinging at (θ=30°). Dotted line represents the true DOA.

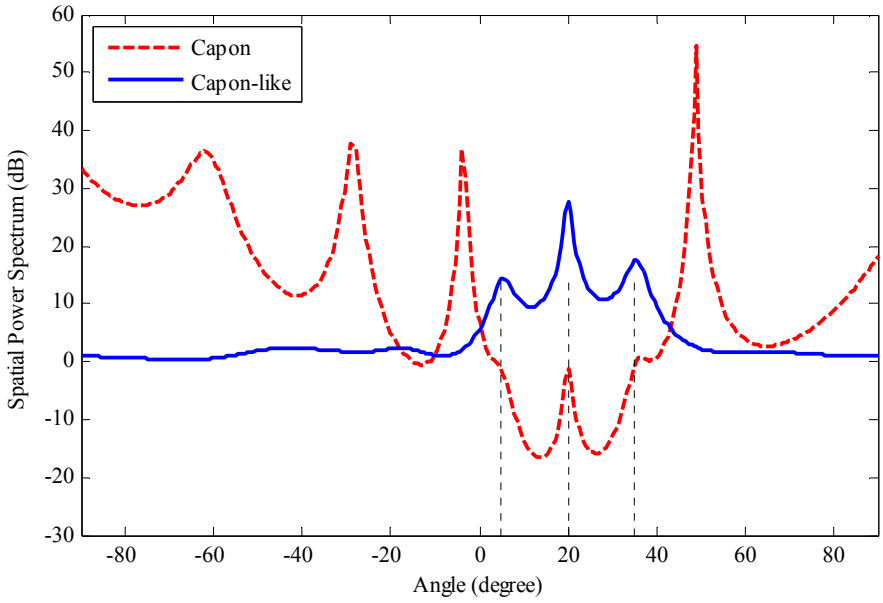

Figure 4.14: Comparison of DOA estimation between the Capon and Capon-like algorithms for multiple signals impinging at (θ=5°), (θ=20°) and (θ=35°). Dotted lines represent the true DOA.

4.2.5 Error of estimation

Next, it is important to compare the estimation results between the Capon and Capon-like algorithm in terms of estimation error. All the simulation results in this section use the RMSE, which is given in (3.13).

In this simulation, it is assumed that there is a single signal impinging the array at 5°. Figure 4.15 shows the RMSE versus SNR for both the Capon and Capon-like algorithms when the number of snapshots is fixed at 100. As the SNR is increased, the RMSE of the Capon-like algorithm is improved significantly, whereas the RMSE of the Capon algorithm does not show any significant changes. It is observed that the Capon-like algorithm produced at least 150 times lower RMSE than the Capon algorithm. The huge estimation error produced by the Capon algorithm is due to the spurious peak positions as seen in Figure 4.13 and Figure 4.14, which lead to false estimations. The observation suggests that the performance of the Capon-like algorithm is vastly superior compared with the Capon algorithm.

Next, the RMSE estimation of both the Capon and Capon-like algorithms are presented in Figure 4.16 with the SNR fixed to 0dB and the number of snapshots varying from 40 to 100. The same pattern in the results is observed, in which the Capon algorithm produced RMSE at least 150 times higher than the Capon algorithm. This observation is likely caused by the spurious peaks present in the Capon algorithm, which lead to a very large estimation error.

Finally, Figure 4.17 illustrates the effect of DOA separation between two signal sources on RMSE for both Capon and Capon-like algorithms. In this case, the first signal remains at 5°, and the second signal is varied between 10° and 20°. The results suggest that the Capon-like algorithm have at least 27 times lower RMSE than the Capon algorithm.

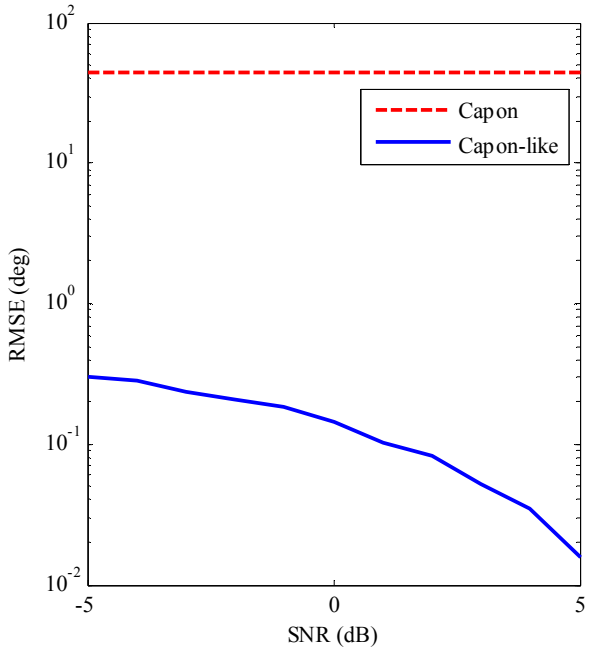

Figure 4.15: RMSE of DOA estimation for various SNR when number of snapshots is 100. The DOA is at ($\theta = 5°$).

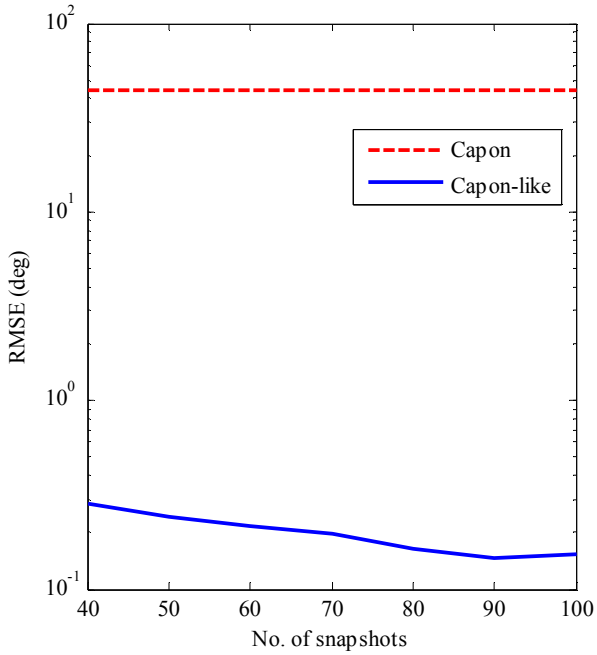

Figure 4.16: RMSE of DOA estimation versus number of snapshots when SNR is 0dB. The DOA is at ($\theta = 5°$).

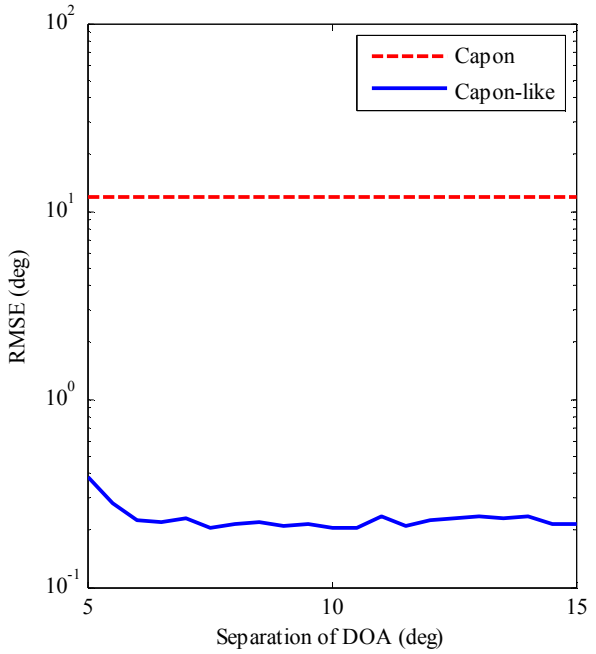

Figure 4.17: RMSE of DOA estimation for various signal separations when number of snapshots is 100 and SNR is 0dB. The DOAs are at ($\theta = 5°$) and ($10° < \theta < 20°$).

4.2.6 Consistency of estimation

In this section, a comparison of estimation consistency was presented between the Capon and Capon-like algorithms. It is assumed that the number of snapshots is 100, SNR level is 0dB, the number of trials is 1000, and the elevation DOA is at θ=5°. As shown in Figure 4.18, the Capon-like algorithm has 90% estimation consistency. On the other hand, the Capon algorithm produced a false estimation at 49°. The results also reflect that the Capon-like algorithm possessed a high reliability to estimate close-to-true DOA. Furthermore, the Capon-like algorithm also eliminates false estimation produced by the Capon algorithm when using the directional antenna array.

The observations made on the spatial spectrum, the estimation error and estimation consistency clearly show that the Capon-like algorithm yields better estimation results than the Capon algorithm. The reason for this is that the Capon-like algorithm takes into account the gain of the directional antenna array at every angular position of the main beam. The Capon algorithm, on the other hand, is designed to work for the isotropic antenna array and does not consider the radiation pattern of directional antenna array. This factor, in turn, leads to a huge difference in terms of estimation results between the two algorithms.

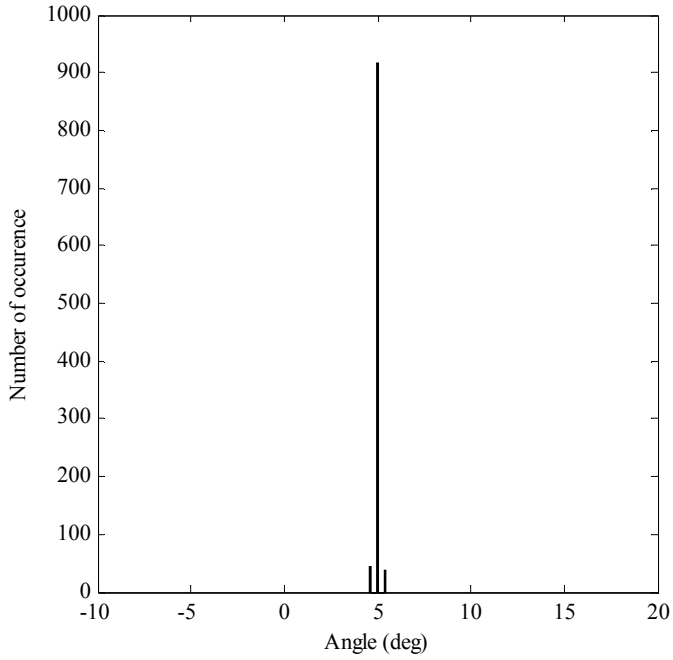

Figure 4.18: Histogram of DOA estimation using the Capon-like algorithm. The DOA is at (θ=5°).

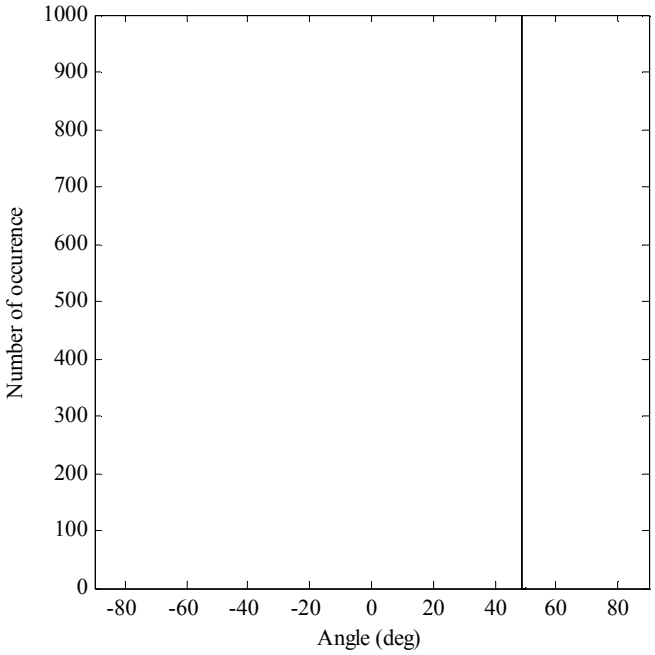

Figure 4.19: Histogram of DOA estimation using the Capon-like algorithm. The DOA is at (θ=5°).

4.3 Capon-like algorithm for azimuth estimation

In this section, the application of the Capon-like algorithm will be extended to azimuth angular estimation. The azimuth estimation process will use the semi-circular antenna array which was introduced in Chapter 3. The performance of both the Capon and Capon-like algorithm will be compared in terms of estimation resolution, estimation error, and estimation consistency.

4.3.1 Semi-circular directional antenna array

A semi-circular array of eight elements is shown in Figure 4.20. The elements are the same as in the linear array shown in Figure 4.4. Spacing between the elements is fixed to 0.5λ, where λ is the wavelength of incoming signal. The radiation pattern of the semi-circular array is shown in Figure 4.21 with the main beam at θ = 0°. The operating frequency of the semi-circular array is 2.45 GHz, as illustrated in Figure 4.22.

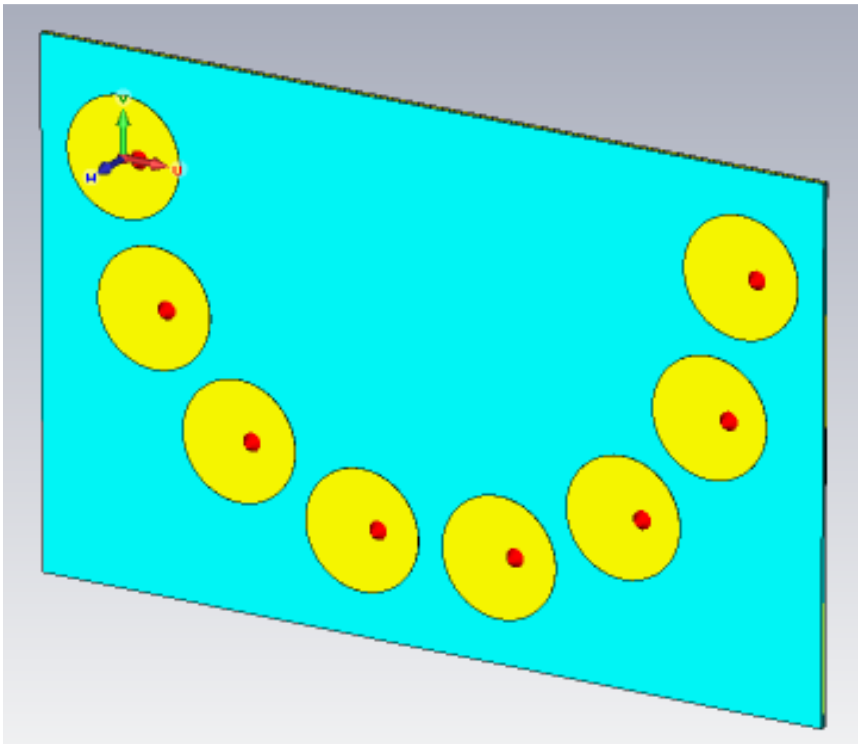

Figure 4.20: A semi-circular array of eight circular patch elements

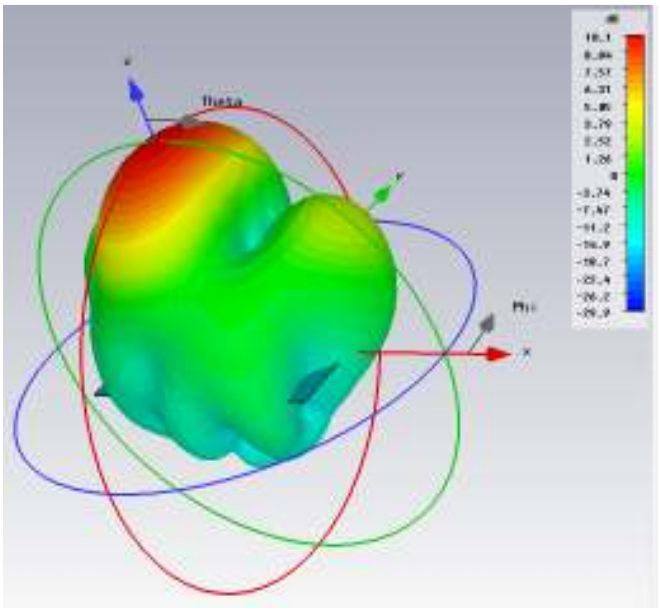

Figure 4.21: Radiation pattern of the semi-circular array

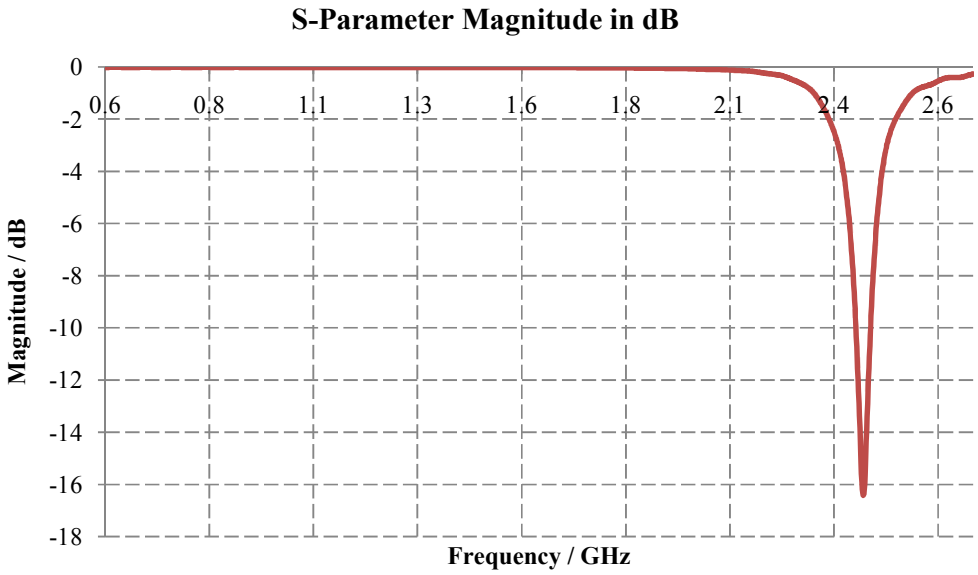

Figure 4.22: Reflection coefficient of the semi-circular array

4.3.2 Angular estimation

Comparison of azimuth estimation between the Capon algorithm and the Capon-like algorithm is performed in this section. It was pointed out in 4.1.3 that the position of the main beam is essential in DOA estimation when using directional antenna array. Therefore, the radiation pattern of the semi-circular array must be obtained before performing the comparison of azimuth estimation. Figure 4.23 – Figure 4.28 illustrate the importance of the main beam position in obtaining an accurate DOA estimation of incoming signal. There are three cases of azimuth estimation for comparing the Capon and Capon-like algorithms.

Firstly, it is assumed that the true DOA is at 5°. The array gain shown in Figure 4.23 is used to calculate the steering vector described in (4.13). Estimation results in Figure 4.24 show that the Capon-like algorithm managed to estimate the true DOA without any spurious peaks. In contrast, the Capon algorithm was unable to estimate the true DOA and there are two spurious peaks at 20° and 340°. Secondly, it is assumed that the true DOA is impinging the array at 180°. Using the array gain shown in Figure 4.25, the estimation result is obtained as illustrated in Figure 4.26. The result shows that the Capon-like algorithm manages to estimate the true DOA. On the other hand, the Capon algorithm produces two false estimations at 160° and 200°. Finally, it is assumed there is a signal impinging the array at 220°. Using the array gain shown in Figure 4.27, estimation results of the Capon and Capon-like algorithms are illustrated in Figure 4.30. As observed in the previous cases, the Capon-like algorithm successfully estimates the true DOA whereas the Capon algorithm fails to do so.

These results clearly depict the superiority of the Capon-like algorithm over the Capon algorithm in azimuth estimation. Moreover, these results also emphasise the importance of main beam position in DOA estimation when using the directional antenna array.

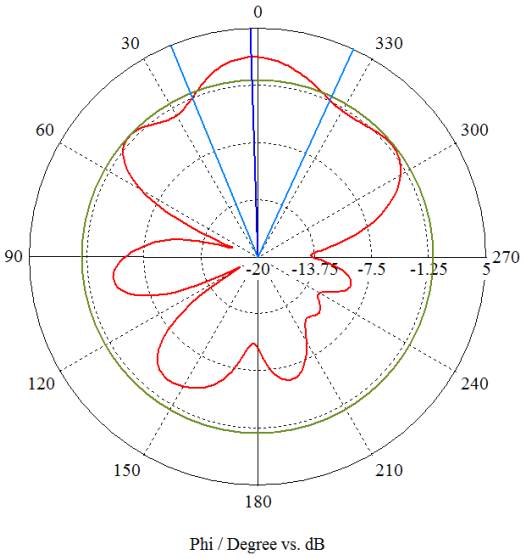

Figure 4.23: Radiation pattern of the semi-circular array for 0°<φ<360° and θ = 90°. The main beam is pointing at φ = 2°.

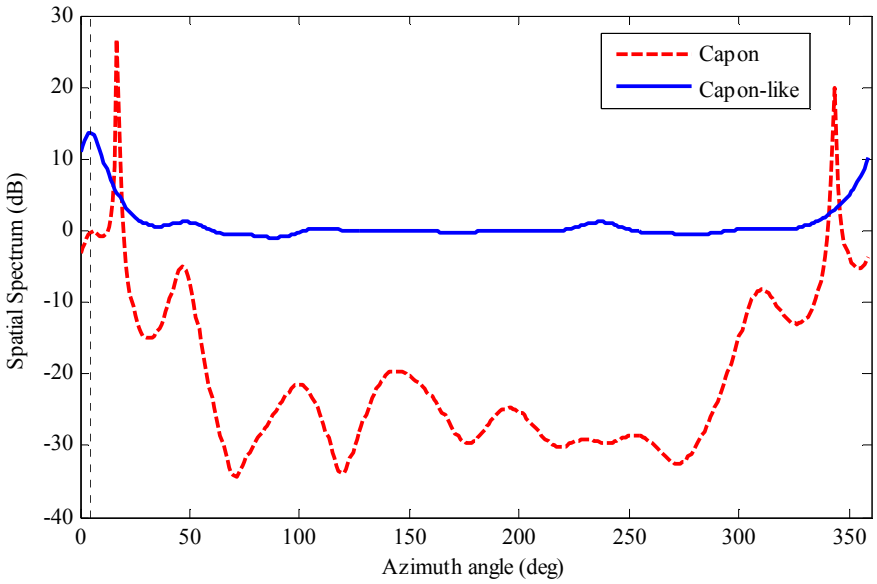

Figure 4.24: Comparison of DOA estimation between the Capon and Capon-like algorithms for signal impinging at (φ=5°). Dotted line represents the true DOA.

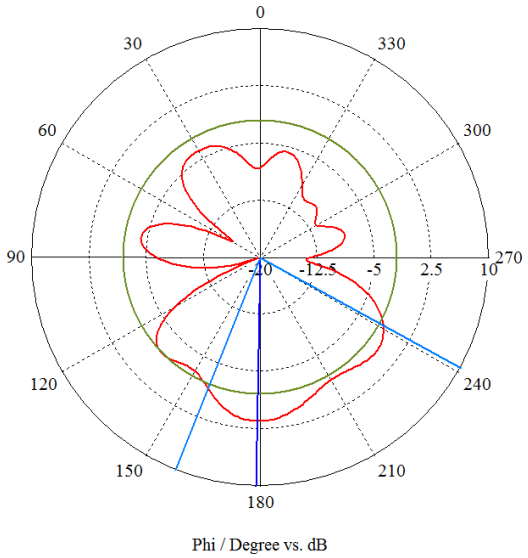

Figure 4.25: Radiation pattern of the semi-circular array for 0°<φ<360° and θ = 90°. The main beam is pointing at φ = 179°.

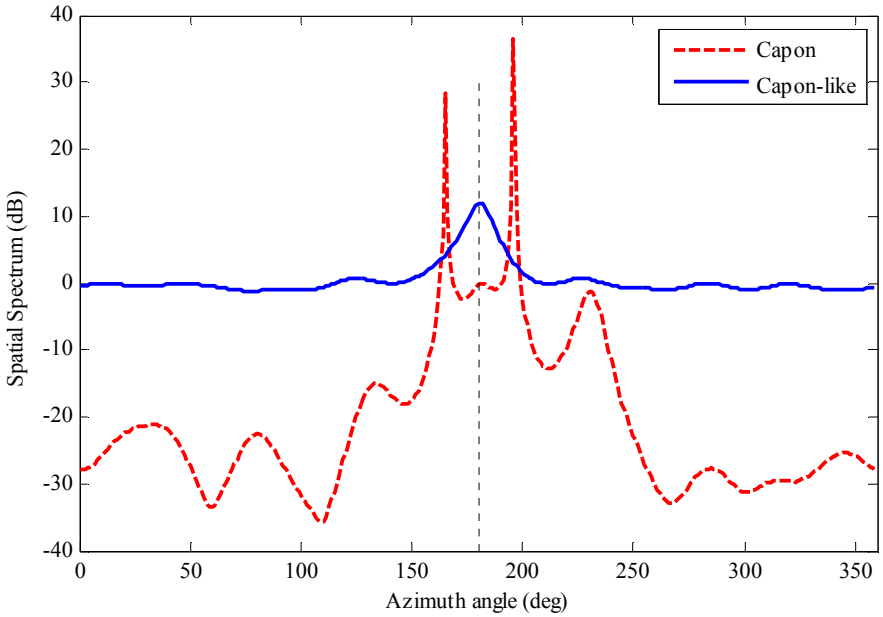

Figure 4.26: Comparison of DOA estimation between the Capon and Capon-like algorithms for signal impinging at (φ=180°). Dotted line represents the true DOA.

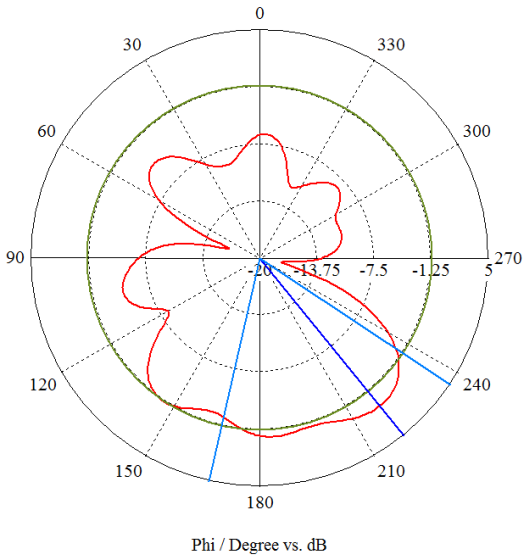

Figure 4.27: Radiation pattern of the semi-circular array for 0°<φ<360° and θ = 90°. The main beam is pointing at φ = 219°.

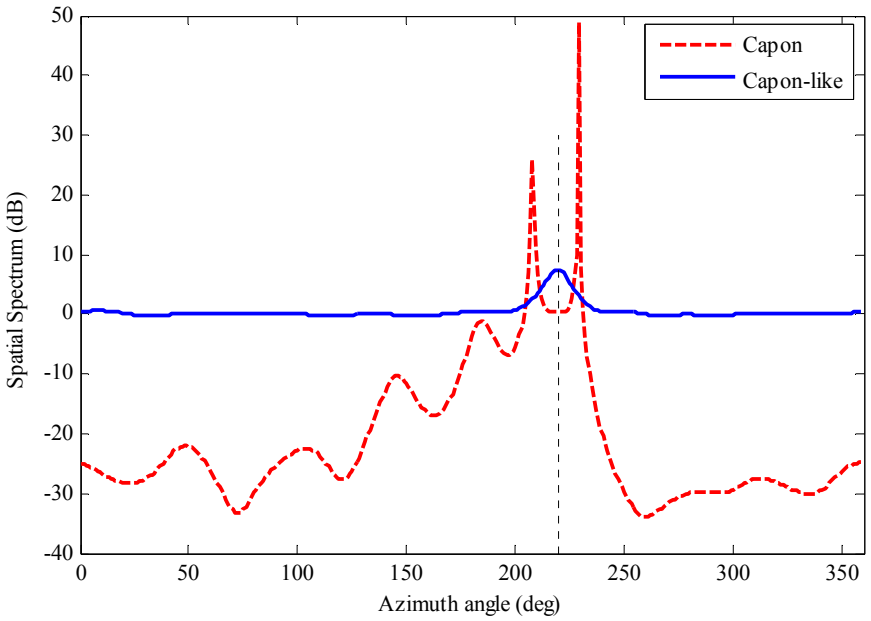

Figure 4.28: Comparison of DOA estimation between the Capon and Capon-like algorithms for signal impinging at (φ=220°). Dotted line represents the true DOA.

4.3.3 Error of estimation

This section presents comparison of estimation error between the Capon and Capon-like algorithms. There are two cases of comparison being considered; estimation error for varied SNR, and for varied number of snapshots. Throughout the simulations, it is assumed that there is one incoming signal impinging the array at (θ=90°, φ=180°).

Figure 4.29 shows the RMSE for both the Capon and Capon-like algorithms when the SNR is fixed at 0dB. It is apparent that the Capon-like produced at least 30 times lower RMSE than the Capon algorithm. The same observation is also obtained when the number of snapshots is fixed to 100 as shown in Figure 4.30. The RMSE of the Capon-like algorithm is improved as the number of snapshots is increased but the RMSE of the Capon algorithm remains unchanged. The Capon-like algorithm is able to produce RMSE up to 75 times lower than the RMSE of the Capon algorithm.

As shown in Figure 4.23 and Figure 4.25, the Capon-like algorithm is able to eliminate spurious estimation unlike the Capon algorithm. This difference helps to produce huge improvement in estimation error. These results also suggest that the array gain information must be considered in azimuth estimation when using directional antenna array.

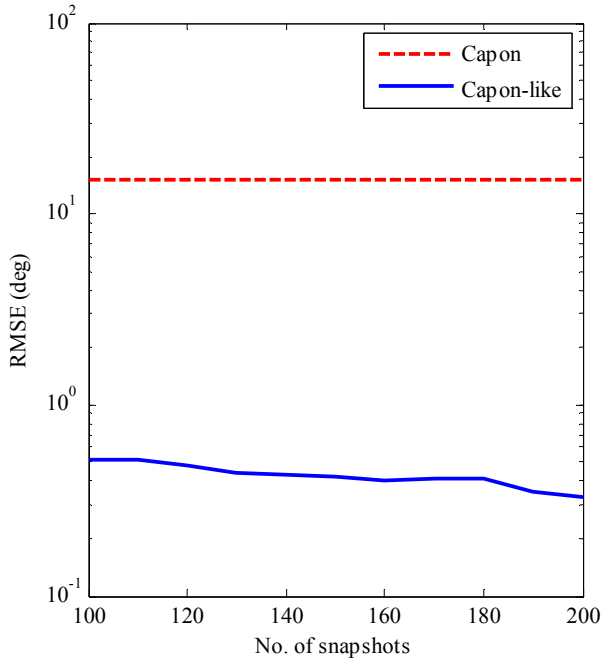

Figure 4.29: RMSE of DOA estimation versus number of snapshots when SNR is 0dB. The DOA is at (φ = 180°).

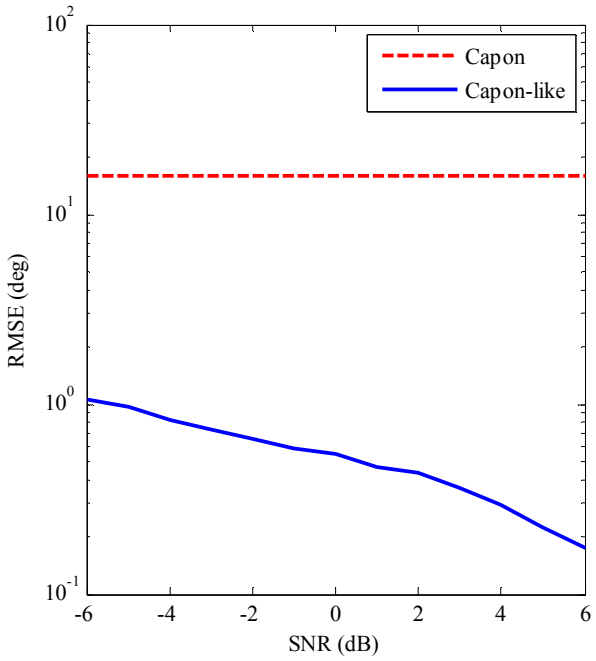

Figure 4.30: RMSE of DOA estimation for various SNR when number of snapshots is 100. The DOA is at (φ = 180°).

4.3.4 Consistency of estimation

This section presents the performance of the Capon and Capon-like algorithms in terms of estimation consistency. It is assumed that the number of snapshots is 100, SNR level is 0dB, and the number of trials is 1000. In the first case, the true DOA is assumed to be $\varphi = 10°$. Figure 4.31 and Figure 4.32 depict that the estimation consistency is 97% and 72% for the Capon and Capon-like algorithms respectively. These results suggest that the Capon algorithm achieves higher consistency than the Capon-like algorithm. However, the estimation of the Capon algorithm occurs at $\varphi = 17°$, slightly off the true DOA. The Capon-like algorithm manages to estimate the correct DOA although with a lower consistency than the Capon algorithm.

In the second case, it is assumed that the true DOA is at $\varphi = 180°$. As shown in Figure 4.33 and Figure 4.34, the Capon algorithm achieves higher consistency than the Capon-like algorithm. Nevertheless, as in the first case, high consistency of the Capon algorithm is achieved at inaccurate estimation. Although the Capon algorithm seems to achieve 96% consistency, 20% higher than the Capon-like algorithm, it occurs at 165°, 15° off the true DOA.

The poor result of the Capon algorithm is caused mainly due to spurious estimation as presented in 4.3.2. The same pattern of results was also shown in 4.2.6, in which the highest occurrence of estimation was far off the true DOA.

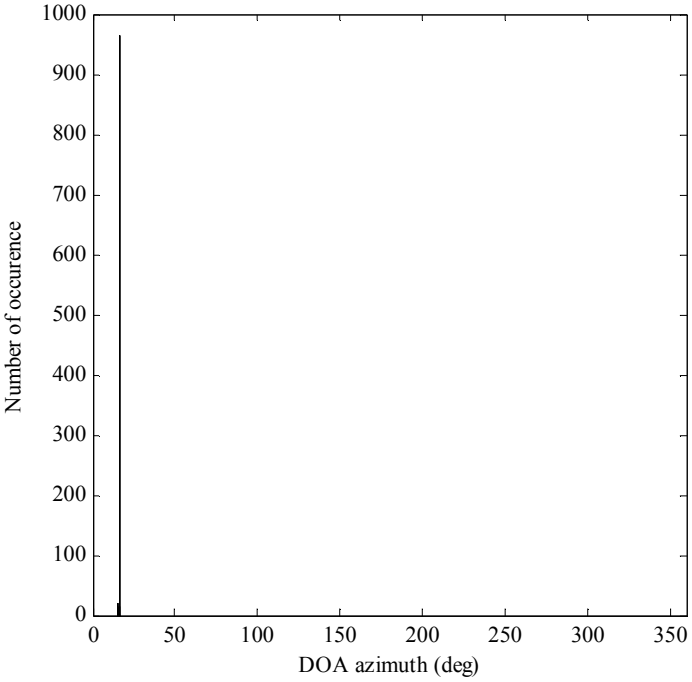

Figure 4.31: Histogram of DOA estimation using Capon-like algorithm. The DOA is at (φ=10°). The highest occurrence is at 17°.

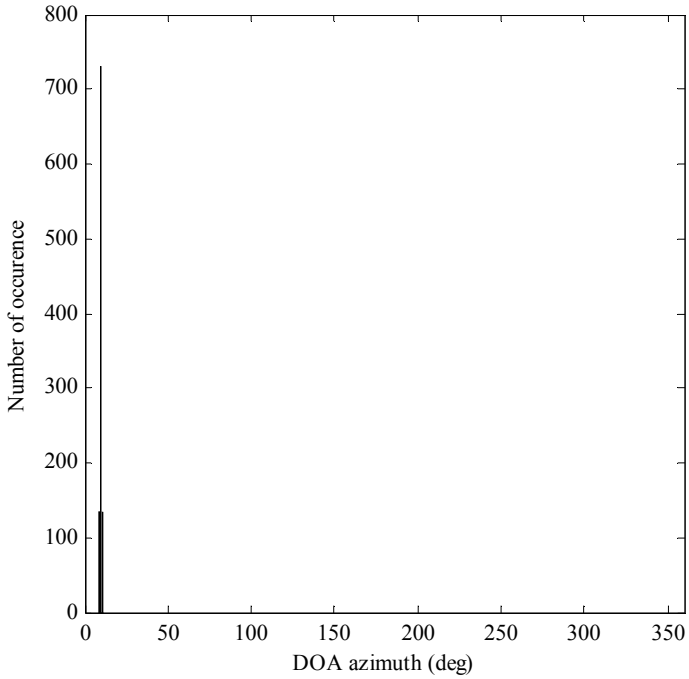

Figure 4.32: Histogram of DOA estimation using Capon-like algorithm. The DOA is at (φ=10°). The highest occurrence is at 10°.

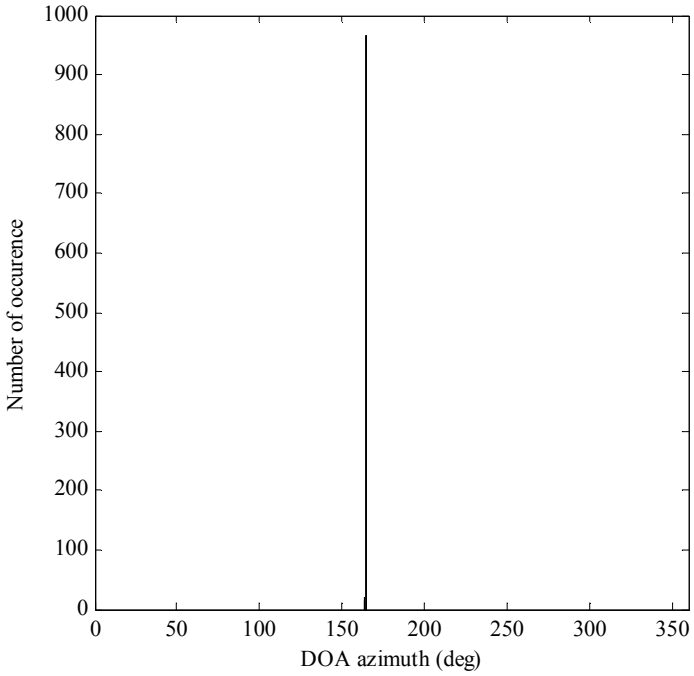

Figure 4.33: Histogram of DOA estimation using Capon algorithm. The DOA is at (φ=180°). The highest occurrence is at 165°.

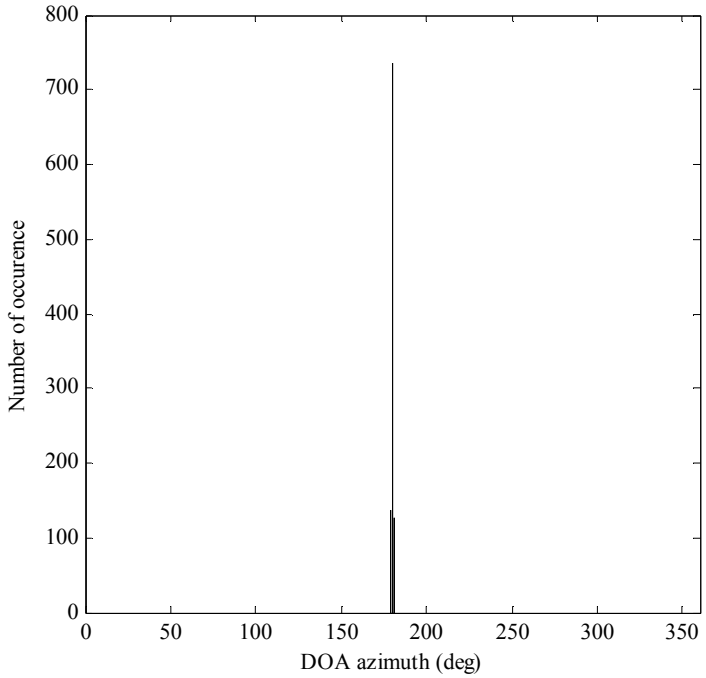

Figure 4.34: Histogram of DOA estimation using Capon-like algorithm. The DOA is at (φ=180°). The highest occurrence is at 180°.

4.4 Summary

This chapter has presented the process of DOA estimation for directional antenna arrays and proposed a modification to the DOA algorithm to suit the characteristics of directional antennas. DOA estimation for isotropic antennas is fairly straightforward to analyse but this is not a real situation as the antenna does not exist. Furthermore, the directional antennas also have unique properties such as gain-phase, which must be taken into account in DOA estimation. Therefore, this chapter has intended to investigate the process of DOA estimation when using directional antenna arrays. In this chapter, three cases of DOA estimation that involved directional antenna arrays have been presented.

In the first part of this chapter, it has been shown that the antenna power concentration is different between the isotropic and directional antennas. Isotropic antennas have uniform power in all direction, whereas the directional antennas focus their power on a distinct direction. As a result, the difference of distribution of power in those antenna arrays affects the process in DOA estimation. Another important point worthy of mention is that the position of the main beam of a directional antenna array plays a significant role in the DOA estimation process. These factors are noticeable when comparing the results of DOA estimation between the two arrays. The DOA of incoming signals can only be estimated if the direction falls within the range of the main beam of directional antenna arrays. Thus, it is essential to move the main beam of the directional antenna array into every angular position in order to have an accurate estimation.

The second part of this chapter proposed a new algorithm to work with directional antenna arrays. The new algorithm is essentially a modified version of the Capon algorithm, which includes the gain information of the directional antenna array. The proposed algorithm depends on an idea that the steering vector in directional antenna arrays should include the gain of a particular angular position. This is in contrast with the case of using the isotropic antenna, which assumes that the gain of antenna array will always be equal to one. The modification leads to the calculation of a spatial power spectrum that considers the antenna array gain in DOA estimation. Simulation

results show that the proposed algorithm managed to estimate the elevation DOA of incoming signals. On the other hand, the Capon algorithm produced many spurious peaks which represent false estimation of direction of incoming signals. Furthermore, comparison study shows that the proposed algorithm has at least 27 times lower estimation error than the Capon algorithm. The proposed algorithm also has 90% higher consistency of estimation than the Capon algorithm.

The final part of this chapter presented the application of the proposed algorithm for azimuth DOA estimation. The azimuth estimation was using the semi-circular array which had been introduced in Chapter 3. Simulation results suggest that the proposed algorithm maintains its superiority over the Capon algorithm in terms of estimation error and estimation consistency. The proposed algorithm produces at least 30 times lower estimation error than the Capon algorithm. Moreover, the proposed algorithm also possesses 20% higher estimation consistency than the Capon algorithm. Furthermore, the Capon algorithm also consistently estimates 15° off the true DOA. A huge improvement of the proposed algorithm is due to its ability to eliminate false estimation compared to the Capon algorithm. In short, the results emphasise that the array gain should be included in steering vector calculation.

This chapter has emphasised the importance of modification in the DOA estimation process as well as in the DOA algorithm. The modification is related to the inclusion of array gain information in DOA estimation when using directional antenna array. The improvement in the estimation result is very significant as shown numerically in simulations. The next chapter will look into the effect of antenna array gain in covariance matrix calculation, an important component in the estimation process. A new method of covariance matrix will be proposed and then applied in elevation and azimuth estimation.

5 Estimation Method for Directional Antenna Arrays

This chapter presents a new method of DOA estimation for directional antenna arrays. In the proposed method, the estimation process is made possible through a modified covariance matrix. The modification is due to an additional determination of antenna array gain in calculating the covariance matrix. The first part of this chapter presents the proposed method and its application in elevation angle estimation. The next part analyses the azimuth angle estimation using the proposed method. In this chapter, DOA estimation is simulated using MATLAB®, and the directional antenna array is simulated using CST Microwave Studio®.

5.1 Elevation angle estimation with modified covariance matrix

In the previous chapter, the importance of gain strength of the directional antenna array was demonstrated. Taking into account the gain strength in the DOA estimation process generates an accurate estimation of the DOA of incoming signals in the directional antenna array. The next step is to investigate another approach of the estimation process in the directional antenna array. In this chapter, an alternate method of calculation to obtain the covariance matrix will be presented, a method which will potentially lead to better results in DOA estimation.

5.1.1 Motivation

The previous chapter has shown that it is vital to modify the existing DOA algorithms to accommodate the characteristic of directional antenna arrays. The modification is also important to differentiate the estimation process whether using isotropic or directional antennas. The changes are driven by the shape of the radiation pattern when the array is pointed in different angular positions. The change in radiation pattern leads to changing of gain strength the directional antenna array. Since the antenna gain is a unique property of an antenna, its changes must be

considered in DOA estimation when using the directional antenna array. This factor is further investigated in this chapter but using a different approach. Rather than employing the antenna array gain in the steering vector, another approach is to utilise it in the calculation of the covariance matrix.

Since the covariance matrix is an important component in estimating the DOA, the characteristic of directional antenna array could be considered to obtain the covariance matrix. This section will present a new method for calculating the covariance matrix. A distinct modification in the proposed method is the inclusion of gain of the antenna array in the covariance matrix calculation. The inclusion will reflect changes of the antenna array gain as the array is swept across a range of 'look directions', either in azimuth or elevation angles.

5.1.2 Proposed method

The proposed method introduces modification in the process to form the covariance method. Unlike in the conventional approach, each entry in the covariance matrix is a combination of output of an element and its corresponding maximum gain at a particular angular position. Suppose a symmetric matrix $\mathbf{G_S}$, composed of element gains, is defined as the following:

$$\mathbf{G}_S = \begin{pmatrix} g_{11} & g_{12} & \cdots & g_{1N} \\ g_{21} & g_{22} & \cdots & g_{2N} \\ \vdots & \vdots & \ddots & \vdots \\ g_{N1} & g_{N2} & \cdots & g_{NN} \end{pmatrix} \tag{5.1}$$

where the diagonal entries (g_{11}, g_{22},$\cdots$, g_{NN}) are the individual element gains and the rest of the entries (g_{12}, g_{13},$\cdots$, g_{1N}) are the gain of two elements. In other words, g_{12} represents the gain of elements 1 and 2, g_{13} is the gain of elements 1 and 3, and so on. The gain of two elements is obtained by turning on only two elements at a time, and the rest of the elements are turned off.

In general, for an array of N elements, a total of $\frac{(N+r-1)!}{r!(N-1)!}$ element gain must be determined to form the $\mathbf{G_S}$ matrix. The approach in the proposed method is to combine the output of an element with its corresponding gain. In other words, the covariance matrix in (4.9) can be rewritten as:

$$\hat{\mathbf{R}}_g = \hat{\mathbf{R}} \bullet \mathbf{G}_S \tag{5.2}$$

It is noted that the element-wise multiplication operation is used rather than the normal matrix multiplication. This is to ensure the entry in new covariance matrix, $\hat{\mathbf{R}}_g$, will pair both the output and corresponding gain of an element.

The next step is to perform the proposed method on the directional antenna array to evaluate its performance in DOA estimation. Figure 5.1 shows eight circular patch elements in a uniform linear array with element separation of 0.5λ. The radiation pattern of the first element (g_1), and between the first element and the subsequent elements (g_{12}, g_{13},$\cdots$, g_{18}) are shown in Figure 5.2. The maximum gain from the radiation pattern will be taken as the first row entries in the matrix $\mathbf{G_S}$. Since there are eight elements in the array, there will be 36 unique element gains that must be defined in order to form the symmetric matrix $\mathbf{G_S}$. In the next section, the proposed method refers to the covariance matrix defined in (5.2) and the conventional method refers to the covariance matrix described in (4.9).

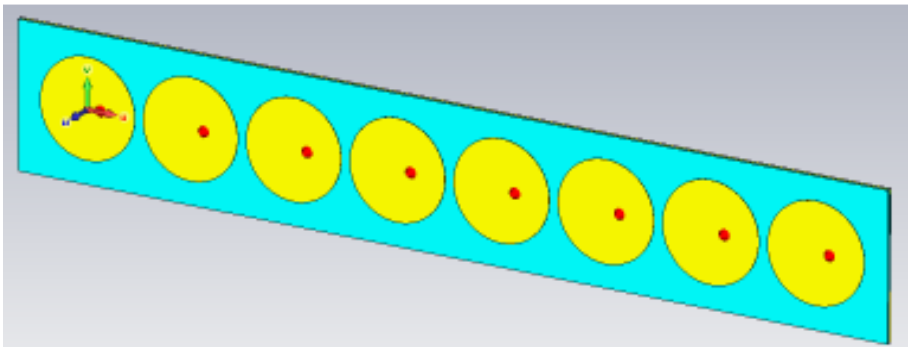

Figure 5.1: Linear array of circular patch elements

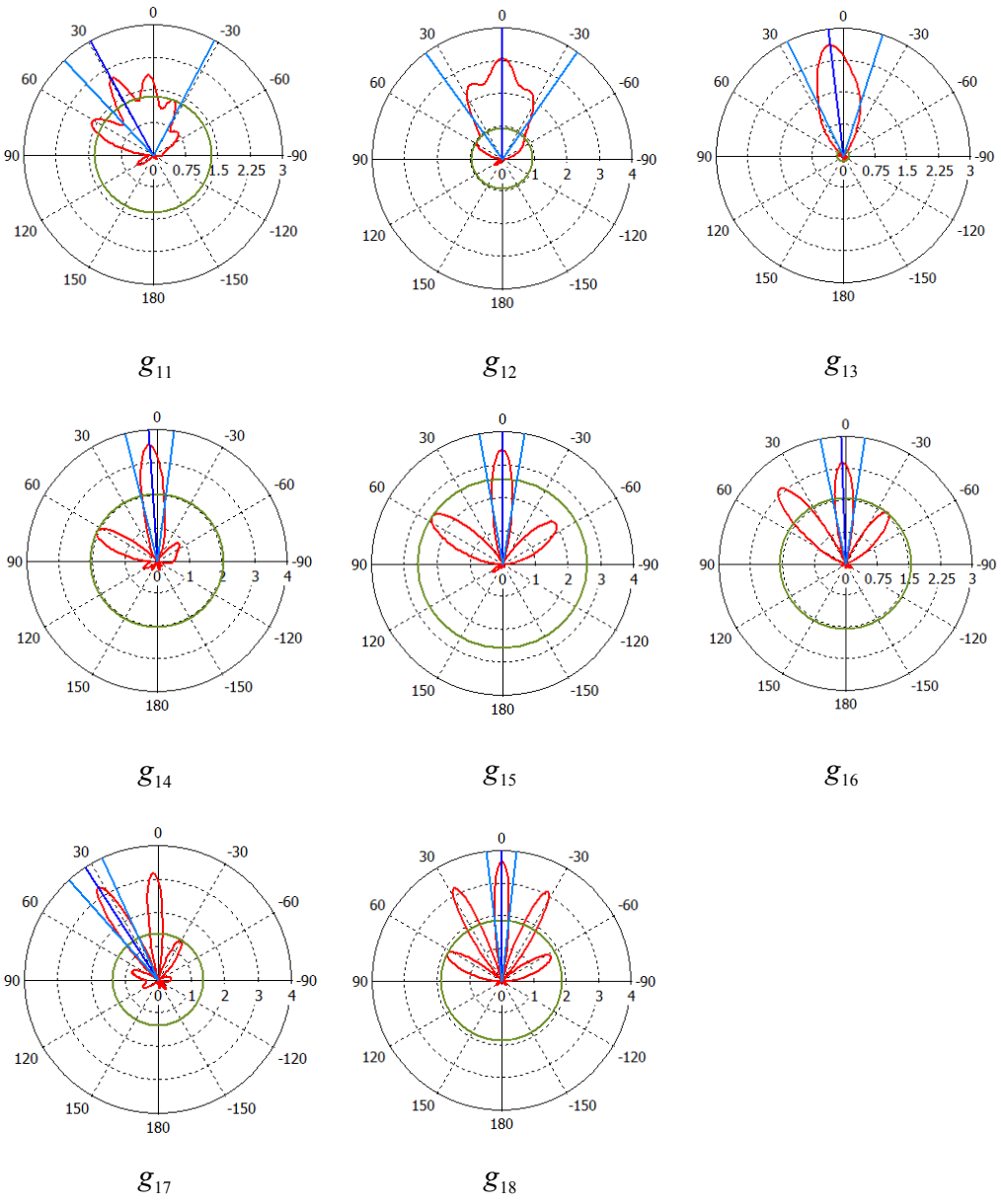

Figure 5.2: Radiation pattern of the first element and its adjacent elements

5.1.3 Resolution of estimation

This section presents simulation results of the proposed method and comparison with the conventional method. All results are obtained using the directional antenna array shown in Figure 5.1. Figure 5.3 and Figure 5.4 which show two cases of DOA estimation using both the conventional and proposed methods. In both cases, the number of snapshots is set at 100, and the SNR is set at 0dB. In the first case, two signals are coming at 0° and 10°, and in the second case, the signals are impinging the array at 25° and 35°.

Estimation results produced in both cases show improvement in estimation resolution using the proposed method. The results clearly show there are two distinct peaks in the spatial spectrum, which means the proposed method could distinguish two signals. The conventional method, on the other hand, only shows a single, flat peak around the incoming signals. This represents the inability of the conventional method to distinguish those signals, which also reflects that it has lower resolution than the proposed method. On that account, the estimation resolution can be improved using the proposed method.

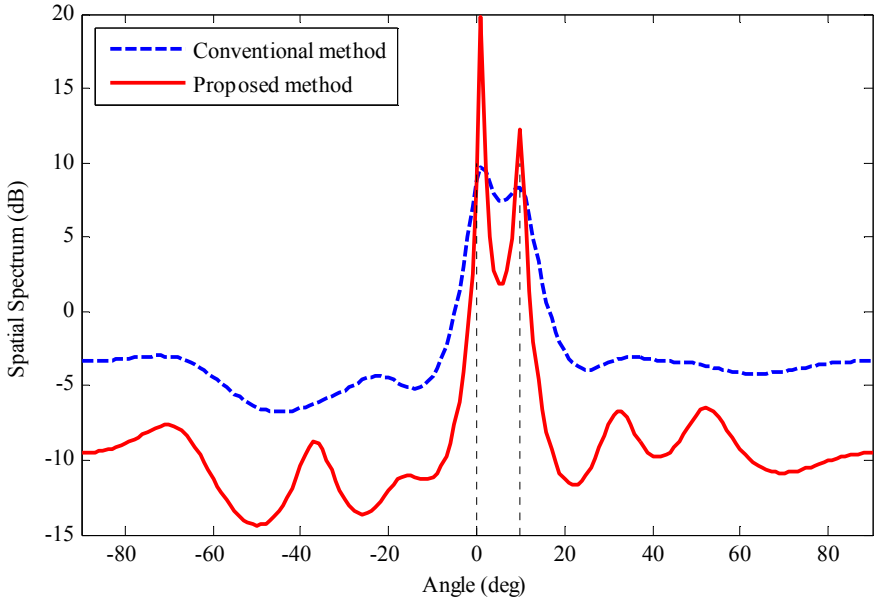

Figure 5.3: DOA estimation comparison between conventional and proposed method for multiple signal estimation at φ=0° and φ=10°. Dotted line represents the true DOA.

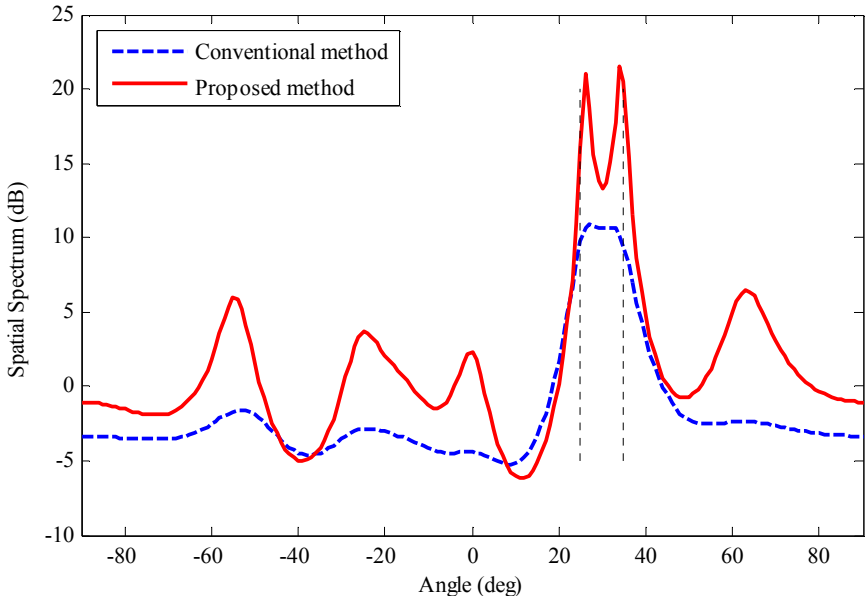

Figure 5.4: DOA estimation comparison between conventional and proposed method for multiple signal estimation at φ=25° and φ=35°. Dotted line represents the true DOA.

5.1.4 Error of estimation

The estimation error is also being investigated and compared between those two methods. In this simulation, it is assumed that there are two signals impinging the array at -4° and 4°.

Figure 5.5 shows the RMSE versus the number of snapshots for both the conventional and proposed methods when the SNR is fixed at 0dB. It is apparent that as the number of snapshots is increased, the estimation error of the proposed method is improved. On the other hand, estimation error from the conventional method is almost unchanged. It is also noted that the estimation error is reduced by up to 65% using the proposed method provided that the number of snapshots is larger than 150.

The RMSE versus SNR is shown in Figure 5.6 when the number of snapshots is set at 100. It is observed that both methods produced almost the same level of estimation error when the SNR is less than 0dB. However, when the SNR exceeds 5dB, the estimation error using the proposed method has reduced significantly. In addition, at high SNR, the proposed method could reduce the estimation error up to 70%. This

result suggests that the proposed method gives a better estimation result when the SNR is kept higher than 5dB.

Finally, the estimation error is compared when the DOA separation between two signal sources is varied. In this analysis, the DOA of the first signal is kept at -5°, DOA of the second signal is varied from 0° to 10°, the number of snapshots is 300, and the SNR is 0dB. Comparison of the estimation error between the two methods is depicted in Figure 5.7. It is observed that the proposed method has up to 85% lower estimation error than the conventional method when DOA of the second signal is between 2° and 8°.

As the separation between the first signal and the second signal gets larger, estimation error of the conventional method improves and slightly outperforms the proposed method. This result confirms that the proposed method yields smaller error than the conventional method when the separation between two signals is less than 13°. It is also apparent that as the signal separation is gets bigger, the proposed method only gives a relatively small improvement in estimation error.

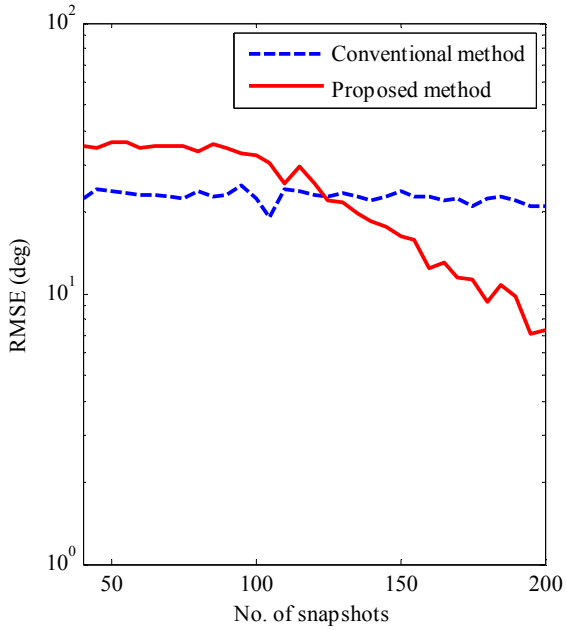

Figure 5.5: RMSE of estimation versus number of snapshots for both methods

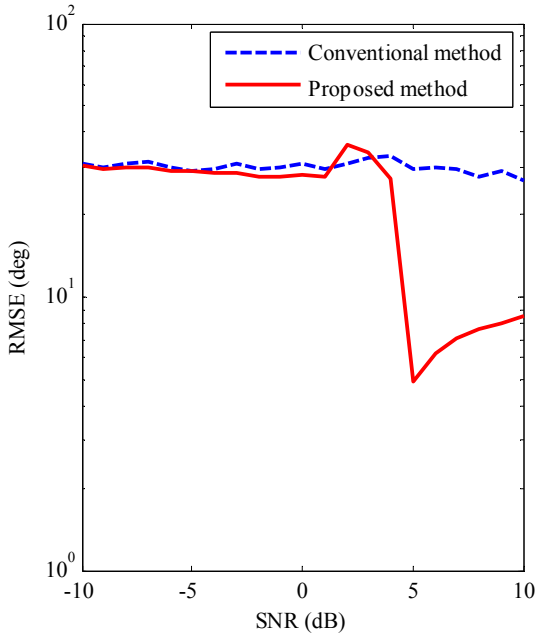

Figure 5.6: RMSE of estimation versus SNR for both methods

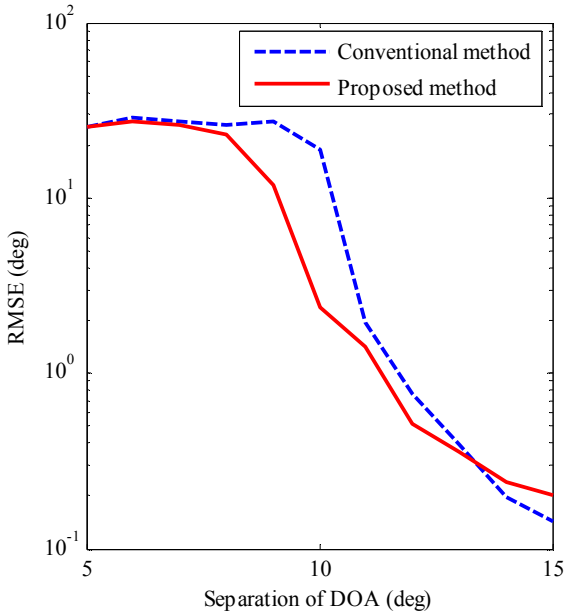

Figure 5.7: RMSE of estimation versus DOA of first signal for both methods

5.1.5 Consistency of estimation

This section compares the consistency of estimation between the conventional and proposed methods. It is assumed that the number of snapshots is 100, SNR level is 0dB, the number of trials is 1000, and the elevation DOA is at θ=25°. Figure 5.8 and Figure 5.9 illustrate that the conventional method and proposed method produce 85% and 78% of estimation consistency respectively. This comparison shows that the conventional method has outperformed the proposed method by 7%.

Simulation results suggest that the proposed method improves the estimation result in terms of estimation resolution and estimation error. The proposed method also shows that the estimation resolution can be achieved as low as 10°, which is a significant improvement compared with the conventional method. In terms of estimation error, the proposed method produced better performance than the conventional method in a large number of snapshots and high SNR. However, the estimation error between the two methods is almost the same regardless of the separation of DOA.

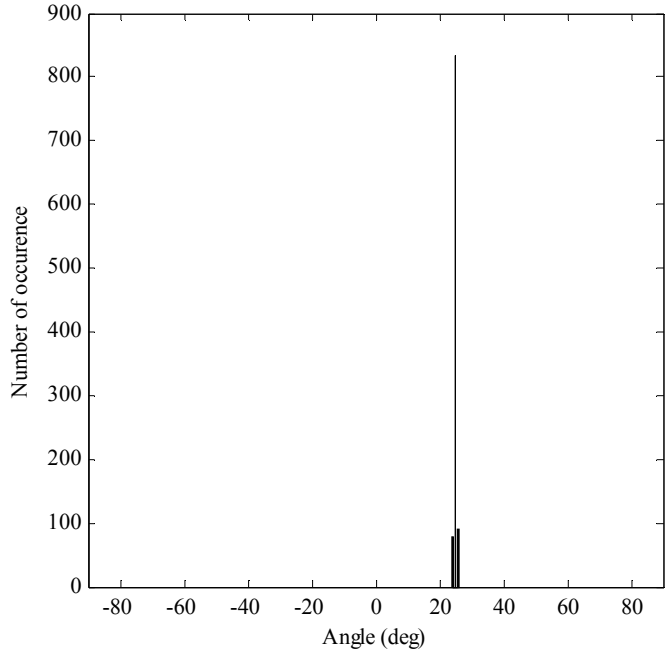

Figure 5.8: Histogram of DOA estimation using the conventional method. The DOA is at (θ=25°).

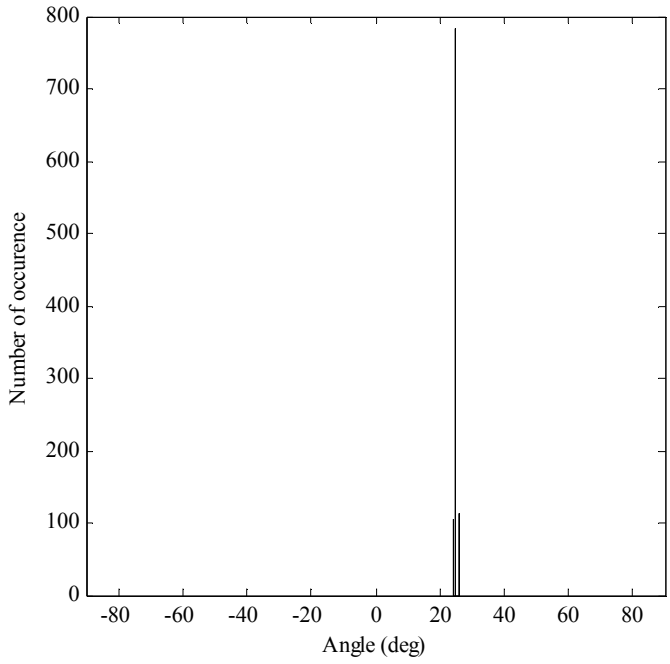

Figure 5.9: Histogram of DOA estimation using the proposed method. The DOA is at (θ=25°).

5.2 Azimuth angle estimation with modified covariance matrix

This section presents application of the proposed method for azimuth angle estimation. Similar to section 4.3, this section also uses semi-circular array as the array configuration for azimuth estimation. Comparison of DOA estimation performance between the conventional and proposed methods is discussed as well.

5.2.1 Semi-circular array for azimuth estimation

Figure 5.10 depicts a semi-circular array with element spacing of 0.5λ, where λ is the wavelength of incoming signal. The radiation pattern of the first element (g_1), and between the first element and the subsequent elements (g_{12}, g_{13},⋯, g_{18}) are illustrated in Figure 5.11.

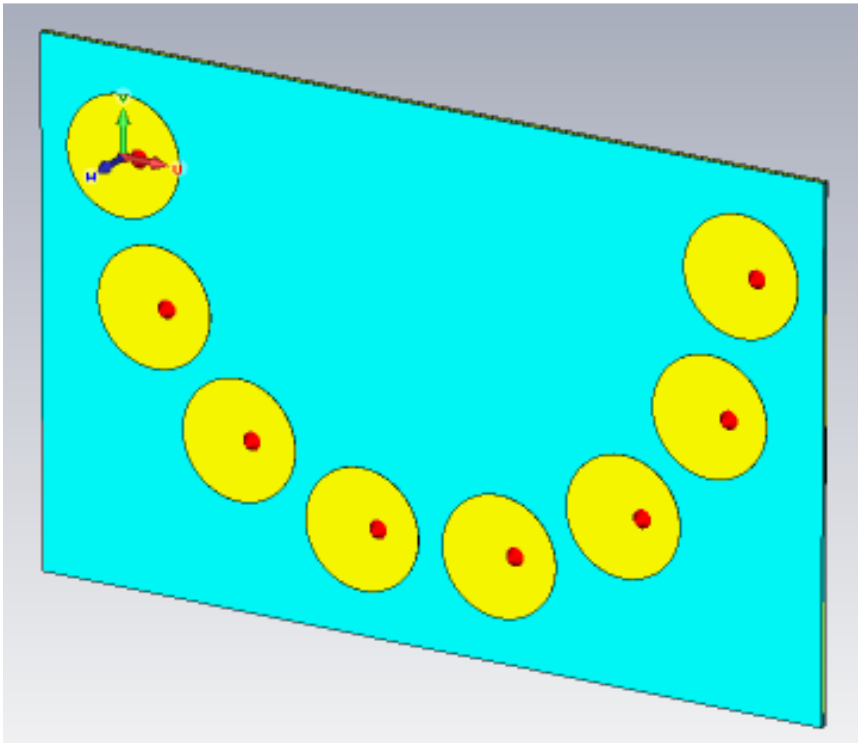

Figure 5.10: Semi-circular array of circular patch elements

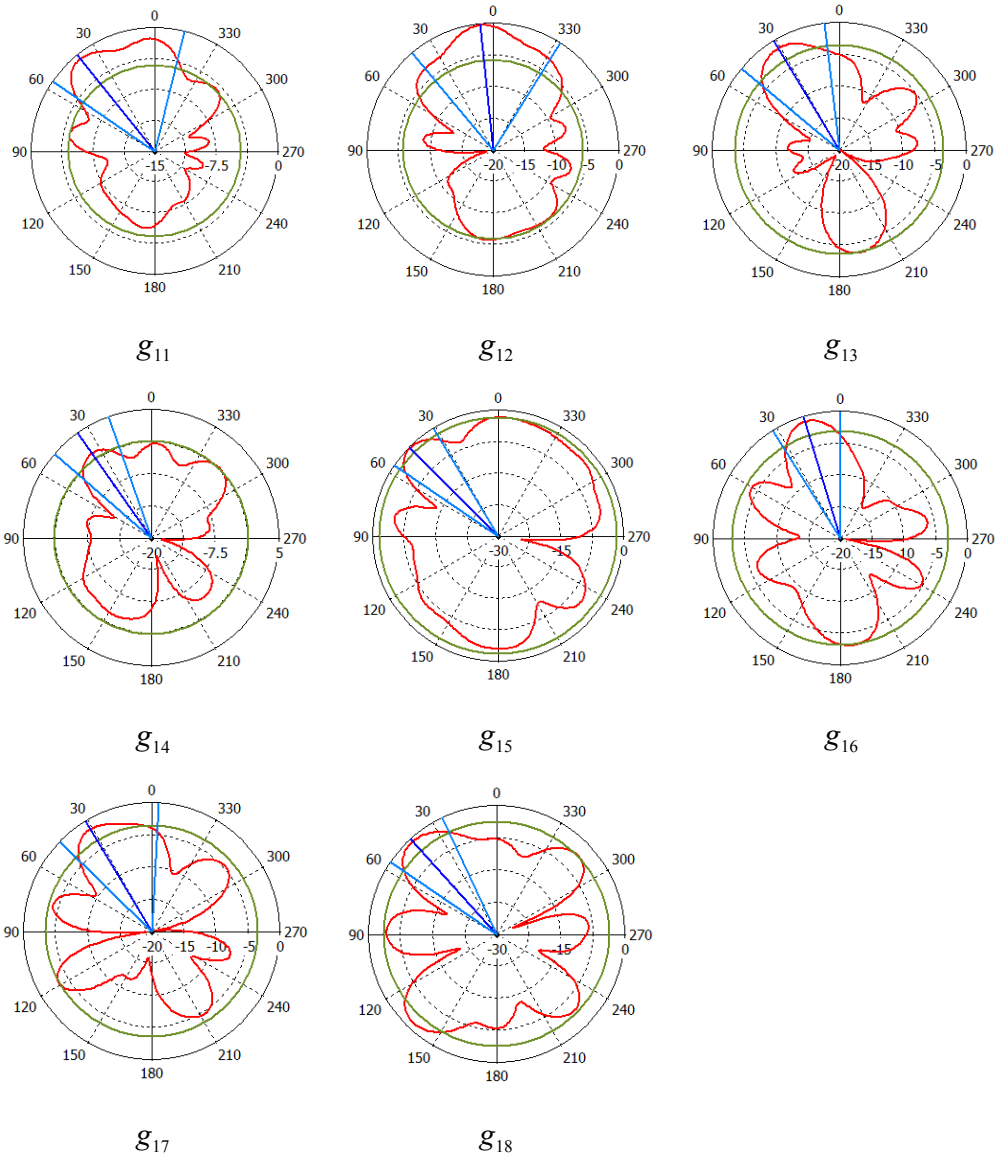

Figure 5.11: Radiation pattern of first element and its adjacent elements

5.2.2 Angular estimation

This section presents comparison of azimuth angle estimation between the conventional and proposed methods. The modified covariance matrix described in (5.2) is used to obtain the azimuth estimation in the proposed method. It is essential to obtain 36 unique element gains to form the symmetric matrix $\mathbf{G_S}$ and thus the modified covariance matrix. There are three cases of azimuth estimation being considered for comparison of angular estimation.

Firstly, the azimuth DOA is assumed at 5°. Figure 5.12 shows that both the conventional and proposed methods are able to estimate the true DOA. This result also illustrates that there are no spurious peaks existing in the spatial spectrum. The same observation is obtained in the second and third case when the true DOA is at 90° and 180° respectively. As shown in Figure 5.13 and Figure 5.14, both methods can estimate the true DOA without any additional false peaks. The results in this section suggest that the proposed method does not possess a significant advantage over the conventional method in azimuth estimation.

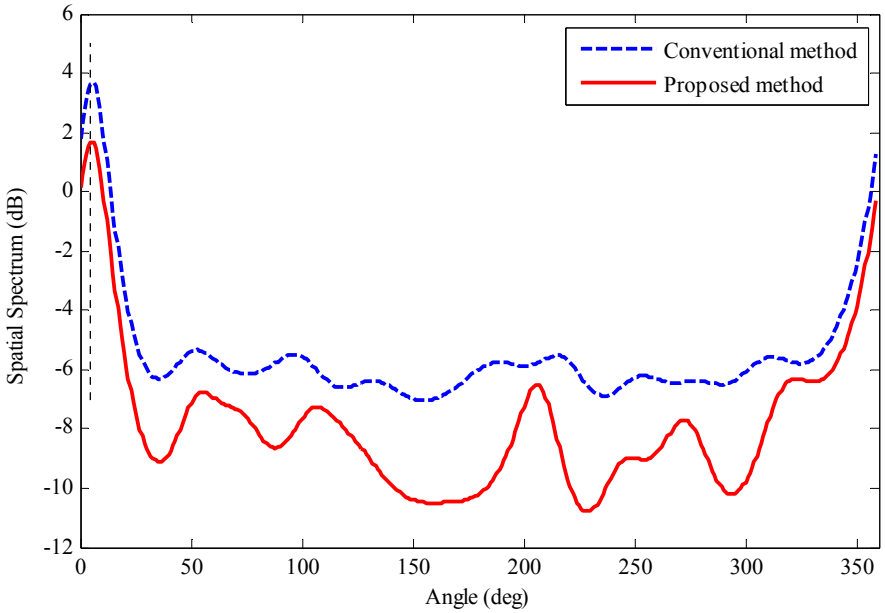

Figure 5.12: Comparison of DOA estimation between conventional and proposed methods for signals impinging at (φ=5°). Dotted line represents the true DOA.

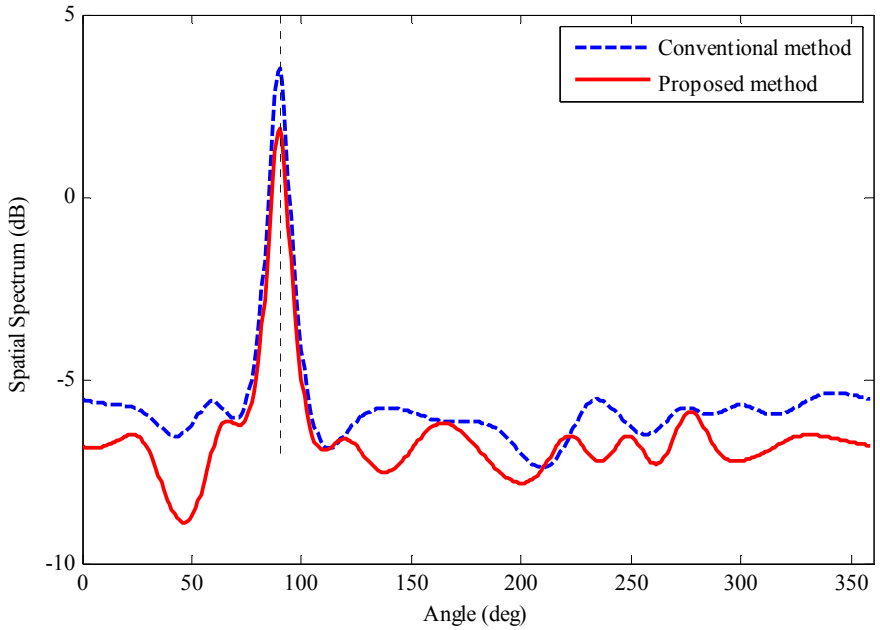

Figure 5.13: Comparison of DOA estimation between conventional and proposed methods for signals impinging at (φ=90°). Dotted line represents the true DOA.

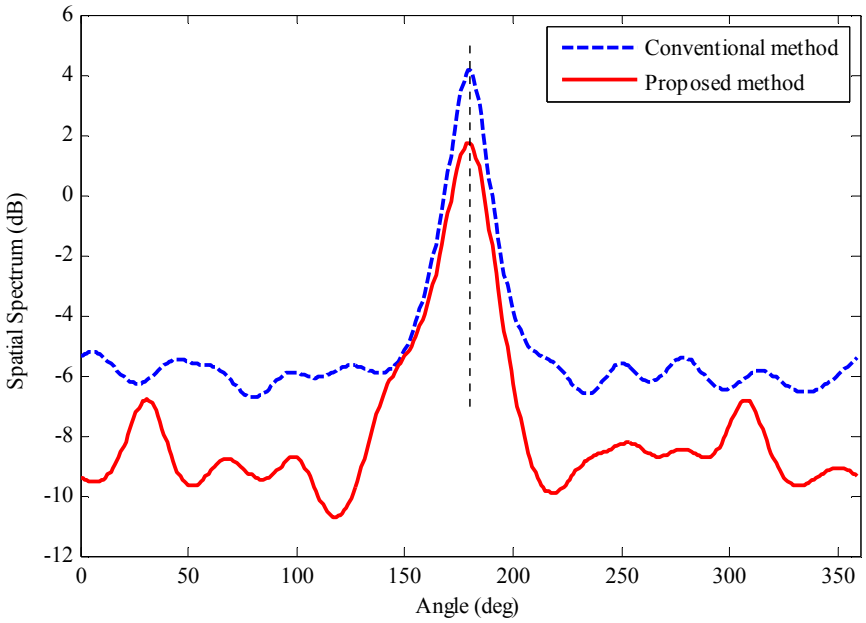

Figure 5.14: Comparison of DOA estimation between conventional and proposed methods for signals impinging at (φ=180°). Dotted line represents the true DOA.

5.2.3 Error of estimation

This section presents a comparison of estimation error between the conventional and proposed methods. In this section, it is assumed that there is one signal source present at (θ=90°, φ=180°). There are two cases of comparison being considered; estimation error for varied SNR and estimation error for varied number of snapshots.

In the first case, Figure 5.15 shows the RMSE of both methods when the number of snapshots is fixed at 100. The result clearly shows that both methods have the same trend in change of RMSE. There is a small difference of RMSE between the two methods when the SNR is between 4dB and 6dB. However, in general, both methods produce the same RMSE for various SNR levels.

The same result is also observed in the second case for various numbers of snapshots as shown in Figure 5.16. Both methods produce the same RMSE except in when the number of snapshots is between 130 and 150, and also between 185 and 200. Nevertheless, the difference of RMSE in this region is considered very small, about 0.1°.

The results in this section suggest that the proposed method offers an insignificant improvement over the conventional method in terms of estimation error. This result follows the trend in angular estimation in 5.2.2 where both methods produce an almost similar pattern of azimuth estimation.

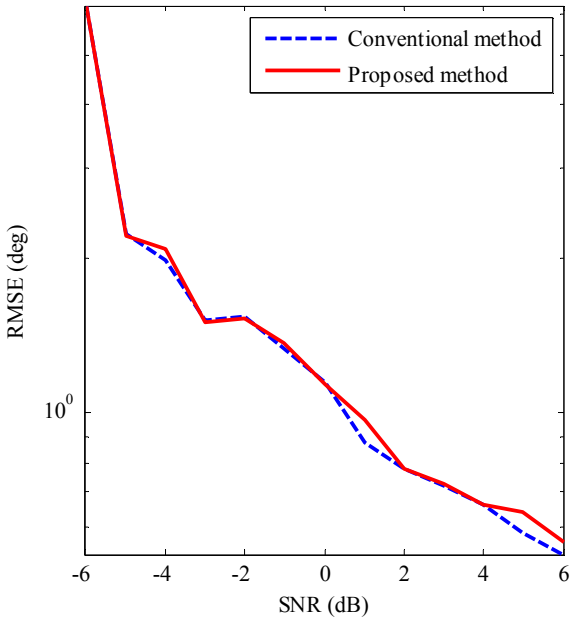

Figure 5.15: RMSE of DOA estimation for various SNR when number of snapshots is 100. The DOA is at (φ = 180°).

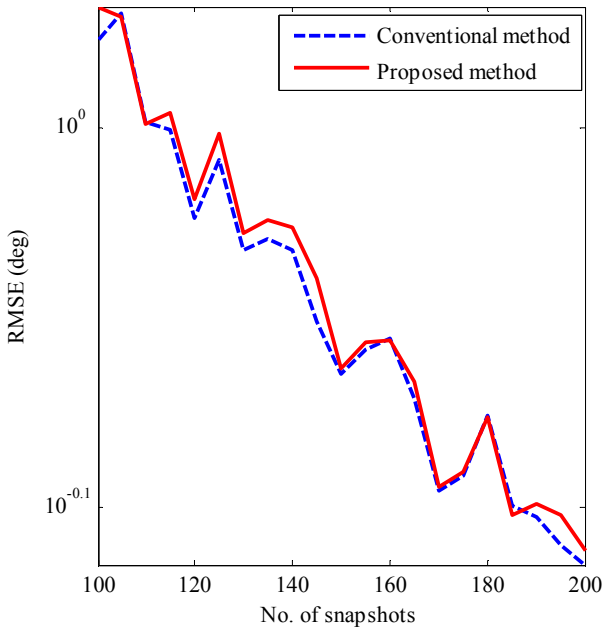

Figure 5.16: RMSE of DOA estimation versus number of snapshots when SNR is 0dB. The DOA is at (φ = 180°).

5.2.4 Consistency of estimation

This section presents comparison of estimation consistency between the conventional and proposed methods in azimuth estimation. It is assumed that the SNR is 0dB, the number of snapshots is 100, and the number of trials is 1000. There are two cases of azimuth DOA being considered: φ=5° and φ=180°. In the first case, the conventional method slightly outperforms the proposed method by 30%. This is due to greater dispersion of estimation away from the true DOA observed in the proposed method. The proposed method produces estimation between 1° and 7°, which is wider than the conventional method that has an estimation range of 4° - 6°.

In the second case, the conventional method outperforms the proposed method once again but by a smaller difference, around 10%. In contrast to the first case, the conventional method has a wider dispersion of azimuth estimation than the proposed method. The conventional method has an estimation between 178° and 182° compared to 179° - 181° in the proposed method. However, the conventional method maintains having a higher consistency than the proposed method.

In general, in terms of estimation consistency, the proposed method does not offer any significant improvement over the conventional method in azimuth estimation. As observed in 5.2.2, both the conventional and proposed methods have the same pattern of azimuth estimation. Therefore, it is not expected that the proposed method could yield higher estimation consistency than the conventional method.

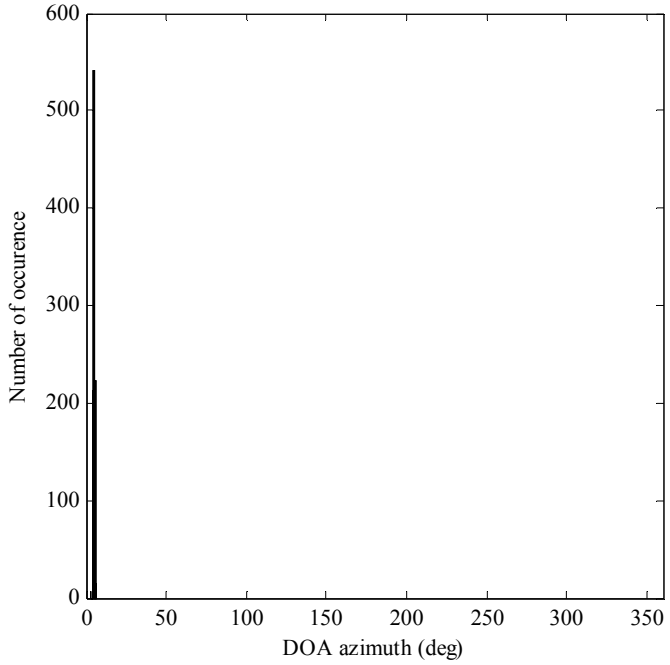

Figure 5.17: Histogram of DOA estimation using the conventional method. The DOA is at (φ=5°).

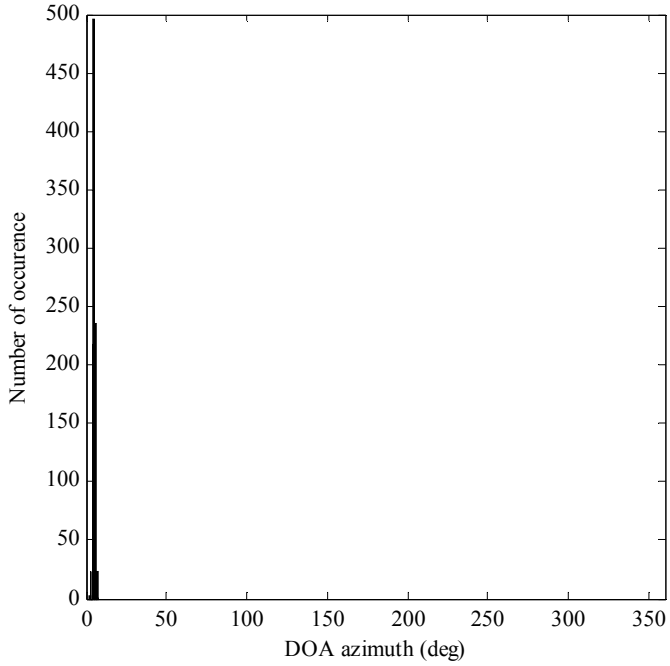

Figure 5.18: Histogram of DOA estimation using the proposed method. The DOA is at (φ=5°).

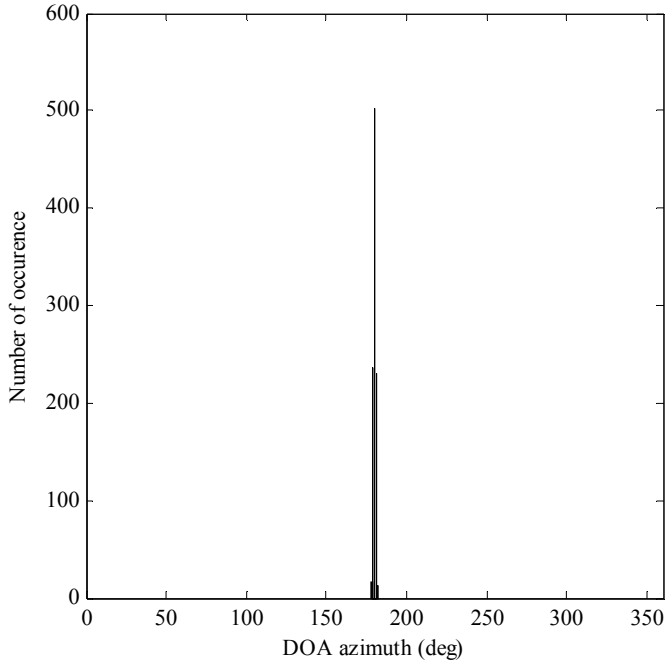

Figure 5.19: Histogram of DOA estimation using the conventional method. The DOA is at (φ=180°).

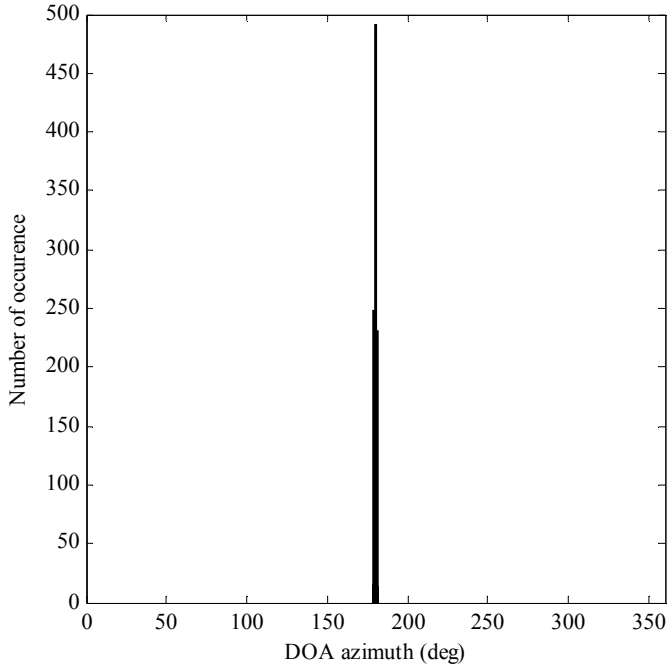

Figure 5.20: Histogram of DOA estimation using the proposed method. The DOA is at (φ=180°).

5.3 Summary

This chapter has presented a new method of DOA estimation for directional antenna arrays in order to suit the characteristics of directional antennas. In the previous chapter, the antenna array gain was used in determining the steering vector. This chapter maintained the importance of utilising the antenna array gain in DOA estimation with a different approach. In this chapter, the proposed method used the individual element gain to form the covariance matrix. The proposed method was then compared with the conventional method that excludes antenna array gain in covariance matrix calculation. In this chapter, the proposed method was applied and analysed in both elevation and azimuth angle estimation.

The first part of this chapter introduced a new method in utilising the gain of directional antenna array in DOA estimation. The proposed method utilises the gain of each of antenna element to calculate the covariance matrix. The method being proposed in this case requires the gain of each element as well as the combination gain of neighbouring elements in each angular position. These values of gain are then fed into the calculation of a new form of the covariance matrix. The proposed method in this chapter has higher complexity compared to the method used in the Capon-like algorithm. The proposed method requires $\frac{(N+r-1)!}{r!(N-1)!}$ of element gains for each angular position in order to form a complete modified covariance matrix. In elevation angle estimation, simulation results suggest that the proposed method could improve the estimation resolution by up to 10°. In addition, using the proposed method could achieve lower estimation error than the conventional method in two conditions. Firstly, when the number of snapshots is more than 150, and secondly, when the SNR is more than 5dB. It has been shown that the proposed method could reduce the estimation of the conventional method between 65% and 70%. Further analysis shows that the proposed method could improve the estimation consistency of the conventional method by up to 7%. Although the improvement offered by the modified covariance matrix is not as significant as in the Capon-like algorithm, it is considered as an option to improve the result of elevation DOA estimation.

In the second part of this chapter, the proposed method was further applied to azimuth DOA estimation. Similar to Chapter 4, the semi-circular array was used as array configuration for azimuth estimation. The results of azimuth angular estimation showed that the proposed method has comparable performance with the conventional method. Both methods are able to estimate the true DOA without any spurious peak existing in the spatial spectrum. Further analysis suggests that the proposed method does not exhibit any significant improvement in terms of estimation error and estimation consistency. The results in azimuth estimation show that the proposed method could not replicate the improvement exhibited in elevation estimation.

6 Conclusions and Future Work

This chapter highlights the main contributions of this thesis and also discusses possible extensions for future work.

6.1 Conclusions

This thesis has addressed problems related to antenna array configurations that could affect the performance of DOA estimation. It has also covered the processing techniques of DOA estimation in directional antenna array. As a result, new antenna array geometries and DOA algorithms have been proposed in order to solve the current problems efficiently.

The problem of DOA estimation in the existing antenna array geometries was addressed in Chapter 3. Three new antenna array geometries were proposed that could improve DOA estimation performance. Two antenna arrays based on the circular array, termed as semi-circular and oval arrays, have been proposed. Another antenna array has also been proposed, which is composed of several linear arrays, termed as the Y-bend array. It has been shown that the semi-circular array has 5.7% better estimation resolution, 76% lower estimation error, and 20% higher estimation consistency than the circular array. The second proposed array, the oval antenna array, could reduce the area required in the circular array between 12.5% and 15% with the same number of elements. In addition, the oval array has 33% better estimation resolution, 60% lower estimation error, and 20% higher estimation consistency than the circular array. The third proposed array, the Y-bend array, achieves 23% smaller estimation resolution, 88% lower estimation error, and 7% higher estimation consistency than the V-shape array. On top of that, a comparison study of DOA performance among the proposed arrays was also carried out. Simulation results suggest that the semi-circular array topped the result chart in all DOA performance criteria. In particular, the semi-circular array has 25% smaller estimation resolution, ten times smaller estimation error, and 5% higher estimation consistency than other proposed arrays.

The problem of DOA estimation using a directional antenna array is addressed in Chapter 4. The existing DOA algorithms are designed to work for the isotropic antenna and these algorithms cannot be applied directly without considering the characteristic of directional antenna array. Estimation processes using the isotropic antenna array and directional antenna array have been investigated and compared in this chapter. The comparison reveals that the radiation pattern of directional antenna array changes during beam steering and this change should be considered in DOA estimation. Therefore, a new DOA algorithm has been presented to accommodate the characteristic of directional antenna arrays. The proposed algorithm takes into account the maximum gain of the directional antenna array when the main beam is pointing in a certain direction. In elevation angle estimation, the proposed algorithm could offer an improvement over the Capon algorithm in three ways. Firstly, the proposed algorithm achieves estimation resolution of up to 1°. Secondly, the proposed algorithm has lowered the estimation error in the Capon algorithm not less than 80%. Thirdly, the proposed algorithm improves the estimation consistency of the Capon algorithm by at least 10%. The proposed algorithm maintains its superiority over the Capon algorithm in azimuth angle estimation. The proposed algorithm achieves 30 times lower estimation error and 20% higher estimation consistency than the Capon algorithm. These results suggest that the proposed algorithm is a candidate to be an effective algorithm in DOA estimation.

In Chapter 5, a new method in DOA estimation was presented by modifying the covariance matrix. The proposed technique combines the output of the individual antenna element and its corresponding gain in the covariance matrix to reflect the characteristic of directional antenna. In elevation angle estimation, the proposed method improves the estimation resolution of the conventional method by 5°. The proposed method also improves the estimation error in elevation estimation by 10%. However, the improvement is significant when either the number of snapshots is greater than 150 or the SNR is larger than 5dB. In azimuth angle estimation, the proposed method does not show a significant advantage over the conventional method. Simulation results illustrate that both methods possess the same pattern of azimuth estimation.

6.2 Future work

This thesis uses the assumption that all incoming signals are stationary. This assumption does not reflect the environment in real applications. A possible extension would be to consider the incoming signal dynamically, which means the DOA estimation needs to combine with tracking algorithms. A source tracking system can be formed as a combination of DOA algorithm and source tracking algorithm such as Kalman filter. This system would also address the problem of time-varying DOA estimation in practical applications. The source tracking is an interesting topic especially when involving the directional antenna array.

Another possible extension is to consider the effect of element position error in evaluating the DOA estimation performance using the proposed arrays. The element position is essential information used to determine the steering vector and thus the accuracy of DOA estimation. Therefore, the effect of element position error in antenna array on DOA estimation is an interesting topic to be investigated further.

One of the biggest concerns in mobile devices is the lifespan of the battery and numerous techniques have been proposed to conserve energy. The focus of this thesis is to improve the performance of DOA estimation but the energy efficient algorithm is also important for future deployment in real applications. A compromise between high gain algorithm and energy consumption needs to be investigated. Optimisation of antenna array configuration as well as DOA algorithm relative to energy efficiency will be an important topic in future research.

APPENDIX

APPENDIX A: Implementation of Bartlett Algorithm in MATLAB

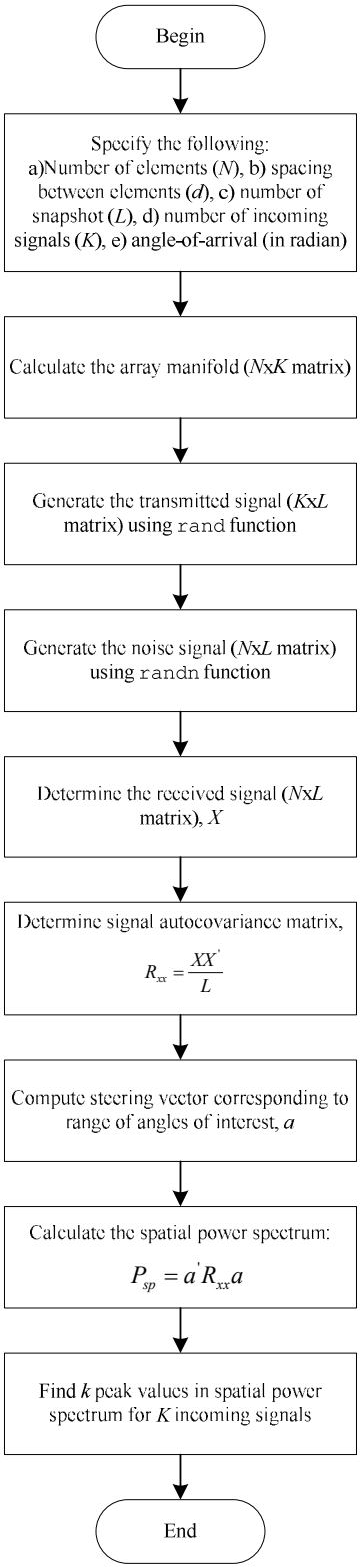

APPENDIX B: Implementation of Capon Algorithm in MATLAB

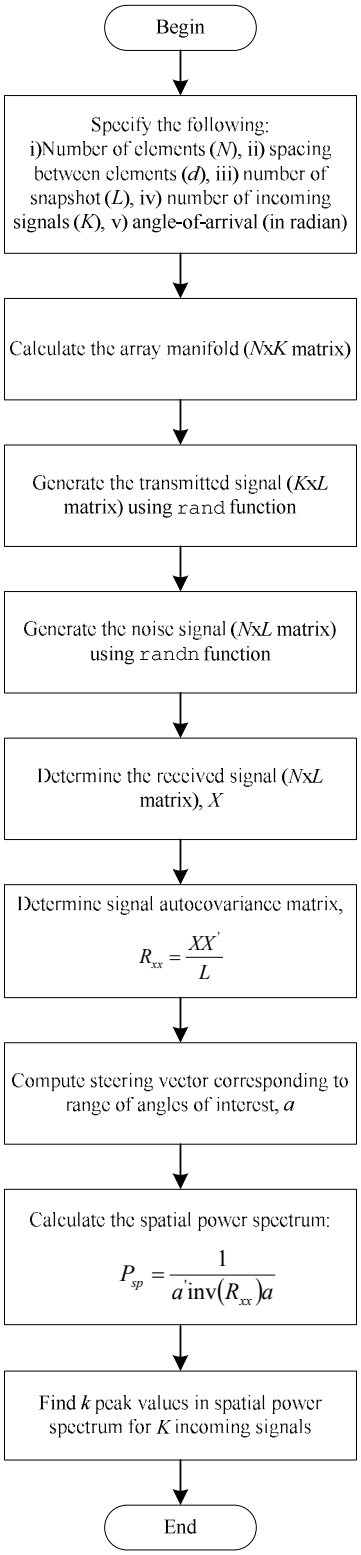

APPENDIX C: Implementation of MUSIC Algorithm in MATLAB

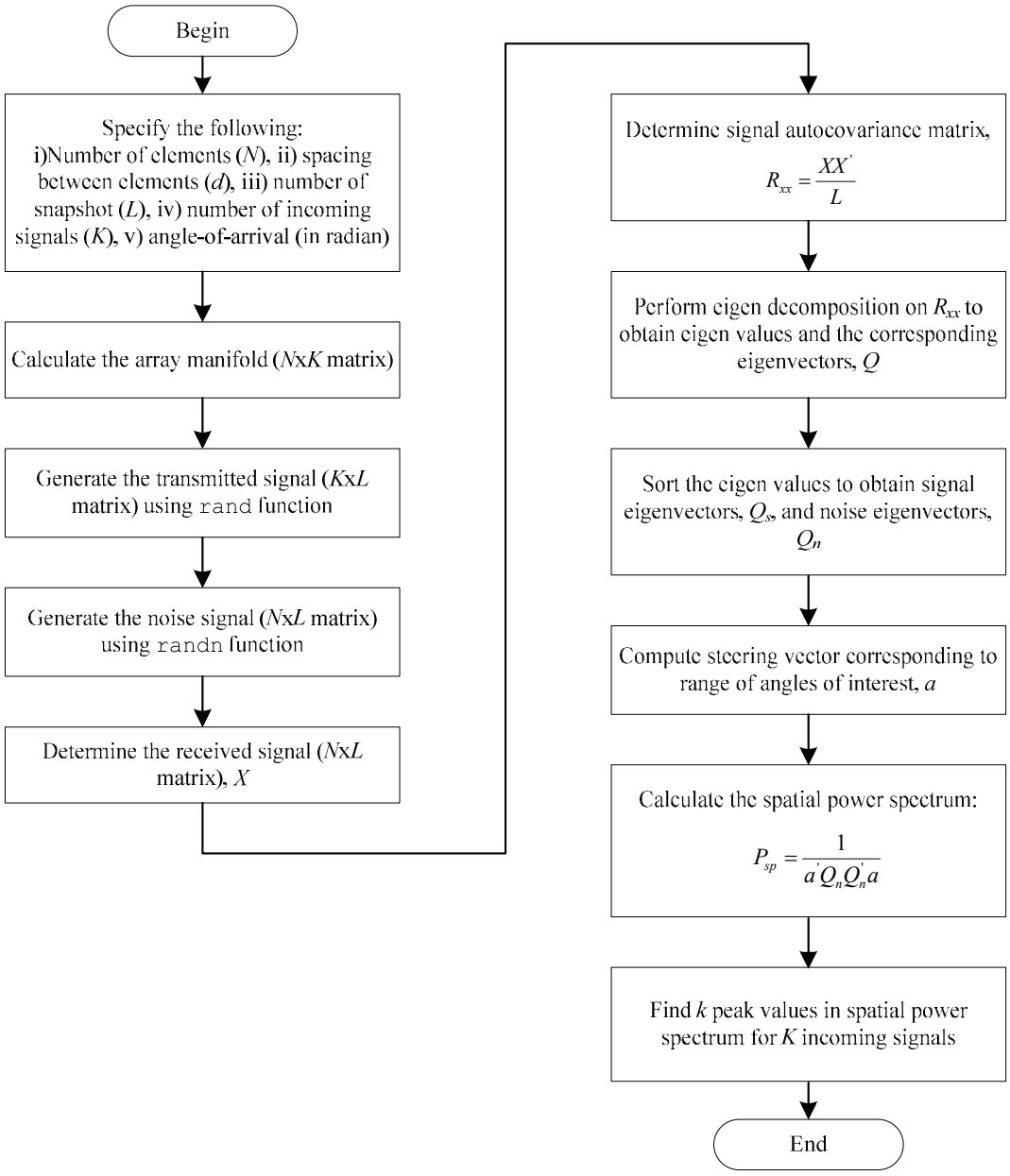

References

[1] G. T. Okamoto, *Smart Antenna Systems and Wireless LANs*, 1st ed. Santa Clara, California: Kluwer Academic, 2002.

[2] C. A. Balanis and P. I. Ioannides, *Introduction to Smart Antenna*. Arizona: Morgan and Claypool, 2007.

[3] J. Foutz, A. Spanias, and M. K. Banavar, *Narrowband Direction of Arrival Estimation for Antenna Arrays*, 1 ed. Arizona State University: Morgan & Claypool, 2008.

[4] R. L. Haupt, *Antenna Arrays: A Computational Approach*. New Jersey: John Wiley and Sons, 2010.

[5] J. Y.-L. Chou, "An Investigation on the Impact of Antenna Array Geometry on Beamforming User Capacity," Master of Science (Engineering), Queen's Universitty, Kingston, Ontario, 2002.

[6] T. S. Rappaport, *Wireless Communications: Principles and Practice*, 2nd ed. Upper Saddle River, NJ: Prentice Hall, 2002.

[7] X. Weikai, W. Lin, and C. Guanrong, "Performance of DCSK Cooperative Communication Systems Over Multipath Fading Channels," *IEEE Transactions on Circuits and Systems I: Regular Papers,* vol. 58, pp. 196-204, 2011.

[8] Z. Lei, L. Ning, and C. Lin, "Reliable Wireless Communication Networks for Demand Response Control," *IEEE Transactions on Smart Grid,* vol. 4, pp. 133-140, 2013.

[9] P. Mary, M. Dohler, J. Gorce, and G. Villemaud, "Packet Error Outage for Coded Systems Experiencing Fast Fading and Shadowing," *IEEE Transactions on Wireless Communications,* vol. 12, pp. 574-585, 2013.

[10] Y. Cho, J. Kim, W. Yang, and C. Kang, *MIMO-OFDM Wireless Communications with MATLAB®*: Wiley-IEEE Press, 2010.

[11] A. Molisch, *Wireless Communications*: Wiley-IEEE Press, 2011.

[12] D. Kim, K. Hyun-Myung, and I. Gi-Hong, "Improved Network-Coded Cooperative Transmission with Low-Complexity Adaptation to Wireless Channels," *IEEE Transactions on Communications,* vol. 59, pp. 2916-2927, 2011.

[13] J. Singh, "A Comparative Study of Error Detection and Correction Coding Techniques," in *Second International Conference on Advanced Computing & Communication Technologies (ACCT)*, 2012, pp. 187-189.

[14] M. A. El-Iskandarani, S. Darwish, and S. M. Abuguba, "Reliable wireless error correction technique for secure image transmission," in *43rd Annual International Carnahan Conference on Security Technology*, 2009, pp. 184-188.

[15] G. Farquharson, P. Lopez-Dekker, and S. J. Frasier, "Contrast-Based Phase Calibration for Remote Sensing Systems With Digital Beamforming Antennas," *IEEE Transactions on Geoscience and Remote Sensing,* vol. 51, pp. 1744-1754, 2013.

[16] K. Shinho and Y. E. Wang, "Two-Dimensional Planar Array for Digital Beamforming and Direction-of-Arrival Estimations," *IEEE Transactions on Vehicular Technology,,* vol. 58, pp. 3137-3144, 2009.
[17] Z. Ren, G. Wang, Q. Chen, and H. Li, "Modelling and simulation of Rayleigh fading, path loss, and shadowing fading for wireless mobile networks," *Simulation Modelling Practice and Theory,* vol. 19, pp. 626-637, 2011.
[18] I. Nicolaescu and D. Stoica, "Smart antennas for wireless communications systems," in *International Conference on Applied Electromagnetics and Communications (ICECom)*, 2010, pp. 1-4.
[19] C. Dau-Chyrh and H. Cheng-Nan, "Smart Antennas for Advanced Communication Systems," *Proceedings of the IEEE,* vol. 100, pp. 2233-2249, 2012.
[20] M. Z. U. Rahman, V. A. Kumar, and G. V. S. Karthik, "A low complex adaptive algorithm for antenna beam steering," in *International Conference on Signal Processing, Communication, Computing and Networking Technologies (ICSCCN)*, 2011, pp. 317-321.
[21] N. Himayat, S. Talwar, A. Rao, and R. Soni, "Interference management for 4G cellular standards [WIMAX/LTE UPDATE]," *IEEE Communications Magazine,* vol. 48, pp. 86-92, 2010.
[22] M. N. O. Sadiku, "Wireless wises up with smart antennas," *IEEE Potentials,* vol. 29, pp. 37-39, 2010.
[23] S. Yutao, J. Vihriala, A. Papadogiannis, M. Sternad, Y. Wei, and T. Svensson, "Moving cells: a promising solution to boost performance for vehicular users," *IEEE Communications Magazine,* vol. 51, pp. 62-68, 2013.
[24] J. R. De Luis and F. De Flaviis, "Frequency Agile Switched Beam Antenna Array System," *IEEE Transactions on Antennas and Propagation,* vol. 58, pp. 3196-3204, 2010.
[25] W. Han, Z. Zhijun, and F. Zhenghe, "A Beam-Switching Antenna Array With Shaped Radiation Patterns," *IEEE Antennas and Wireless Propagation Letters,* vol. 11, pp. 818-821, 2012.
[26] E. P. Tsakalaki, D. Wilcox, E. de Carvalho, C. B. Papadias, and T. Ratnarajah, "Spectrum sensing using single-radio switched-beam antenna systems," in *7th International ICST Conference on Cognitive Radio Oriented Wireless Networks and Communications (CROWNCOM)*, 2012, pp. 118-123.
[27] T. N. Kaifas and J. N. Sahalos, "Design and Performance Aspects of an Adaptive Cylindrical Beamforming Array," *IEEE Antennas and Propagation Magazine,* vol. 54, pp. 51-65, 2012.
[28] J. A. Srar and C. Kah-Seng, "Adaptive RLMS algorithm for antenna array beamforming," in *IEEE Region 10 Conference TENCON*, 2009, pp. 1-6.
[29] P. Nicopolitidis, V. Kakali, G. Papadimitriou, and A. Pomportsis, "On Performance Improvement of Wireless Push Systems via Smart Antennas," *IEEE Transactions on Communications,* vol. 60, pp. 312-316, 2012.
[30] A. J. Fenn, *Adaptive Antennas and Phased Arrays for Radar and Communications*. Massachusets Institute of Technology: Artech House Publishers, 2008.
[31] C. A. Balanis, *Modern Antenna Handbook*. New Jersey: John Wiley and Sons, 2008.

[32] H.-S. Lui, H. T. Hui, and M. S. Leong, "Investigation of Direction-of-Arrival Estimation using Uniform Linear Arrays with Different Antenna Separations and Array Apertures," presented at the Asia Pacific Microwave Conference, 2008.
[33] L. C. Godara, *Smart Antennas*. Boca Raton: CRC Press LLC, 2004.
[34] Z. Chen, G. Gokeda, and Y. Yu, *Introduction to Direction-of-Arrival Estimation*. Norwood, Massachusetts: Artech House, 2010.
[35] P. Rocca, R. L. Haupt, and A. Massa, "Sidelobe Reduction Through Element Phase Control in Uniform Subarrayed Array Antennas," *IEEE Antennas and Wireless Propagation Letters,* vol. 8, pp. 437-440, 2009.
[36] G. D. Hopkins, J. Ratner, A. Traille, and V. Tripp, "Aperture efficiency of amplitude, weighting distributions for array antennas," presented at the IEEE Aerospace Conference, 2007.
[37] C. A. Balanis, *Antenna Theory: Analysis and Design*, 3rd ed. New Jersey: John Wiley & Sons Inc., 2005.
[38] C. Wenquan, X. Yang, Z. Bangning, L. Aijun, Y. Tongbin, and G. Daosheng, "A Low-Cost Compact Patch Antenna With Beam Steering Based on CSRR-Loaded Ground," *IEEE Antennas and Wireless Propagation Letters,* vol. 10, pp. 1520-1523, 2011.
[39] Y. Sheng-Hong and C. Tah-Hsiung, "A Beam-Steering and -Switching Antenna Array Using a Coupled Phase-Locked Loop Array," *IEEE Transactions on Antennas and Propagation,* vol. 57, pp. 638-644, 2009.
[40] L. Haitao, S. Gao, and L. Tian-Hong, "Compact Dual-Band Antenna With Electronic Beam-Steering and Beamforming Capability," *IEEE Antennas and Wireless Propagation Letters,* vol. 10, pp. 1349-1352, 2011.
[41] J. Jia-jia, D. Fa-jie, C. Jin, L. Yan-chao, and H. Xiang-ning, "Mixed Near-Field and Far-Field Sources Localization Using the Uniform Linear Sensor Array," *IEEE Sensors Journal,* vol. 13, pp. 3136-3143, 2013.
[42] P. Ioannides and C. A. Balanis, "Uniform circular arrays for smart antennas," *IEEE Antennas and Propagation Magazine,* vol. 47, pp. 192-206, 2005.
[43] C. M. Tan, P. Fletcher, M. A. Beach, A. R. Nix, M. Landmann, and R. S. Thoma, "On the Application of Circular Arrays in Direction Finding Part I: Investigation into the estimation algorithms," in *1st Annual COST 273 Workshop*, 2002.
[44] T. Kuroda, N. Kikuma, and N. Inagaki, "DOA estimation and pairing method in 2D-ESPRIT using triangular antenna array," *Electronics & Communications in Japan, Part 1: Communications,* vol. 86, pp. 59-68, 2003.
[45] M. Ghavami, "Wideband smart antenna theory using rectangular array structures," *IEEE Transactions onSignal Processing,* vol. 50, pp. 2143-2151, 2002.
[46] P. Ioannides and C. A. Balanis, "Uniform circular arrays for smart antennas," in *IEEE Antennas and Propagation Society International Symposium*, 2004, pp. 2796-2799 Vol.3.
[47] Y. Zhongfu, L. Xiang, and X. Xu, "DOA Estimation With Circular Array via Spatial Averaging Algorithm," *IEEE Antennas and Wireless Propagation Letters,* vol. 6, pp. 74-76, 2007.

[48] P. Ioannides and C. A. Balanis, "Uniform circular and rectangular arrays for adaptive beamforming applications," *IEEE Antennas and Wireless Propagation Letters,* vol. 4, pp. 351-354, 2005.

[49] K. Yo Han, K. Yeung Jun, Y. Hyun-Il, Y. Won Young, and C. Yong-Soo, "2-D DoA Estimation with Cell Searching for a Mobile Relay Station with Uniform Circular Array," *IEEE Transactions on Communications,* vol. 58, pp. 2805-2809, 2010.

[50] K. Yo-Han, K. Yeong-Jun, Y. Hyun-Il, Y. Won-Young, and C. Yong-Soo, "DoA estimation with cell searching for mobile relay stations with uniform circular array," in *IEEE 20th International Symposium on Personal, Indoor and Mobile Radio Communications*, 2009, pp. 993-997.

[51] H. Gazzah and S. Marcos, "Cramer-Rao bounds for antenna array design," *IEEE Transactions on Signal Processing,* vol. 54, pp. 336-345, 2006.

[52] T. Filik and T. E. Tuncer, "Uniform and nonuniform V-shaped planar arrays for 2-D direction-of-arrival estimation," *Radio Science,* vol. 44, pp. 1-12, 2009.

[53] A. Manikas, A. Alexiou, and H. R. Karimi, "Comparison of the ultimate direction-finding capabilities of a number of planar array geometries," *IEE Proceedings - Radar, Sonar and Navigation,* vol. 144, pp. 321-329, 1997.

[54] S. W. Ellingson, "Design and evaluation of a novel antenna array for azimuthal angle-of-arrival measurement," *IEEE Transactions on Antennas and Propagation,* vol. 49, pp. 971-979, 2001.

[55] Y. Hua, T. K. Sarkar, and D. D. Weiner, "An L-shaped array for estimating 2-D directions of wave arrival," *IEEE Transactions on Antennas and Propagation,* vol. 39, pp. 143-146, 1991.

[56] J. Liang and D. Liu, "Joint Elevation and Azimuth Direction Finding Using L-Shaped Array," *IEEE Transactions on Antennas and Propagation,* vol. 58, pp. 2136-2141, 2010.

[57] S. Xin-Yu and Z. Jian-Jiang, "2-D DOA estimation employing L-shape array without estimation failure and pair matching failure," *International Journal of Electronics,* vol. 97, pp. 349-363, 2010.

[58] G. Wang, J. Xin, N. Zheng, and A. Sano, "Computationally Efficient Subspace-Based Method for Two-Dimensional Direction Estimation with L-Shaped Array," *IEEE Transactions on Signal Processing,* vol. 59, pp. 3197-3212, 2011.

[59] X. Zhang, J. Li, and L. Xu, "Novel two-dimensional DOA estimation with L-shaped array," *EURASIP Journal on Advances in Signal Processing,* pp. 1-7, 2011.

[60] L.-y. Xu, X.-f. Zhang, Z.-z. Xu, and M. Yu, "Joint 2D-DOA and Frequency Estimation for L-Shaped Array using Iterative Least Squares Method," *International Journal of Antennas and Propagation,* pp. 1-8, 2012.

[61] N. Tayem and H. M. Kwon, "L-shape 2-dimensional arrival angle estimation with propagator method," *IEEE Transactions on Antennas and Propagation,* vol. 53, pp. 1622-1630, 2005.

[62] F. Harabi, H. Changuel, and A. Gharsallah, "A new estimation of direction of arrival algorithm with a special antenna shape," *Smart Materials & Structures,* vol. 16, pp. 2595-2599, 2007.

[63] Y. Yantao, L. Hoi-Shun, N. Choon Hock, and H. Hon Tat, "Improved DOA Estimations Using the Receiving Mutual Impedances for Mutual Coupling Compensation: An Experimental Study," *IEEE Transactions on Wireless Communications,* vol. 10, pp. 2228-2233, 2011.

[64] L. Bin, Z. Zhi-Guo, and C. Shing-Chow, "DOA Estimation and Tracking of ULAs with Mutual Coupling," *IEEE Transactions on Aerospace and Electronic Systems,* vol. 48, pp. 891-905, 2012.

[65] L. Aifei, L. Guisheng, Z. Cao, Y. Zhiwei, and X. Qing, "An Eigenstructure Method for Estimating DOA and Sensor Gain-Phase Errors," *IEEE Transactions on Signal Processing,* vol. 59, pp. 5944-5956, 2011.

[66] L. Bin and C. Shing-Chow, "Direction-of-Arrival Estimation in Subarrays-Based Linear Sparse Arrays with Gain/Phase Uncertainties," *IEEE Transactions on Aerospace and Electronic Systems,* vol. 49, pp. 2268-2280, 2013.

[67] L. Zhang-Meng and Z. Yi-Yu, "A Unified Framework and Sparse Bayesian Perspective for Direction-of-Arrival Estimation in the Presence of Array Imperfections," *IEEE Transactions on Signal Processing,* vol. 61, pp. 3786-3798, 2013.

[68] I. J. Gupta and A. A. Ksienski, "Effect of mutual coupling on the performance of adaptive arrays," *IEEE Transactions on Antennas and Propagation,* vol. 31, pp. 785-791, 1983.

[69] F. Sellone and A. Serra, "A Novel Online Mutual Coupling Compensation Algorithm for Uniform and Linear Arrays," *IEEE Transactions on Signal Processing,* vol. 55, pp. 560-573, 2007.

[70] K. R. Dandekar, L. Hao, and X. Guanghan, "Experimental study of mutual coupling compensation in smart antenna applications," *IEEE Transactions on Wireless Communications,* vol. 1, pp. 480-487, 2002.

[71] R. S. Adve and T. K. Sarkar, "Compensation for the effects of mutual coupling on direct data domain adaptive algorithms," *IEEE Transactions on Antennas and Propagation,* vol. 48, pp. 86-94, 2000.

[72] N. Boon Chong and S. Chong Meng Samson, "Sensor-array calibration using a maximum-likelihood approach," *IEEE Transactions on Antennas and Propagation,* vol. 44, pp. 827-835, 1996.

[73] C. M. S. See, "Sensor array calibration in the presence of mutual coupling and unknown sensor gains and phases," *Electronics Letters,* vol. 30, pp. 373-374, 1994.

[74] B. Friedlander and A. J. Weiss, "Direction finding in the presence of mutual coupling," *IEEE Transactions on Antennas and Propagation,* vol. 39, pp. 273-284, 1991.

[75] S. Fabrizio and S. Alberto, "A Novel Online Mutual Coupling Compensation Algorithm for Uniform and Linear Arrays," *IEEE Transactions on Signal Processing,* vol. 55, pp. 560-573, 2007.

[76] Y. Zhongfu, D. Jisheng, X. Xu, and W. Xiaopei, "DOA Estimation for Uniform Linear Array with Mutual Coupling," *IEEE Transactions on Aerospace and Electronic Systems,* vol. 45, pp. 280-288, 2009.

[77] E. K. L. Hung, "A critical study of a self-calibrating direction-finding method for arrays," *IEEE Transactions on Signal Processing,* vol. 42, pp. 471-474, 1994.

[78] B.-h. Wang, Y.-l. Wang, and H. Chen, "A robust DOA estimation algorithm for uniform linear array in the presence of mutual coupling," in *IEEE Antennas and Propagation Society International Symposium*, 2003, pp. 924-927 vol.3.

[79] L. Min and Y. Luxi, "Blind Calibration and DOA Estimation With Uniform Circular Arrays in the Presence of Mutual Coupling," *IEEE Antennas and Wireless Propagation Letters,* vol. 5, pp. 315-318, 2006.

[80] L. C. Godara, "Application of antenna arrays to mobile communications. II. Beam-forming and direction-of-arrival considerations," *Proceedings of the IEEE,* vol. 85, pp. 1195-1245, 1997.

[81] D. H. Johnson, "The application of spectral estimation methods to bearing estimation problems," *Proceedings of the IEEE,* vol. 70, pp. 1018-1028, 1982.

[82] J. Capon, "High-resolution frequency-wavenumber spectrum analysis," *Proceedings of the IEEE,* vol. 57, pp. 1408-1418, 1969.

[83] W. Hong and M. Kaveh, "On the performance of signal-subspace processing-- Part I: Narrow-band systems," *IEEE Transactions on Acoustics, Speech and Signal Processing,* vol. 34, pp. 1201-1209, 1986.

[84] R. Schmidt, "Multiple emitter location and signal parameter estimation," *IEEE Transactions on Antennas and Propagation,* vol. 34, pp. 276-280, 1986.

[85] R. T. Williams, S. Prasad, A. K. Mahalanabis, and L. H. Sibul, "An improved spatial smoothing technique for bearing estimation in a multipath environment," *IEEE Transactions on Acoustics, Speech and Signal Processing,* vol. 36, pp. 425-432, 1988.

[86] P. Stoica and K. C. Sharman, "Maximum likelihood methods for direction-of-arrival estimation," *IEEE Transactions on Acoustics, Speech and Signal Processing,* vol. 38, pp. 1132-1143, 1990.

[87] L. C. Godara, "Applications of antenna arrays to mobile communications. I. Performance improvement, feasibility, and system considerations," *Proceedings of the IEEE,* vol. 85, pp. 1031-1060, 1997.